CHEMISTRY
A European Journal

Supporting Information

Thermodynamic Programming of Erbium(III) Coordination Complexes for Dual Visible/Near-Infrared Luminescence

Bahman Golesorkhi,[a] Laure Guénée,[b] Homayoun Nozary,[a] Alexandre Fürstenberg,[a] Yan Suffren,[c, e] Svetlana V. Eliseeva,[d] Stéphane Petoud,*[d] Andreas Hauser,*[c] and Claude Piguet*[a]

chem_201802277_sm_miscellaneous_information.pdf

Supporting Information

(107 pages)

Appendix 1: Thermodynamics analysis of melting processes for L4-L9.

The influence of terminal substituents on the intermolecular cohesion in the solid state can be investigated by differential scanning calorimetry (Figures S3-S8). The traces of energy fluxes recorded at low scanning rate (0.5 K/min) reveal standard Ehrenfest first-order melting processes, from which the associated enthalpic (ΔH_m) and entropic (ΔS_m) contributions can be easily deduced by integration (columns 2-3 in Table A1-1).[42] Plots of enthalpic (ΔH_m) versus entropic (ΔS_m) contributions display approximate linear *H*/*S* compensations in agreement with the existence of a unique minimal intermolecular contact distance between polyaromatic entities in the solid state for both the bisbzimpy (**L4-L6**) and terpy (**L7-L9**) series (Figure A1-1a).[41]

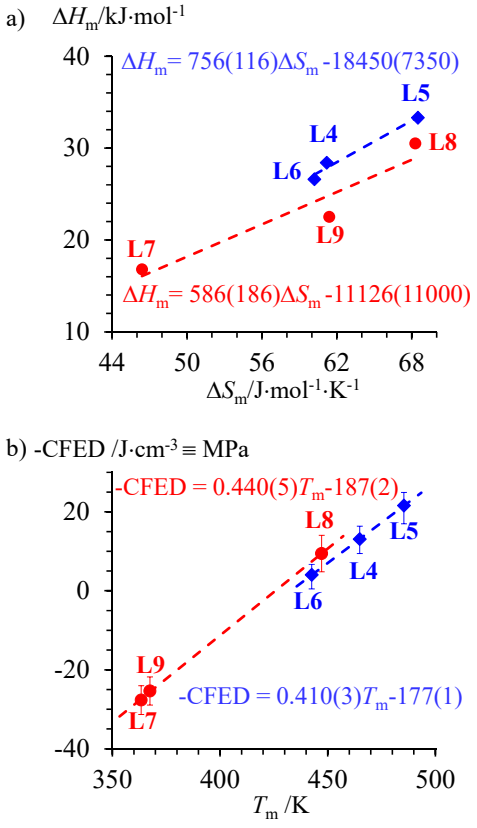

Figure A1-1 Plots of a) enthalpic *versus* entropic contributions for the melting processes modelled with eq. (A1-1) and b) cohesion free energy densities (-CFED computed at $T^{ref} = 428.5$ K) versus melting temperatures for ligands **L4-L9**. Local linear trendlines are shown together with their respective equations. The bisbzimpy series is plotted in blue and the terpy series in red.

Table A1-1 Thermodynamic parameters pertinent to the melting processes (ΔH_m, ΔS_m, T_m, $\Delta G_m^{T^{ref}}$),[42] molecular volumes (V_m), molar volumes (V_{mol}) and cohesion free energy densities (CFED, Eq. (A1-3)) for **L4**-**L9**.

L*k*	ΔH_m /kJ·mol^{-1}	ΔS_m /J·mol^{-1}·K^{-1}	T_m [a] /K	ΔG_m^{Tref} [b] /kJ·mol^{-1}	V_m [c] /Å^3	V_{mol} [d] /cm^3·mol^{-1}	CFED [e] /J·cm^{-3}
L4	28.4(1)	61(1)	464.9	2.2(5)	276.4	166.4	-13(3)
L5	33.3(2)	69(1)	485.4	3.9(6)	303.9	183.0	-21(3)
L6	26.6(1)	60(1)	442.6	0.8(5)	331.1	199.4	-4(3)
L7	16.8(1)	46(1)	363.4	-3.1(4)	185.0	111.4	28(4)
L8	30.5(2)	68(1)	447.2	1.2(6)	217.0	130.7	-9(5)
L9	22.5(1)	61(1)	367.5	-3.8(5)	249.6	150.3	25(4)

[a] Melting temperatures are taken at the onset of the DSC trace. [b] $\Delta G_m^{T^{ref}} = \Delta H_m - T^{ref}\Delta S_m$ are calculated at $T^{ref} = (1/N)\sum_{i=1}^{N} T_{m,i} = 428.5$ K. [c] Taken as the Connolly volume of the molecule in the solid state.[53] [d] $V_{mol} = N_A \cdot V_m$ where N_A is Avogadro's number. [e] $\mathrm{CFED} = -\Delta G_m^{T^{ref}} / V_{mol}$.

According to Eq. (A1-1),[41e] the different slopes displayed by the two red and blue *H*/*S* series in Figure A1-1a can be accounted for by the existence of two different phase volume expansions $\Delta\ln(\Omega_{1,2})$ accompanying the melting processes ($R\Delta\ln(\Omega_{1,2}^{bisbzimpy})$ = 24(10) J·mol^{-1}·K^{-1} and $R\Delta\ln(\Omega_{1,2}^{terpy})$ = 19(19) J·mol^{-1}·K^{-1}).

$$\Delta H_m = T_{comp}\Delta S_m - RT_{comp}\Delta\ln(\Omega_{1,2}) \quad \text{(A1-1)}$$

The magnitude of $1/\Omega$ can be then considered as a novel coordinate in the extended extra-thermodynamic relationship depicted in Eq. (A1-2) where *M* is some constant characterizing the system for which $p_\Omega^2/2M$ corresponds to its kinetic energy.[41]

$$\Delta H_m = T'_{comp}\left[\Delta S_m + R\Delta\ln(\Omega_{1,2})\right] - RT'_{comp}\Delta\ln(M_{1,2}) \quad \text{(A1-2)}$$

The restored straight line (within experimental uncertainties) observed for the plot of ΔH_m versus $\Delta S_m + R\Delta\ln(\Omega_{12})$ built for **L4**-**L9** (Figure A1-2) demonstrates that all ligands belong to the same

thermodynamic *H/S* family, for which the perturbation imposed by terminal alkyl substitutions of increasing sizes (R = H < CH_3 < CH_2CH_3) similarly affects the energy cohesion in the solid state; the only difference arises from minor changes in specific volume expansions.[41]

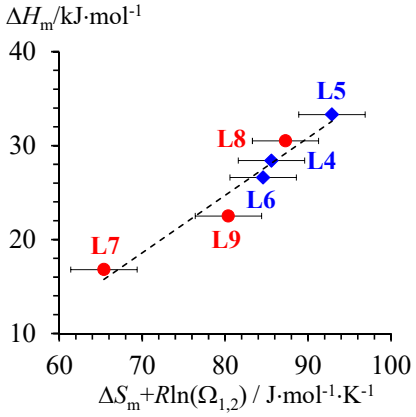

Figure A1-2 Plots of a) enthalpic *versus* entropic contributions to the melting processes modelled with Eq. (A1-2) for ligands **L4-L9**. The linear trendline is shown in black. The bisbzimpy series is plotted in red and the terpy series in blue.

The second step in the thermodynamic analysis consists in plotting in Figure A1-1b the cohesive Gibbs free energy densities (CFED) given in Eq. (A1-3), where V_{mol} is the molar volume and T^{ref} is a reference temperature taken as the average of the melting temperatures (columns 5-8 in Table A1-1) as a function of the transition temperatures (T_m).[42] The resulting pseudo-linear traces represents the phase boundaries produced by the 'chemical pressure' induced by successive perturbations within a *H/S* family (right part of Eq. (A1-3)).[42] The approximate single trace observed for ligands **L4-L9** points to similar dependence of the intermolecular energy cohesion on successive terminal alkylation for both series (Figure A1-1b).

$$\text{CFED} = \frac{\Delta G_{\text{cohesion}}^{T^{\text{ref}}}}{V_{\text{mol}}} = \frac{\Delta H_{\text{m}} - T^{\text{ref}}\Delta S_{\text{m}}}{V_{\text{mol}}} \approx \frac{\Delta V_{\text{melting}}}{V_{\text{mol}}}\Delta P_{\text{chemical}} \qquad \text{(A1-3)}$$

Moving along the boundary line, the connection of two terminal methyl groups (**L4**→**L5** or **L7**→**L8**), induces larger cohesive energies in the solid state as measured by the development of positive 'chemical pressures' ($\Delta P_{chemical}$ = CFED(**L4**)-CFED(**L5**) = 9(4) MPa or CFED(**L7**)-CFED(**L8**)

= 37(4) MPa) and the concomitant increase of the melting temperatures (Figure A1-1b). This behavior can be reasonably assigned to the increase of the molecular polarizability produced by the larger molar volume, this without significant disruption of the intermolecular packing interactions. On the contrary, the introduction of an additional methylene (CH_2) rotor in ethyl groups as found in **L6** and **L9**, provides non-linear three-carbon chains, the various conformations of which may notably affect intermolecular packing possibilities. The associated severe loss in 'chemical pressure' observed along the boundary (**L5**→**L6** or **L8**→**L9**) reduces the melting temperature of **L6** and **L9** despite their larger molecular weight and polarizabilities (Figure A1-1b). In other words, the H→CH_3→CH_2CH_3 sequence produces two successive, but opposite alterations of intermolecular cohesion. The introduction of methyl groups improves cohesion due the increase in molecular polarizability, while the extension by additional methylene rotors to give ethyl substituents severely disrupts inter-aromatic stacking.

Appendix 2: Thermodynamics analysis of Er-ligand affinities and interligand interactions in acetonitrile solutions for L4-L9.

Pertinent Born-Haber cycles allow the partition of the experimental Er-ligand affinities (Eq. (A2-1) and Scheme A2-1a) and interligand interactions (Eq. (A2-2) and Scheme A2-2b) measured in solution into their gas-phase counterpart modulated by the various solvation energies.[A2-1]

$$\Delta G^{\mathrm{Er},\mathbf{L}\boldsymbol{k}}_{\mathrm{affinity,solv}} = \Delta G^{\mathrm{Er},\mathbf{L}\boldsymbol{k}}_{\mathrm{affinity,gas}} + \Delta G^{\mathrm{Er}\mathbf{L}\boldsymbol{k}}_{\mathrm{solv}} - \left(\Delta G^{\mathrm{Er}}_{\mathrm{solv}} + \Delta G^{\mathbf{L}\boldsymbol{k}}_{\mathrm{solv}}\right) \quad \text{(A2-1)}$$

$$\Delta E^{\mathbf{L}\boldsymbol{k},\mathbf{L}\boldsymbol{k}}_{\mathrm{solv}} = \Delta E^{\mathbf{L}\boldsymbol{k},\mathbf{L}\boldsymbol{k}}_{\mathrm{gas}} + \left(\Delta G^{\mathrm{Er}}_{\mathrm{solv}} + \Delta G^{\mathrm{Er}(\mathbf{L}\boldsymbol{k})_2}_{\mathrm{solv}}\right) - 2\Delta G^{\mathrm{Er}\mathbf{L}\boldsymbol{k}}_{\mathrm{solv}} \quad \text{(A2-2)}$$

a) Intrinsic affinity

$$\begin{array}{ccc} \mathrm{Er}^{3+}_{(\mathrm{gas})} + \mathbf{L}\boldsymbol{k}_{(\mathrm{gas})} & \overset{\Delta G^{\mathrm{Er},\mathbf{L}\boldsymbol{k}}_{\mathrm{affinity,gas}}}{\rightleftharpoons} & [\mathrm{Er}(\mathbf{L}\boldsymbol{k})]^{3+}_{(\mathrm{gas})} \\ \Big\updownarrow \Delta G^{\mathrm{Er}}_{\mathrm{solv}} \quad \Big\updownarrow \Delta G^{\mathbf{L}\boldsymbol{k}}_{\mathrm{solv}} & & \Big\updownarrow \Delta G^{\mathrm{Er}\mathbf{L}\boldsymbol{k}}_{\mathrm{solv}} \\ [\mathrm{Er}]^{3+}_{(\mathrm{solv})} + \mathbf{L}\boldsymbol{k}_{(\mathrm{solv})} & \underset{\Delta G^{\mathrm{Er},\mathbf{L}\boldsymbol{k}}_{\mathrm{affinity,solv}}}{\rightleftharpoons} & [\mathrm{Er}(\mathbf{L}\boldsymbol{k})]^{3+}_{(\mathrm{solv})} \end{array}$$

b) Interligand interaction

$$\begin{array}{ccc} 2[\mathrm{Er}(\mathbf{L}\boldsymbol{k})]^{3+}_{(\mathrm{gas})} & \overset{\Delta E^{\mathbf{L}\boldsymbol{k},\mathbf{L}\boldsymbol{k}}_{\mathrm{gas}}}{\rightleftharpoons} & \mathrm{Er}^{3+}_{(\mathrm{gas})} + [\mathrm{Er}(\mathbf{L}\boldsymbol{k})_2]^{3+}_{(\mathrm{gas})} \\ \Big\updownarrow \Delta G^{\mathrm{Er}\mathbf{L}\boldsymbol{k}}_{\mathrm{solv}} & & \Big\updownarrow \Delta G^{\mathrm{Er}}_{\mathrm{solv}} \quad \Big\updownarrow \Delta G^{\mathrm{Er}(\mathbf{L}\boldsymbol{k})_2}_{\mathrm{solv}} \\ 2[\mathrm{Er}(\mathbf{L}\boldsymbol{k})]^{3+}_{(\mathrm{solv})} & \underset{\Delta E^{\mathbf{L}\boldsymbol{k},\mathbf{L}\boldsymbol{k}}_{\mathrm{solv}}}{\rightleftharpoons} & \mathrm{Er}^{3+}_{(\mathrm{solv})} + [\mathrm{Er}(\mathbf{L}\boldsymbol{k})_2]^{3+}_{(\mathrm{solv})} \end{array}$$

Scheme A2-1. Thermodynamic cycles used for rationalizing a) intrinsic Er-ligand **L*k*** affinities and b) interligand interactions.

The various solvation energies can be roughly estimated with the help of Born Eq. (A2-3),[A2-2] which is adapted for spherical ions of R_i radii and bearing z charges, and of Onsager Eq. (A2-4),[A2-3] which stands for neutral pseudo-spherical dipolar molecules possessing R_{vdw} van der Waals radii and μ dipole moments ($N_{Av} = 6.023 \cdot 10^{23}$ mol^{-1} is Avogadro's number, $e = 1.602 \cdot 10^{-19}$ C is the elementary charge, $\varepsilon_0 = 8.859 \cdot 10^{-12}$ C$^2 \cdot$N$^{-1} \cdot$m^{-2} is the vacuum permittivity, ε_r is the relative dielectric permittivity).

$$\Delta G^{0}_{\text{solv}} = -\frac{z^2 e^2 N_{\text{av}}}{8\pi\varepsilon_0 R_{\text{i}}} \cdot \left(1 - \frac{1}{\varepsilon_{\text{r}}}\right) \quad \text{(A2-3)}$$

$$\Delta G^{0}_{\text{solv}} = -\frac{\mu^2 N_{\text{av}}}{4\pi\varepsilon_0 \left(R_{\text{vdw}}\right)^3} \cdot \left(\frac{\varepsilon_{\text{r}} - 1}{2\varepsilon_{\text{r}} + 1}\right) \quad \text{(A2-4)}$$

Let's start with intrinsic affinities $\Delta G^{\text{Er,L}\boldsymbol{k}}_{\text{affinity,solv}}$ modeled with Eq. (A2-1). Since the solvation energies of neutral dipolar molecules (Eq. (A2-4)) are several orders of magnitude smaller than those obtained for charged objects of similar size (Eq. (A2-3)),[A2-4] $\left|\Delta G^{\mathbf{L}\boldsymbol{k}}_{\text{solv}}\right|$ is largely dominated by $\left|\Delta G^{\text{ErL}\boldsymbol{k}}_{\text{solv}}\right|$ in Eq. (A2-1) and the stepwise increase in size accompanying the connection of alkyl groups along the series R=H (**L4** or **L7**) < R=CH_3 (**L5** or **L8**) < R=CH_2CH_3 (**L6** or **L9**) gradually limits the favorable contribution of $\Delta G^{\text{ErL}\boldsymbol{k}}_{\text{solv}}$ to $\Delta G^{\text{Er,L}\boldsymbol{k}}_{\text{affinity,solv}}$ (Eq. (A2-1)). This effect is leveled out by the inductive effects which boost the affinity of **L*k***$_{(\text{gas})}$ for $Er^{3+}{}_{(\text{gas})}$, and makes $\Delta G^{\text{Er,L}\boldsymbol{k}}_{\text{affinity,gas}}$ more negative along the H < methyl < ethyl series. Considering the two latter opposite contributions, the effect of $\left|\Delta G^{\text{ErL}\boldsymbol{k}}_{\text{solv}}\right|$ is magnified for the small ligands and it dominates the trend for the terpy series. The loss in solvation along **L7→L8→L9** therefore reduces their affinities for Er(III), and $\Delta G^{\text{Er,L}\boldsymbol{k}}_{\text{affinity,solv}}$ becomes less negative (left part of Figure 5a). For the larger ligands of the bisbzimpy series, the solvation energies are significantly reduced and the inductive effect dominates. Consequently, $\Delta G^{\text{Er,L}\boldsymbol{k}}_{\text{affinity,gas}}$ and $\Delta G^{\text{Er,L}\boldsymbol{k}}_{\text{affinity,solv}}$ concomitantly become more negative along **L4→L5→L6** (right part of Figure 5a).

The analysis of interligand interactions $\Delta E^{\mathbf{L}\boldsymbol{k},\mathbf{L}\boldsymbol{k}}_{\text{solv}}$ modeled with Eq. (A2-2) follows the same strategy with the initial neglect of weak dipole-dipole interactions responsible for $\Delta E^{\mathbf{L}\boldsymbol{k},\mathbf{L}\boldsymbol{k}}_{\text{gas}}$,[A2-4] which leaves $\Delta G^{\text{Er(L}\boldsymbol{k}\text{)}_2}_{\text{solv}} - 2\Delta G^{\text{ErL}\boldsymbol{k}}_{\text{solv}}$ as the dominant variable contributions upon successive alkyl substitution. Introducing Born Eq. (A2-3) into Eq. (A2-2) gives

$$\Delta G^{\text{Er(L}\boldsymbol{k}\text{)}_2}_{\text{solv}} - 2\Delta G^{\text{ErL}\boldsymbol{k}}_{\text{solv}} = -\frac{z^2 e^2 N_{\text{av}}}{8\pi\varepsilon_0} \cdot \left(1 - \frac{1}{\varepsilon_{\text{r}}}\right)\left(\frac{1}{R^{\text{Er(L}\boldsymbol{k}\text{)}_2}} - \frac{1}{R^{\text{Er(L}\boldsymbol{k}\text{)}}}\right) > 0 \quad \text{(A2-5)}$$

The latter positive contribution ($R^{\mathrm{Er}(\mathbf{Lk})_2} > R^{\mathrm{Er}(\mathbf{Lk})}$) is maximized for small ligands and we therefore predict that $\Delta E_{\mathrm{solv}}^{\mathbf{Lk},\mathbf{Lk}}$ decreases when the molecular volume increases (**L7** > **L8** > **L9** > **L4** > **L5** > **L6**). This trend is experimentally detected for the first four members of the series (left part of Figure 5b), but **L5** and **L6** significantly deviate from the rule (right part of Figure 5b). This noticeable discrepancy is diagnostic for the operation of unusually strong repulsive and destabilizing interligand interactions in the triple-stranded helix $[\mathrm{Er}(\mathbf{L5})_3]^{3+}$ (methyl substituted), but especially in $[\mathrm{Er}(\mathbf{L6})_3]^{3+}$ where the ethyl substituents are known (see Appendix 1) to prevent interaromatic packing. To conclude, the thermodynamic stabilities of the $[\mathrm{Er}(\mathbf{Lk})_n]^{3+}$ (n = 1-3) complexes in acetonitrile are globally comparable for all six ligands, while minor variations along the series can be rationalized by a fine balance between inductive effect and size-dependent solvation energies. Specific inter-strand interactions can be highlighted in $[\mathrm{Er}(\mathbf{L5})_3]^{3+}$ and $[\mathrm{Er}(\mathbf{L6})_3]^{3+}$ when three bulky extended aromatic ligands are wrapped around small Er^{3+}.

References

[A2-1] a) C. J. Cramer, D. G. Truhlar, *Acc. Chem. Res.* **2008**, *41*, 760-768; b) S. A. Cotton, P. R. Raithby, *Coord. Chem. Rev.* **2017**, *340*, 220-231; c) G. Schreckenbach, *Chem. Eur. J.* **2017**, *23*, 3797-3803.

[A2-2] a) M. Born, *Zeit. Phys.* **1920**, *1*, 45-48; b) R. H. Stokes, *J. Phys. Chem.* **1964**, *86*, 979-982; c) P. W. Atkins, A. J. MacDermott, *J. Chem. Educ.* **1982**, *59*, 359-360; d) T. Abe, *Bull. Chem. Soc. Jpn* **1991**, *64*, 3035-3038.

[A2-3] a) L. Onsager, *J. Am. Chem. Soc.* **1936**, *58*, 1486-1492; b) D. V. Matyushov, *J. Chem. Phys.* **2004**, *120*, 1375-1382; c) L. E. Johnson, S. J. Benight, R. Barnes, B. H. Robinson, *J. Phys. Chem. B* **2015**, *119*, 5240-5250.

[A2-4] L. Babel, T. N. Y. Hoang, L. Guénée, C. Besnard, T. A. Wesolowski, M. Humbert-Droz, C. Piguet, *Chem. Eur. J.* **2016**, *22*, 8113-8123.

Appendix 3: Experimental section

Chemicals were purchased from Fluka AG, Aldrich or Acros and used without further purification unless otherwise stated. $Er(ClO_4)_3{\cdot}xH_2O$ and $Er(CF_3SO_3)_3{\cdot}xH_2O$ were prepared from the corresponding oxides (Aldrich, 99.99%).[S1] The Ln content of solid salts was determined by complexometric titrations with Titriplex III (Merck) in the presence of urotropine and xylene orange.[S2] The synthesis of $[Er(NCCH_3)_8][Al(OC(CF_3)_3)_4]$[49] was carried out with rigorous exclusion of air and water. Dry glove box or Schlenk techniques were employed, using purified nitrogen or argon (H_2O and O_2 < 1 ppm). Acetonitrile, dichloromethane and hexane were distilled over calcium hydride. Toluene and tetrahydrofuran were distilled under nitrogen over sodium.

Caution! *Dry perchlorates may explode and should be handled in small quantities and with the necessary precautions.*[S3]

Preparation of 2,6-bis(1′-methyl-benzimidazol-2′-yl)pyridine (L4). 2,6-bis(2-benzimidazolyl-2-yl)pyridine (2.0 g, 6.42 mmol, 1 eq)[S4] in DMF (60 mL) was slowly added to a suspension of NaH (0.5 g, 13.48 mmol, 2.1 eq) in DMF (40 mL) at rt. After 30 min, methyl iodide (0.82 mL, 1.9 g, 13.16 mmol, 2.05 eq) was added dropwise. The mixture was stirred at rt for 16 h and then quenched with ethanol (1.0 mL). Water (30 mL) was added and the crude product was extracted with ethyl acetate (3×100 mL). The combined organic phases were dried over anhydrous Na_2SO_4, filtered, and evaporated to dryness. The residue was purified by crystallization in hot acetonitrile to give white crystals of **L4** (1.8 g, yield: 82%). Mp: 192 °C. ^{1}H NMR (CD_3CN; 400 MHz), δ/ppm: 4.30 (s, 6H), 7.33-7.43 (m, 4H), 7.62 (d, ^3J = 8.0 Hz, 2H), 7.79 (d, ^3J = 8.0 Hz, 2H), 8.14 (t, ^3J = 8.0 Hz, 1H), 8.42 (d, ^3J = 8.0 Hz, 2H). Elem. analyses calcd for $C_{21}H_{17}N_5$: C 74.32, H 5.05, N 20.63; found C 74.80, H 5.46, N 19.78. ESI-MS ($CHCl_3$, soft positive mode): *m*/*z* 340.1 ($[M+H]^+$), 362.4 ($[M+Na]^+$), 679.5 ($[2M+H]^+$), 701.5 ($[2M+Na]^+$).

Preparation of 4-(*N*-methylamino)-3-nitrotoluene (5b). 4-Bromo-3-nitrotoluene (**1**, 10.0 g, 46.29 mmol, 1 eq) and methylamine (33% in methanol, 14.3 mL, 463.00 mmol, 10 eq) were heated at 130

°C for 24 h in an autoclave. The mixture was evaporated to dryness and the residual red oil shaken with concentrated hydrochloric acid (75 mL). The organic phase was separated, extracted with concentrated hydrochloric acid (3×30 mL) and the combined aqueous phases were neutralized (pH 9) with aqueous NaOH (5 M). The resulting solution was extracted with dichloromethane (3×300 mL) and the combined organic phases were dried over anhydrous Na_2SO_4, filtered, and evaporated to dryness. The residue was purified by crystallization in hot hexane to give orange crystals of **5b** (6.4 g, yield: 83%). ^{1}H NMR ($CDCl_3$; 400 MHz), δ/ppm: 2.30 (s, 3H), 3.04 (s, 3H), 6.79 (d, ^3J = 8.0 Hz, 1H), 7.32 (d, ^3J = 8.0 Hz, 1H), 8.01 (s, 1H). ESI-MS ($CHCl_3$, soft positive mode): *m*/*z* 167.1 ($[M+H]^+$)

Preparation of bis[*N*-methyl-*N*-(4′-methyl-2′-nitrophenyl)]-pyridine-2,6-dicarboxamide (8b). Pyridine-2,6-dicarboxylic acid (**6**, 1.0 g, 6.0 mmol, 1 eq) and DMF (100 μL) were refluxed in thionyl chloride (18 mL, 240 mmol, 40 eq) for 2 h. Excess thionyl chloride was distilled from the reaction mixture, which was then co-evaporated with dry CH_2Cl_2 (3 × 20 mL) and dried under vacuum. The solid was re-dissolved in freshly distilled CH_2Cl_2 (50 mL) and slowly added to a solution of 4-(*N*-methylamino)-3-nitrotoluene (**5b**, 2.1 g, 12.6 mmol, 2.1 eq) in CH_2Cl_2 (100 mL). The resulting mixture was refluxed for 24 h and the pH value was kept close to pH 9 by adding small amounts of *N,N*-diisopropylethylamine. The mixture was partitioned between CH_2Cl_2 (120 mL) and half-saturated aqueous NH_4Cl (60 mL). The organic phase was separated and the aqueous phase was further extracted with CH_2Cl_2 (2 × 150 mL). The combined organic phases were dried with anhydrous Na_2SO_4, filtered, and evaporated to dryness. The crude product was purified by column chromatography (Silicagel; CH_2Cl_2/Hexane, 30:70→100:0) to give **8b** as a yellow powder (2.6 g, yield: 92%). 1H NMR ($CDCl_3$; 400 MHz), δ/ppm: 2.19-2.50 (m, 6H, aryl CH_3), 3.19-3.52 (m, 6H, CH_3), 7.10-7.88 (m, 9H, aromatic). ESI-MS ($CHCl_3$, soft positive mode): *m*/*z* 464.0 ($[M+H]^+$).

Preparation of 2,6-bis(1′-methyl-5′-methylbenzimidazol-2′-yl)pyridine (L5). Compound **8b** (2.5 g, 5.48 mmol, 1 eq) was dissolved in ethanol-water (4:1, 600 mL). Activated iron powder (9.18 g, 164.4 mmol, 30 eq) and concentrated hydrochloric acid (37%, 15.3 mL, 180 mmol) were added and the mixture refluxed for 20 h. Water (100 mL) was then added, excess of iron filtered off and ethanol

was evaporated. The resulting mixture was poured into CH_2Cl_2 (100 mL), $Na_2(H_2edta)\cdot 2H_2O$ (H_4edta = N,N,N′,N′-ethylenediaminetetraacetic acid; 24.8 g, 66.7 mmol, 12.1 eq) dissolved in water (100 mL) was added and the resulting stirred mixture neutralized (pH > 9) with aqueous NH_4OH (12%). Concentrated hydrogen peroxide (30%, 10 mL) was added cautiously under vigorous stirring. After 15 min, the organic phase was separated and the aqueous phase extracted with CH_2Cl_2 (2 × 200 mL). The combined organic phases were dried over anhydrous Na_2SO_4, filtered, and evaporated to dryness. The residue was purified by crystallization in hot acetonitrile to give pale yellow crystals of **L5** (1.8 g, yield: 90%). Mp: 212 °C. ^{1}H NMR ($CDCl_3$; 400 MHz), δ/ppm: 2.55 (s, 6H), 4.24 (s, 6H), 7.22 (d, ^3J = 8.0 Hz, 2H), 7.36 (d, ^3J = 8.0 Hz, 2H), 7.67 (s, 2H), 8.05 (t, ^3J = 8.0 Hz, 1H), 8.41 (d, ^3J = 8.0 Hz, 2H). ^{13}C NMR ($CDCl_3$; 101 MHz), δ/ppm: 21.65 (2 CH_3), 32.53 (2 CH_3), 109.43 (2 CH), 119.86 (2 CH), 125.09 (2 CH), 125.23 (2 CH), 132.57 (2 C_{quat}), 135.36 (2 C_{quat}), 137.97 (CH), 142.92 (2 C_{quat}), 149.64 (2 C_{quat}), 150.14 (2 C_{quat}). Elem. analyses calcd for $C_{23}H_{21}N_5$: C 75.18, H 5.76, N 19.06; found C 74.78, H 5.73, N 19.03. ESI-MS ($CHCl_3$, soft positive mode): m/z 368.0 ($[M+H]^+$), 735.3 ($[2M+H]^+$).

Preparation of 1-(4-bromo-3-nitrophenyl)ethanol (3). Sodium borohydride (1.3 g, 33.8 mmol, 1.5 eq) was slowly added to a stirred solution of 4-bromo-3-nitroacetophenone (5.5 g, 22.54 mmol, 1 eq) in methanol (150 mL) at 0 °C, and the mixture was allowed to warm to rt. After stirring for 1 h. The reaction mixture was evaporated to dryness and water (50 mL) was added and the aqueous phase was extracted with ethyl acetate (2 × 100 mL). The combined organic phases were washed with brine and dried over anhydrous Na_2SO_4, filtered, and evaporated to dryness. The crude product was purified by column chromatography (Silicagel; CH_2Cl_2/methanol, 99:1) to give **3** as a pale yellow powder (5.4 g, yield: 97%). ^{1}H NMR ($CDCl_3$; 400 MHz), δ/ppm: 1.535 (d, ^3J = 4.0, 3H), 2.00 (s, br, OH), 4.98 (q, ^3J = 8.0 Hz, 1H), 7.46 (d, ^3J = 8.0 Hz, 1H), 7.72 (d, ^3J = 8.0 Hz, 1H), 7.89 (s, 1H). ESI-MS ($CHCl_3$, soft positive mode): m/z 246.4 ($[M+H]^+$).

Preparation of 1-bromo-4-ethyl-2-nitrobenzene (4). The crude alcohol **3** (5.4 g, 21.88 mmol, 1 eq) was dissolved in CH_2Cl_2 (150 mL). Triphenylphosphine (8.6 g, 32.82 mmol, 1.5 eq) and imidazole

(2.24 g, 32.94 mmol, 1.5 eq) were then added and the mixture was cooled to 0 °C. Molecular iodine (8.3 g, 32.70 mmol, 1.6 eq) was added, the cold bath was removed, and after stirring for 3 h, water (100 mL) was added. The organic phase was separated and the aqueous phase was extracted with CH_2Cl_2 (2 × 100 mL). The combined organic phases were washed with brine and dried over anhydrous Na_2SO_4, filtered, and evaporated to dryness and the crude product was dried at rt under high vacuum for 1.5 h. The product was then dissolved in DMSO (75 mL) and the solution was cooled to 0 °C. Sodium borohydride (1.7 g, 44.97 mmol, 2 eq) was slowly added, the reaction mixture was allowed to warm to rt and stirred for 30 min, and then cooled to 0 °C once more. Water (50 mL) was added and the mixture was extracted with ethyl acetate (3 × 50 mL). The combined organic phases were washed with brine and dried over anhydrous Na_2SO_4, filtered, and evaporated to dryness to afford the crude product as a yellow solid. This product was dissolved in a minimum volume of CH_2Cl_2 and then a mixture of hexane/Et_2O (1:1; 100 mL) was added. After gentle shaking, Ph_3PO started to precipitate. The mixture was then filtered through a silica pad, which was washed with Et_2O until no more product could be eluted, as monitored by TLC. This procedure removed most of the Ph_3PO formed as a byproduct. The eluent was collected and concentrated under reduced pressure, and the crude product was purified by column chromatography (Silicagel; hexane/ethyl acetate, 90:10) to give **4** (2.9 g, yield: 55%) as a yellow oil. ^{1}H NMR ($CDCl_3$; 400 MHz), δ/ppm: 1.29 (t, ^3J = 8.0, 3H), 2.72 (q, ^3J = 8.0 Hz, 2H), 7.29 (d, ^3J = 8.0 Hz, 1H), 7.65 (d, ^3J = 8.0 Hz, 1H), 7.70 (s, 1H). ESI-MS ($CHCl_3$, soft positive mode): *m*/*z* 230.3 ($[M+H]^+$).

Preparation of 4-ethyl-*N*-methyl-2-nitro-benzenamine (5c). Compound **4** (2.9 g, 12.5 mmol, 1 eq) and methylamine (33% in methanol, 20.0 mL, 161.1 mmol, 10 eq) were heated at 130 °C for 48 h in an autoclave. The mixture was evaporated to dryness and the residual red oil was shaken with concentrated hydrochloric acid (40 mL). The organic phase was separated, extracted with concentrated hydrochloric acid (3×40 mL) and the combined aqueous phases were neutralized (pH 9) with aqueous NaOH (5 M). The resulting solution was extracted with dichloromethane (3×100 mL) and the combined organic phases were dried over anhydrous Na_2SO_4, filtered, and evaporated

to dryness. The residue was purified by column chromatography (Silicagel; CH_2Cl_2/Hexane, 90:10) to give **5c** (2.2 g, yield: 99%). ^{1}H NMR ($CDCl_3$; 400 MHz), δ/ppm: 1.24 (t, ^3J = 8.0, 3H), 2.60 (q, ^3J = 8.0 Hz, 2H), 3.04 (s, 3H), 6.81 (d, ^3J = 12.0 Hz, 1H), 7.36 (d, ^3J = 8.0 Hz, 1H), 8.02 (s, 1H). ESI-MS ($CHCl_3$, soft positive mode): m/z 181.1 ($[M+H]^+$)

Preparation of bis[*N*-methyl-*N*-(4′-ethyl-2′-nitrophenyl)]-pyridine-2,6-dicarboxamide (8c). Pyridine-2,6-dicarboxylic acid (**6**, 1.0 g, 5.9 mmol, 1 eq) and DMF (100 μL) were refluxed in thionyl chloride (17.1 mL, 236.0 mmol, 40 eq) for 2 h. Excess thionyl chloride was distilled from the reaction mixture, which was then co-evaporated with dry CH_2Cl_2 (3 × 20 mL) and dried under vacuum. The solid was re-dissolved in freshly distilled CH_2Cl_2 (50 mL) and slowly added to a solution of 4-(*N*-methylamino)-3-nitrotoluene (**5c**, 2.2 g, 12.4 mmol, 2.1 eq) in CH_2Cl_2 (100 mL). The resulting mixture was heated to reflux for 24 h and the pH value was kept close to pH 9 by adding small amounts of *N,N*-diisopropylethylamine. The mixture was partitioned between CH_2Cl_2 (150 mL) and half-saturated aqueous NH_4Cl (60 mL). The organic phase was separated and the aqueous phase was further extracted with CH_2Cl_2 (2 × 150 mL). The combined organic phases were dried with anhydrous Na_2SO_4, filtered, and evaporated to dryness. The crude product was purified by column chromatography (Silicagel; CH_2Cl_2/methanol, 100: 0→98:2) to give **8c** (2.2 g, yield: 77%). 1H NMR ($CDCl_3$; 400 MHz), δ/ppm: 1.17-1.36 (m, 6H, aryl CH_3), 2.64-2.83 (m, 4H, aryl CH_2), 3.30-3.60 (m, 6H, CH_3), 7.10-7.89 (m, 9H, aromatic). ESI-MS ($CHCl_3$, soft positive mode): m/z 492.4 ($[M+H]^+$).

Preparation of 2,6-bis(1′-methyl-5′-ethylbenzimidazol-2′-yl)pyridine (L6). Compound **8c** (2.2 g, 4.48 mmol, 1 eq) was dissolved in ethanol-water (4:1, 600 mL). Activated iron powder (7.5 g, 134.4 mmol, 30 eq) and concentrated hydrochloric acid (37%, 13.0 mL, 147.8 mmol) were added and the mixture refluxed for 20 h. Water (100 mL) was then added, excess of iron filtered off and ethanol was evaporated. The resulting mixture was poured into CH_2Cl_2 (100 mL), $Na_2(H_2edta)\cdot 2H_2O$ (H_4edta = N,N,N′,N′-ethylenediaminetetraacetic acid, 20.1 g, 66.7 mmol, 12.1 eq) dissolved in water (100 mL) was added and the resulting stirred mixture was neutralized (pH > 9) with aqueous NH_4OH (12%). Concentrated hydrogen peroxide (30%, 10 mL) was added cautiously under vigorous stirring.

After 15 min, the organic phase was separated and the aqueous phase extracted with CH_2Cl_2 (2 × 200 mL). The combined organic phases were dried over anhydrous Na_2SO_4, filtered, and evaporated to dryness. The residue was purified by crystallization in hot acetonitrile to give pale orange needle crystals of L3 (0.9 g, yield: 50%). Mp: 169 °C. ^{1}H NMR ($CDCl_3$; 400 MHz), δ/ppm: 1.35 (t, ^3J = 8.0 Hz, 6H), 2.84 (q, ^3J = 8.0 Hz, 4H), 4.22 (s, 6H), 7.25 (d, ^3J = 8.0 Hz, 2H), 7.38 (d, ^3J = 8.0 Hz, 2H), 7.71 (s, 2H), 8.03 (t, ^3J = 8.0 Hz, 1H), 8.41 (d, ^3J = 8.0 Hz, 2H). ^{13}C NMR ($CDCl_3$; 101 MHz), δ/ppm: 16.32 (2 CH_3), 29.08 (2 CH_2), 32.50 (2 CH_3), 109.55 (2 CH), 118.63 (2 CH), 124.27 (2 CH), 125.06 (2 CH), 135.52 (2 C_{quat}), 137.94 (2 C_{quat}), 139.30 (CH), 142.92 (2 C_{quat}), 149.65 (2 C_{quat}), 150.14 (2 C_{quat}). Elem. analyses calcd for $C_{23}H_{21}N_5$: C 75.92, H 6.37, N 17.71; found C 75.41, H 6.34, N 17.49. ESI-MS ($CHCl_3$, soft positive mode): *m*/*z* 395.8 ($[M+H]^+$), 791.5 ($[2M+H]^+$).

Preparation of 2-bromo-5-methylpyridine (10). To a mechanically stirred mixture of HBr (48%, 40.4 mL, 357.1 mmol, 8 eq) and 2-amino-5-picoline (**9**, 10.0 g, 92.6 mmol, 1 eq), bromine (14.24 mL, 280.0 mmol, 3 eq) was added dropwise during 90 min at -5 °C. A 200 mL aqueous $NaNO_2$ solution (16.0 g, 231.0 mmol, 2.5 eq) was added dropwise during 2 h and the temperature was kept below 0 °C. The mixture was neutralized with aqueous NaOH while the temperature was kept below 0 °C, then warmed to rt and extracted with CH_2Cl_2 (2 × 200 mL). The combined organic phases were washed with aqueous $Na_2S_2O_3$ and dried over anhydrous Na_2SO_4, filtered, and evaporated to dryness. The crude product was purified by sublimation (40 °C, 0.05 mbar) to give **10** (8.1 g, yield: 50%) as a pale yellow crystals. ^{1}H NMR ($CDCl_3$; 400 MHz), δ/ppm: 2.49 (s, 3H), 7.74 (d, ^3J = 8.0 Hz, 1H), 7.89 (d, ^3J = 8.0 Hz, 1H), 8.52 (s, 1H). ESI-MS ($CHCl_3$, soft positive mode): *m*/*z* 172.4 and 174.4 ($[M+H]^+$).

Preparation of 5-methyl-2-tributylstannyl pyridine (11). A solution of 2-bromo-5-methylpyridine (**10**, 3.6 g, 20.84 mmol, 1 eq) in THF (90 mL) was cooled to -78 °C and *n*-BuLi (13.81 mL, 22.1 mmol, 1.06 eq) was added dropwise during 10 min. After stirring for 2 h at -78 °C, tributyltin chloride (7.9 g, 24.31 mmol, 1.1 eq) was added and the mixture was stirred for another 2 h at -78 °C. The mixture was allowed to warm to r.t. and then saturated aqueous NH_4Cl (40 mL) was added. The

resulting precipitate was dissolved by adding water, and the layers were separated. The aqueous layer was extracted with diethyl ether (3 × 100 mL). The combined organic phases were washed with brine and dried over anhydrous Na_2SO_4, filtered, and evaporated to dryness. The crude product was purified by column chromatography (Alumina; petroleum ether/ethyl acetate, 95: 5) to give **11** (6.7 g, yield: 83%) as a yellow oil. ^{1}H NMR ($CDCl_3$; 400 MHz), δ/ppm: 0.89 (t, ^3J = 8.0 Hz, 9H), 1.13 (t, ^3J = 8.0 Hz, 6H), 1.34 (tq, ^3J = 8.0 Hz, 6H), 1.58 (m, 6H), 2.29 (s, 3H), 7.31 (m, 2H), 8.61 (s, 1H). ESI-MS ($CHCl_3$, soft positive mode): *m*/*z* 384.5 ($[M+H]^+$), 326.1 ($[M-Bu]^+$), 268.3 ($[M-2Bu]^+$), 209.9 ($[M-3Bu]^+$).

Preparation of 5,5″-dimethyl-2,2′:6′,2″-terpyridine (L8). 2,6-Dibromopyridine (**14**, 1.9 g, 8.2 mmol, 1 eq), **11** (6.3 g, 16.5 mmol, 2.01 eq) and $Pd(PPh_3)_4$ (379 mg, 0.164 mmol, 0.04 eq) were heated in toluene (100 mL) for 16 h. After cooling to r.t, saturated NH_4Cl (40 mL) was added and the organic phase separated. The aqueous phase was extracted with toluene (3 × 50 mL). The combined organic phases were dried over anhydrous Na_2SO_4, filtered, and evaporated to dryness. Concentrated hydrochloric acid was added (30 mL) to the residue, and then washed with CH_2Cl_2 (3 × 200 mL). The aqueous phase was cautiously neutralized by solid sodium hydroxide. The aqueous phase was separated and extracted with CH_2Cl_2 (3 × 100 mL). The combined organic phases were dried with anhydrous Na_2SO_4, filtered, and evaporated to dryness. The crude product was purified by column chromatography (Silicagel; CH_2Cl_2/methanol, 100: 0→97:3) and crystallized in hot acetonitrile to give white needles of **L8** (1.4 g, yield: 51%). Mp: 174 °C. ^{1}H NMR ($CDCl_3$; 400 MHz), *δ*/ppm: 2.43 (s, 6H), 7.67 (d, ^3J = 8.0 Hz, 2H), 7.94 (t, ^3J = 8.0 Hz, 1H), 8.40 (d, ^3J = 8.0 Hz, 2H), 8.52 (d, ^3J = 8.0 Hz, 2H), 8.54 (s, 2H). ^{13}C NMR ($CDCl_3$; 101 MHz), *δ*/ppm: 18.42 (2 CH_3), 120.35 (2 CH), 120.69 (2 CH), 133.37 (2 C_{quat}), 137.34 (2 CH), 137.77 (CH), 149.54 (2 CH), 153.82 (2 C_{quat}), 155.40 (2 C_{quat}). Elem. analyses calcd for $C_{23}H_{21}N_5$: C 78.13, H 5.79, N 16.08; found C 77.70, H 5.76, N 15.96. ESI-MS ($CHCl_3$, soft positive mode): *m*/*z* 262.0 ($[M+H]^+$), 523.3 ($[2M+H]^+$).

Preparation of 5-ethyl-2-tributylstannyl pyridine (13). To a solution of 2-dimethylaminoethanol (6.5 g, 72.4 mmol, 3.1 eq) in hexane (15 mL) cooled at 0 °C, was added dropwise *n*-BuLi (1.6 M

solution in hexane, 90 mL, 144.7 mmol, 6.2 eq). After 15 min, a solution of 3-ethylpyridine (**12**, 2.5 g, 23.3 mmol, 1 eq) in hexane (15 mL) was added dropwise and the orange solution stirred for 1 h at 0 °C. After cooling at -78 °C, a solution of tributyltin chloride (28.5 g, 84.0 mmol, 3.6 eq) in THF (20 mL) was added dropwise. The reaction mixture was kept at -78 °C for 1 h and then allowed to warm to r.t. Hydrolysis at 0 °C with water (30 mL) was followed by extraction with diethyl ether (3 × 100 mL). The combined organic phases were dried with anhydrous Na_2SO_4, filtered, and the solvent was evaporated. The oily crude product was purified by Kugelrohr type distillation (150 °C, 1×10^{-3} Torr) to give **13** (4.7 g, yield: 51%) as a yellow oil. 1H NMR (DMSO-d_6; 400 MHz), δ/ppm: 0.84 (t, ^3J = 8.0 Hz, 9H), 1.05 (t, ^3J = 8.0 Hz, 6H), 1.18 (t, ^3J = 8.0 Hz, 3H) 1.28 (tq, ^3J = 8.0 Hz, 6H), 1.52 (m, 6H), 2.57 (q, ^3J = 8.0 Hz, 2H), 7.36 (d, ^3J = 8.0 Hz, 1H), 7.46 (d, ^3J = 8.0 Hz, 1H), 8.56 (s, 1H). ESI-MS ($CHCl_3$, soft positive mode): *m*/*z* 399.0 ($[M+H]^+$), 340.6 ($[M-Bu]^+$), 282.5 ($[M-2Bu]^+$), 226.6 ($[M-3Bu]^+$).

Preparation of 5,5″-diethyl-2,2′:6′,2″-terpyridine (L9). 2,6-Dibromopyridine (**14**, 1.3 g, 5.65 mmol, 1 eq), **13** (4.7 g, 11.9 mmol, 2.01 eq) and $Pd(PPh_3)_4$ (261 mg, 0.226 mmol, 0.04 eq) were heated in toluene (100 mL) for 16 h. After cooling to r.t, saturated NH_4Cl (40 mL) was added and the organic phase separated. The aqueous phase was extracted with toluene (3 × 50 mL). The combined organic phases were dried over anhydrous Na_2SO_4, filtered, and evaporated to dryness. Concentrated hydrochloric acid was added (30 mL) to the residue, and then washed with CH_2Cl_2 (3 × 200 mL). The aqueous phase was cautiously neutralized with solid sodium hydroxide. The aqueous phase was separated and extracted with CH_2Cl_2 (3 × 100 mL). The combined organic phases were dried with anhydrous Na_2SO_4, filtered, and evaporated to dryness. The crude product was purified by column chromatography (Silicagel; CH_2Cl_2/methanol, 100: 0→97:3) and crystalized in hot acetonitrile to give white needles of **L9** (0.8 g, yield: 49%). Mp: 94 °C. ^{1}H NMR ($CDCl_3$; 400 MHz), *δ*/ppm: 1.33 (t, ^3J = 8.0 Hz, 6H), 2.76 (q, ^3J = 8.0 Hz, 6H), 7.70 (d, ^3J = 8.0 Hz, 2H), 7.95 (t, ^3J = 8.0 Hz, 1H), 8.41 (d, ^3J = 8.0 Hz, 2H), 8.55 (d, ^3J = 8.0 Hz, 2H), 8.57 (s, 2H). ^{13}C NMR ($CDCl_3$; 101 MHz), *δ*/ppm: 15.36 (2 CH_3), 26.02 (2 CH_2), 120.37 (2 CH), 120.84 (2 CH), 136.18 (2 C_{quat}), 137.76 (2 CH), 139.58

(CH), 148.84 (2 CH), 154.08 (2 C_{quat}), 155.44 (2 C_{quat}). Elem. analyses calcd for $C_{23}H_{21}N_5$: C 78.86, H 6.62, N 14.52; found C 78.71, H 6.62, N 14.61. ESI-MS ($CHCl_3$, soft positive mode): *m*/*z* 290.8 ($[M+H]^+$), 313.8 ($[M+Na]^+$).

Preparation of $[Er(L4)_2(O_3SCF_3)_2](CF_3SO_3)$, $[Er(L7)_2(O_3SCF_3)_2](CF_3SO_3)$ and $Er(L8)_2(O_3SCF_3)_3$. Reaction **L*k*** (*k* = 3, 7 and 8, 3.0 eq) with $[Er(CF_3SO_3)_3]$ (1.0 eq) in acetonitrile followed by crystallization induced by slow diffusion of diethyl ether into a saturated acetonitrile solution of the complex provided crystals of $[Er(\mathbf{L4})_2(CF_3SO_3)_2](CF_3SO_3)\cdot 2CH_3CN$ (**1**), $[Er(\mathbf{L7})_2(CF_3SO_3)_2](CF_3SO_3)\cdot 1.5C_2H_5CN$ (**2**, recristallized from propionitrile), $[Er(\mathbf{L8})_2(CF_3SO_3)_3]$ (**3**) suitable for X-ray diffraction. Separation from the mother liquor followed by air drying gave satisfying elemental analysis for $[Er(\mathbf{L4})_2(O_3SCF_3)_2](CF_3SO_3)\ 0.4CH_3CN\cdot 1.2H_2O$ (calcd for C 41.29, H 2.85, N 10.93; found C 41.37, H 3.11, N 10.83), $[Er(\mathbf{L7})_2(CF_3SO_3)_2](CF_3SO_3)\cdot 0.6CH_3CN$ (calcd for C 37.12, H 2.18, N 8.41; found C 37.14, H 2.35, N 8.23; $[Er(\mathbf{L8})_2(CF_3SO_3)_3]$ (calcd for C 39.08, H 2.66, N 7.39; found C 38.87, H 2.61, N 7.26. ESI-MS (CH_3CN, positive mode) for: **1** *m*/*z* 1144.8 ($[Er(\mathbf{L4})_2(O_3SCF_3)_2]^+$), 498.2 ($[Er(\mathbf{L4})_2(O_3SCF_3)]^{2+}$), 395.3 ($[Er(\mathbf{L4})_3]^{3+}$), 340.5 ($[\mathbf{L4}+H]^+$), 282.1 ($[Er(\mathbf{L4})_2]^{3+}$); **2** *m*/*z* 931.7 ($[Er(\mathbf{L7})_2(O_3SCF_3)_2]^+$), 391.6 ($[Er(\mathbf{L7})_2(O_3SCF_3)]^{2+}$), 326.3 ($[Er(\mathbf{L7})_2(F)]^{2+}$), 346.4 ($[Er(\mathbf{L7})_2(F)(CH_3CN)]^{2+}$), 234.3 ($[\mathbf{L7}+H]^+$), 211.1 ($[Er(\mathbf{L7})_2]^{3+}$); **3** *m*/*z* 988.6 ($[Er(\mathbf{L8})_2(O_3SCF_3)_2]^+$), 419.2 ($[Er(\mathbf{L8})_2(O_3SCF_3)]^{2+}$), 374.3 ($[Er(\mathbf{L8})_2(F)(CH_3CN)]^{2+}$), 317.2 ($[Er(\mathbf{L8})_3]^{3+}$), 262.2 ($[\mathbf{L8}+H]^+$), 230.2 ($[Er(\mathbf{L8})_2]^{3+}$).

Preparation of $[Er(L\mathit{k})_3](ClO_4)_3$ (*k* = 6-9): Reaction **L*k*** (3.0 eq) with $[Er(ClO_4)_3]\cdot xH_2O$ (1.0 eq) in acetonitrile for **L7** and **L9**, or acetonitrile/propionitrile/dichloromethane for **L6** and **L9,** followed by crystallization induced by slow evaporation provided crystals of $[Er(\mathbf{L6})_3](ClO_4)_3\cdot 1.5CH_3CN$ (**4**), $[Er(\mathbf{L7})_3](ClO_4)_3$ (**5**), $[Er(\mathbf{L8})_3](ClO_4)_3$ (**6**), $[Er(\mathbf{L9})_3](ClO_4)_3\cdot 1.5CH_3CN$ (**7**) suitable for X-ray diffraction studies. Separation from the mother liquor followed by air drying gave satisfying elemental analysis for $[Er(\mathbf{L6})_3](ClO_4)_3\cdot 1.5CH_3CN$ calcd for: (calcd C 54.91, H 4.37, N 13.78; found C 54.55, H 4.86, N 13.52), $[Er(\mathbf{L7})_3](ClO_4)_3$ (calcd C 46.38, H 2.85, N 10.82; found C 46.38, H 2.88,

N 10.87), [Er(**L8**)$_3$](ClO$_4$)$_3$ (calcd C 49.02, H 3.63, N 10.09; found C 48.96, H 3.65, N 10.15) and [Er(**L9**)$_3$](ClO$_4$)$_3$·0.8CH$_3$CN·2.6H$_2$O (calcd C 49.02, H 4.50, N 9.57; found C 49.70, H 4.25, N 9.75. ESI-MS (CH$_3$CN, positive mode) for: **4** *m*/*z* 1552.98 ([Er(L3)$_3$(ClO$_4$)$_2$]$^+$), 726.51 ([Er(**L6**)$_3$(ClO$_4$)]$^{2+}$), 529.2 ([Er(**L6**)$_2$(ClO$_4$)]$^{2+}$), 451.88 ([Er(**L6**)$_3$]$^{3+}$); **5** *m*/*z* 832.3 ([Er(**L7**)$_2$(ClO$_4$)$_2$]$^+$), 366.6 ([Er(**L7**)$_2$(ClO$_4$)]$^{2+}$), 289.1 ([Er(**L7**)$_3$]$^{3+}$), 234.3 ([**L7**+H]$^+$); **6** *m*/*z* 888.5 ([Er(**L8**)$_2$(ClO$_4$)$_2$]$^+$), 394.7 ([Er(**L8**)$_2$(ClO$_4$)]$^{2+}$), 317.2 ([Er(**L8**)$_3$]$^{3+}$), 262.2 ([**L8**+H]$^+$); **7** *m*/*z* 944.7 ([Er(**L9**)$_2$(ClO$_4$)$_2$]$^+$), 423.0 ([Er(**L9**)$_2$(ClO$_4$)]$^{2+}$), 345.1 ([Er(**L9**)$_3$]$^{3+}$), 290.3 ([**L9**+H]$^+$).

Preparation of [(L*k*)$_2$Er(OH)$_2$Er(L*k*)$_2$](ClO$_4$)$_4$ (*k* = 4 and 5). Reaction of **L*k*** (3.0 eq) with [Er(ClO$_4$)$_3$]·*x*H$_2$O (1.0 eq) in a mixture of acetonitrile/ propionitrile/ benzonitrile (4:2:1) followed by crystallization induced by slow evaporation provided crystals of [(**L4**)$_2$Er(OH)$_2$Er(**L4**)$_2$](ClO$_4$)$_4$·2C$_6$H$_5$CN·4CH$_3$CN (**8**) and [(**L5**)$_2$Er(OH)$_2$Er(**L5**)$_2$](ClO$_4$)$_4$·C$_6$H$_5$CN ·7.5CH$_3$CN (**9**) suitable for X-ray diffraction studies. Separation from the mother liquor followed by air drying gave satisfying elemental analysis for [(**L4**)$_2$Er(OH)$_2$Er(**L4**)$_2$](ClO$_4$)$_4$ ·1.6CH$_3$CN·1.5C$_6$H$_5$CN (calcd C 50.01, H 3.51, N 13.79; found C 50.13, H 3.58, N 13.81) and [(**L5**)$_2$Er(OH)$_2$Er(**L5**)$_2$](ClO$_4$)$_4$·0.8CH$_3$CN·4.4C$_6$H$_5$CN (calcd C 54.83, H 4.05, N 12.96; found C 54.90, H 4.17, N 12.97. ESI-MS (CH$_3$CN, positive mode) for: **8** *m*/*z* 679.3 ([2**L4**+H]$^+$), 472.5 ([Er(**L4**)$_2$(ClO$_4$)]$^{2+}$), 395.0 ([Er(**L4**)$_3$]$^{3+}$), 431.5 ([Er(**L4**)$_2$(OH)]$^{2+}$), 340.3 ([**L4**+H]$^+$); **9** *m*/*z* 1019.1 ([(**L5**)$_2$Er(OH)$_2$Er(**L5**)$_2$(ClO$_4$)$_2$]$^{2+}$), 735.2 ([2**L5**+H]$^+$), 645.6 ([(**L5**)$_2$Er(OH)$_2$Er(**L5**)$_2$(ClO$_4$)]$^{3+}$), 500.7 ([Er(**L5**)$_2$(ClO$_4$)]$^{2+}$), 459.5 ([Er(**L5**)$_2$(OH)]$^{2+}$), 423.0 ([Er(**L5**)$_3$]$^{3+}$), 368.2 ([**L5**+H]$^+$).

Preparation of [(L4)$_2$Er(O(CH$_3$)NO)$_2$Er(L4)$_2$](ClO$_4$)$_6$. Reaction **L4** (3.0 eq) with [Er(ClO$_4$)$_3$]·*x*H$_2$O (1.0 eq) in a mixture of acetonitrile/ propionitrile/ nitromethane (2:2:1) followed by crystallization induced by slow evaporation provided crystals of [(**L4**)$_2$Er(CH$_3$NO$_2$)$_2$Er(**L4**)$_2$](ClO$_4$)$_6$·CH$_3$NO$_2$ (**10**) suitable for X-ray diffraction studies. Separation from the mother liquor followed by air drying gave satisfying elemental analysis for [(**L1**)$_2$Er(O(CH$_3$)NO)$_2$Er(**L1**)$_2$](ClO$_4$)$_6$·2.2C$_2$H$_5$CN (calcd C 43.88, H 3.36, N 13.38; found C 44.2,

H 3.23, N 13.30. ESI-MS (CH_3CN, positive mode) *m*/*z* 1004.6, 665.5, 451.9, 340.5 ([**L4**+H]$^+$), 282.5 ([Er(**L4**)$_2$]$^{3+}$), 170.8 ([**L4**+2H]$^{2+}$).

Preparation of K[Al(OC(CF$_3$)$_3$)$_4$].[S5] $LiAlH_4$ (purified by several successive extractions with dry diethyl ether and then dried at 80 °C under high vacuum, 1.5 g, 39.9 mmol, 1 eq) was suspended in dry toluene (100 mL). Perfluoro-tert-butanol (22.8 mL, 163.6 mmol, 4.1 eq) was added at 0 °C during 30 min. The reaction mixture was then stirred for 1 h at 0 °C and another 1 h at r.t. The mixture was heated to reflux overnight (use two reflux condensers). Cooling this solution for one hour to -20 °C led to the precipitation of a colorless powder. The supernatant solution was decanted and all the volatiles were removed (at least 1 h under high vacuum). The crude residue was carefully suspended in dry diethyl ether (60 mL) and a saturated aqueous KCl (60 mL) was added dropwise. The mixture was stirred vigorously for 2 h at r.t and then the organic phase separated. The aqueous phase was extracted with toluene (3 × 50 mL). The combined organic phases were washed by saturated aqueous KCl (40 mL) and evaporated to dryness. The residue was re-dissolved in diethyl ether and filtered. The filtrate was evaporated to dryness and the residue was exposed to high vacuum for at least 2 h to give K[Al(OC(CF$_3$)$_3$)$_4$] (18.1 g, yield: 45%) as a pale yellow powder.

Preparation of [Ag(NCCH$_3$)$_4$][Al(OC(CF$_3$)$_3$)$_4$].[S6] K[Al(OC(CF$_3$)$_3$)$_4$] (5.0 g, 5.0 mmol, 1 eq) and silver nitrate (844 mg, 4.7 mmol, 1 eq) were mixed in acetonitrile (40 mL) in the dark. The mixture was stirred for 20 min and then diethyl ether (40 mL) was added. The solvent and volatiles were removed in vacuum and the residue was dissolved in CH_2Cl_2 (40 mL) and filtered. The filtrate was evaporated to dryness and the residue was exposed to high vacuum for at least 2 h to give [Ag(NCCH$_3$)$_4$][Al(OC(CF$_3$)$_3$)$_4$] (3.0 g, yield: 49%) as a light sensitive off-white powder. ^{1}H NMR (CD_3CN; 400 MHz), *δ*/ppm: 1.99 (s, CH_3). ^{19}F NMR (CD_3CN; 376.5 MHz), *δ*/ppm: -76.01 (s). Elem. analyses calcd for [Ag(NCCH$_3$)$_4$][Al(OC(CF$_3$)$_3$)$_4$]·4.8CH_2Cl_2: C 23.26, H 0.98, N 4.52; found C 20.89, H 1.10, N 3.51.

Preparation of $[Er(NCCH_3)_8][Al(OC(CF_3)_3)_4]$.[49] Anhydrous $ErCl_3$ (137 mg, 0.5 mmol, 1 eq) and $[Ag(NCCH_3)_4][Al(OC(CF_3)_3)_4]$ (1.9 g, 1.55 mmol, 3.1 eq) were mixed in acetonitrile (50 mL) in the darkness at r.t. The reaction mixture was stirred for 10 min and the precipitate was allowed to settle down. After cautious filtration, the filtrate was evaporated to dryness under vacuum. The residue was washed several times with CH_2Cl_2 (7 × 15 mL), dried in vacuum to give $[Er(NCCH_3)_8][Al(OC(CF_3)_3)_4]$ (1.0 g, yield: 58%) as an off-white powder. ^1H NMR (CD_3CN; 400 MHz), *δ*/ppm: 1.99 (s, CH_3). 13C NMR ($CDCl_3$; 101 MHz), δ/ppm: 117.26 (CN). ^{19}F NMR (CD_3CN; 376.5 MHz), *δ*/ppm: -76.0 (s). Elem. analyses calcd for $[Er(NCCH_3)_8][Al(OC(CF_3)_3)_4]\cdot 19.9CH_2Cl_2\cdot 3.2CH_3CN$: C 20.77, H 1.42, N 3.00; found C 20.58, H 1.17, N 3.28.

Spectroscopic and analytical measurements

^1H, ^{19}F and ^{13}C NMR spectra were recorded at 293 K on Bruker Avance 400 MHz and Bruker DRX-300 MHz spectrometers. Chemical shifts are given in ppm with respect to TMS (^1H) or C_6F_6 (^{19}F). Spectrophotometric titrations were performed with a J&M diode array spectrometer (Tidas series) connected to an external computer. In a typical experiment, 20 cm^3 of ligand in acetonitrile (10^{-4} M) were titrated at 293 K with a solution of erbium salt (10^{-3} M) in acetonitrile under an inert atmosphere. After each addition of 0.1 mL, the absorbance was recorded using Hellma optrodes (optical path length 0.1 cm) immersed in the thermostated titration vessel and connected to the spectrometer. Mathematical treatment of the spectrophotometric titrations was performed with factor analysis[46] and with the SPECFIT program.[47] Pneumatically-assisted electrospray (ESIMS) mass spectra were recorded from 10^{-4} M (ligands) and 10^{-3} M (complexes) solutions on an Applied Biosystems API 150EX LC/MS System equipped with a Turbo Ionspray source. Elemental analyses were performed by K. L. Buchwalder from the Microchemical Laboratory of the University of Geneva. Electronic spectra in the UV-Vis region were recorded at 293 K from solutions in CH_3CN with a Perkin-Elmer Lambda 1050 using quartz cells of 0.1 or 1.0 mm path length. Solid-state diffuse reflectance spectra were recorded using UV/Vis/NIR Perkin-Elmer Lambda 900 in reflectance (*R*) mode fitted with an

integrating sphere. The pure or MgO-diluted samples were placed between two 1.0 mm path length quartz cells whose background cell was filled with pure MgO. The signal of pure MgO was used as the baseline. The spectra were then converted into absorbance using *Kubelka-Munk* function ($(1-R)^2/2R$). Solid-state luminescence data were collected on samples either mounted directly onto copper plates using conductive silver glue or placed in quartz suprasil certified capillaries and tubes. Solution emission spectra were recorded on CH_3CN solution sample of compounds using quartz suprasil certified tubes. Emission spectra were measured on a Horiba Scientific Fluorolog 3 spectrofluorimeter equipped with a visible photomultiplier tube (PMT) (220-850 nm, R928P or 185-1010 nm, R2658P; Hamamatsu). The infrared luminescence spectra were recorded either on a Horiba Scientific Fluorolog 3 spectrofluorimeter equipped with a NIR solid-state InGaAs detector cooled to 77 K (800-1600 nm, DSSIGA020L; Horiba Scientific), a NIR PMT (950-1650 nm, H10330-75; Hamamtsu) or a Bruker IFS 66/S spectrometer equipped with an InGaAs diode (780-1725 nm; D424). High resolution NIR emission spectra were recorded upon excitation with a 447 nm diode laser. The low temperature emission spectra were recorded using either a FL-1013 liquid nitrogen dewar Horiba Scientific Fluorolog 3 accessory or an optical closed-cycle cryostat capable of reaching low temperatures down to 5 K in an helium atmosphere (Oxford Instruments CCC1100T, or Sumitono SHI-950/Janis Research CCS-500/204). Luminescence lifetimes were determined under excitation at 355 nm provided by a Nd:YAG laser (YG 980; Quantel). Signals were detected with help of either a CCD detector (in the visible region) or a Hamamatsu H10330-75 PMT (in the NIR region). The output signals from the detectors were fed into a bandpass digital oscilloscope (TDS-724C or 754-C; Tektronix), transferred to a PC for data analysis. Appropriate filters were utilized to remove the laser light, the Rayleigh scattered light and associated harmonics from the emission spectra. Emission spectra were corrected for instrumental functions. Fluorescence lifetimes on the nanosecond timescale were measured using the time-correlated single-photon counting (TCSPC) technique. Excitation was performed at 320 nm at a repetition rate between 8.46 and 78.8 MHz with the output of the Extend-UV module of a picosecond pulsed SuperK Extreme supercontinuum laser (NKT

Photonics). Fluorescence was collected at 90° and focused into an optical fiber guiding the light to the entrance of a Horiba Triax 190 monochromator set at 380 nm (for L1-L3) or 370 nm (for L4-L6) with fully open slits. The fluorescence was then detected on a photomultiplier (PicoQuant PMA 192) connected to a TCSPC lifetime analysis module (PicoQuant PicoHarp 300). The full-width at half maximum of the instrument response function (IRF) was about 180 ps. All measurements were performed in a 1-cm quartz cell at a sample concentration of 10 μM in acetonitrile. The fluorescence decays were analysed by iterative reconvolution of a trial mono- or biexponential function with the measured IRF. The accuracy on the extracted lifetimes is about 0.1 ns.

X-ray crystallography

Summary of crystal data, intensity measurements and structure refinements for were collected in Tables S1, S14, S21, S31. The crystals were mounted on MiTeGen kapton cryoloops with protection oil. X-ray data collections were performed with an Agilent SuperNova Dual diffractometer equipped with a CCD Atlas detector (Cu[Kα] radiation). The structures were solved by using direct methods.[S8] Full-matrix least-square refinements on F^2 were performed with SHELX2014.[S8] CCDC 1834821-1834833 contains the supplementary crystallographic data. The cif files can be obtained free of charge via www.ccdc.cam.ac.uk/conts/retrieving.html (or from the Cambridge Crystallographic Data Centre, 12 Union Road, Cambridge CB2 1EZ, UK; fax: (+ 44) 1223-336-033; or deposit@ccdc.cam.ac.uk).

References

[S1] J. F. Desreux, in *Lanthanide Probes in Life, Chemical and Earth Sciences*; J.-C. G. Bünzli and G. R. Choppin, Eds., Elsevier: Amsterdam, 1989; chap. 2.

[S2] G. Schwarzenbach, *Complexometric Titrations*; Chapman & Hall: London, 1957 p. 8.

[S3] a) W. C. Wolsey, *J. Chem. Educ.* **1973**, *50*, A335-A337; b) J.-L. Pascal, F. Favier, *Coord. Chem. Rev.* **1998**, *178-180*, 865-902.

[S4] a) A. W. Addison, T. N. Rao, C. G. Wahlgren, *J. Heterocyl. Chem.* **1983**, *20*, 1481-1484; b) C. Piguet, B. Bocquet, E. Müller, A. F. Williams, *Helv. Chim. Acta* **1989**, *72*, 323-337.

[S5] I. Krossing, *Chem. Eur. J.* **2001**, *7*, 490-502.

[S6] Y. Li, F. E. Kühn, *J. Organomet. Chem.* **2008**, *693*, 2465-2467.

[S7] SHELXS97 G. M. Sheldrick, *Acta Crystallogr. A* **2008**, *64*, 112–122.

[S8] G. M. Sheldrick, *Acta Crystallogr. Sect. C Struct. Chem.* **2015**, *71*, 3–8.

Table S1 Summary of Crystal Data, Intensity Measurements and Structure Refinements for Ligands **L5**, **L6**, **L8** and **L9**.

	L5	**L6**	**L8**	**L9**
Empirical formula	C23H21N5	C25H25N5	C17H15N3	C19H19N3
Formula weight	367.45	395.50	261.32	289.37
Temperature	180(2) K	240(2)K	180(2)K	180(2)K
Wavelength	1.54184 Å	1.54184 Å	1.54184 Å	1.54184 Å
Crystal System, Space group	Monoclinic, $P2_1/c$	Monoclinic, $I2/a$	Monoclinic, $I2/a$	Monoclinic, $C2/c$
Unit cell dimensions	a = 14.0739(4) Å b = 7.0564(2) Å c = 18.7071(6) Å α = 90° β = 94.384(3)° γ = 90°	a = 8.4966(3) Å b = 12.8837(5) Å c = 19.7197(7) Å α = 90° β = 101.540(4)° γ = 90°	a = 17.0585(5) Å b = 6.47731(18) Å c = 24.6079(7) Å α = 90° β = 90.616(3)° γ = 90°	a = 15.2924(2) Å b = 6.48765(11) Å c = 31.7533(5) Å α = 90° β = 92.2110(14)° γ = 90°
Volume in Å^3	1852.38(11)	2115.03(13)	2718.86(14)	3147.96(9)
Z, Calculated density	4, 1.318 Mg/m^3	4, 1.242 Mg/m^3	8, 1.277 Mg/m^3	8, 1.221 Mg/m^3
Absorption coefficient	0.636 mm^{-1}	0.592 mm^{-1}	0.605 mm^{-1}	0.569 mm^{-1}
F(000)	776	840	1104	1232
Theta range for data collection	4.74 to 73.73°	4.577 to 73.10 °	3.59 to 73.25 °	5.58 to 73.37 °
Limiting indices	-14<=h<=17, -8<=k<=4, -23<=l<=21	-6<=h<=10, -15<=k<=11, -23<=l<=24	-20<=h<=9, -7<=k<=8, -30<=l<=29	-18<=h<=18, -7<=k<=7, -38<=l<=27
Reflections collected / unique	6561 / 3627 [R(int) = 0.0211]	3797 / 2061 [R(int) = 0.0191]	4941 / 2508 [R(int) = 0.0182]	5450 / 3066 [R(int) = 0.0153]
Completeness to theta	67.50°/ 99.8 %	67.50°/ 99.5%	67.50°/ 94.6 %	67.50°/ 99.8 %
Data / restraints / parameters	3627 / 0 / 258	2061 / 0 / 144	2508 / 0 / 184	3066 / 0 / 202
Goodness-of-fit on $F2$	1.033	1.063	1.037	1.077
Final R indices [$I>2\sigma(I)$]	$R1$ = 0.0407, $\omega R2$ = 0.1056	$R1$ = 0.0543, $\omega R2$ = 0.1497	$R1$ = 0.0423, $\omega R2$ = 0.1151	$R1$ = 0.0447, $\omega R2$ = 0.1226
R indices (all data)	$R1$ = 0.0499, $\omega R2$ = 0.1129	$R1$ = 0.0627, $\omega R2$ = 0.1597	$R1$ = 0.0525, $\omega R2$ = 0.1235	$R1$ = 0.0503, $\omega R2$ = 0.1279
Largest diff. peak and hole	0.236 and -0.188 e·Å^{-3}	0.201 and -0.205 e·Å^{-3}	0.193 and -0.158 e·Å^{-3}	0.217 and -0.218 e·Å^{-3}

Table S2 Selected bond distances (Å) and bond angles (°) for ligand **L4**.[39]

Bond distances (Å)

Atom 1	Atom 2	Distance	Atom 1	Atom 2	Distance
C(1)	N(1)	1.341(2)	C(5)	N(1)	1.347(2)
C(6)	N(2)	1.323(2)	C(7)	N(2)	1.392(2)
C(6)	N(3)	1.375(2)	C(12)	N(3)	1.378(2)
C(13)	N(3)	1.459(2)	C(14)	N(4)	1.327(2)
C(15)	N(4)	1.387(2)	C(14)	N(5)	1.381(2)
C(20)	N(5)	1.379(2)	C(21)	N(5)	1.463(2)
C(1)	C(2)	1.397(3)	C(1)	C(14)	1.437(2)
C(2)	C(3)	1.375(3)	C(3)	C(4)	1.383(3)
C(4)	C(5)	1.389(3)	C(5)	C(6)	1.475(2)
C(7)	C(8)	1.396(3)	C(7)	C(12)	1.401(3)
C(8)	C(9)	1.382(3)	C(9)	C(10)	1.401(3)
C(10)	C(11)	1.378(3)	C(11)	C(12)	1.400(3)
C(15)	C(16)	1.400(3)	C(15)	C(20)	1.401(3)
C(16)	C(17)	1.382(3)	C(17)	C(18)	1.398(3)
C(18)	C(19)	1.375(3)	C(19)	C(20)	1.395(3)

Angles (°)

At. 1	At. 2	At. 3	Angle	At. 1	At. 2	At. 3	Angle
C(1)	N(1)	C(5)	118.0(1)	C(6)	N(2)	C(7)	104.6(1)
C(6)	N(3)	C(12)	106.6(1)	C(6)	N(3)	C(13)	129.7(2)
C(12)	N(3)	C(13)	123.4(2)	C(14)	N(4)	C(15)	105.2(1)
C(14)	N(5)	C(20)	106.4(1)	C(14)	N(5)	C(21)	131.4(1)
C(20)	N(5)	C(1)	122.2(1)	N(1)	C(1)	C(2)	122.3(2)
N(6)	C(1)	C(14)	118.4(1)	C(2)	C(1)	C(14)	119.3(2)
C(1)	C(2)	C(3)	119.0(2)	C(2)	C(3)	C(4)	119.3(2)
C(3)	C(4)	C(5)	118.5(2)	N(1)	C(5)	C(4)	122.8(2)
N(1)	C(5)	C(6)	116.9(1)	C(4)	C(5)	C(6)	120.3(2)
N(2)	C(6)	N(3)	113.1(1)	N(2)	C(6)	C(5)	123.1(1)
N(3)	C(6)	C(5)	123.7(2)	N(2)	C(7)	C(8)	130.4(2)
N(2)	C(7)	C(12)	110.0(2)	C(8)	C(7)	C(12)	119.4(2)
C(7)	C(8)	C(9)	118.3(2)	C(8)	C(9)	C(10)	121.5(2)
C(9)	C(10)	C(11)	121.4(2)	C(10)	C(11)	C(12)	116.6(2)
N(3)	C(12)	C(7)	105.7(1)	N(3)	C(12)	C(11)	131.5(2)
C(7)	C(12)	C(11)	122.7(2)	N(4)	C(14)	N(5)	112.6(1)
N(4)	C(14)	C(1)	122.0(1)	N(5)	C(14)	C(1)	125.4(1)
N(4)	C(15)	C(16)	130.5(2)	N(4)	C(15)	C(20)	109.8(2)
C(16)	C(15)	C(20)	119.6(2)	C(15)	C(16)	C(17)	117.7(2)
C(16)	C(17)	C(18)	121.8(2)	C(17)	C(18)	C(19)	121.5(2)
C(18)	C(19)	C(20)	116.8(2)	N(5)	C(20)	C(15)	106.1(1)
N(5)	C(20)	C(19)	131.3(2)	C(15)	C(20)	C(19)	122.6(2)

Table S3 Selected least-squares planes data for ligand **L4**.

Least-squares planes

Least-squares planes description	Abbreviation	Max. deviation/Å	Atom
Benzimidazole 1 C(7) C(8) C(9) C(10) C(11) C(12) N(3) C(6) N(2)	Bz1	0.046	C(13)
Pyridine N(1) C(1) C(2) C(3) C(4) C(5)	Py	0.025	C(7)
Benzimidazole 2 C(15) C(16) C(17) C(18) C(19) C(20) N(5) C(14) N(4)	Bz2	0.019	N(6)

Interplanar angles (°)

	Bz1	Py	Bz2
Bz1		36.80(6)	42.75(5)
Py			7.11(6)
Bz2			

Table S4 Selected bond distances (Å) and bond angles (°) for ligand **L5**.

Bond distances (Å)

Atom 1	Atom 2	Distance	Atom 1	Atom 2	Distance
C(9)	N(1)	1.3220(19)	C(3)	C(5)	1.411(2)
C (1)	N(1)	1.3818(18)	C(3)	C(4)	1.508(2)
C (9)	N(2)	1.3744(18)	C(5)	C(6)	1.380(2)
C(7)	N(2)	1.3779(18)	C(6)	C(7)	1.3997(19)
C(8)	N(2)	1.4574(18)	C(9)	C(10)	1.4790(18)
C(10)	N(3)	1.3430(18)	C(10)	C(11)	1.3931(19)
C(14)	N(3)	1.3443(17)	C(11)	C(12)	1.382(2)
C(15)	N(4)	1.3247(17)	C(12)	C(13)	1.384(2)
C(16)	N(4)	1.3830(19)	C(14)	C(15)	1.473(2)
C(15)	N(5)	1.3727(17)	C(16)	C(17)	1.400(2)
C(22)	N(5)	1.3797(18)	C(17)	C(18)	1.380(2)
C(23)	N(5)	1.4569(16)	C(18)	C(20)	1.410(2)
C(1)	C(7)	1.397(2)	C(18)	C(19)	1.510(2)
C(1)	C(2)	1.400(2)	C(20)	C(21)	1.383(2)
C(2)	C(3)	1.387(2)	C(21)	C(22)	1.393(2)

Angles (°)

At. 1	At. 2	At. 3	Angle	At. 1	At. 2	At. 3	Angle
C(9)	N(1)	C(1)	104.96(12)	N(3)	C(10)	C(11)	123.14(13)
C(9)	N(2)	C(7)	105.83(11)	N(3)	C(10)	C(9)	119.51(12)
C(9)	N(2)	C(8)	130.80(12)	C(11)	C(10)	C(9)	117.34(13)
C(7)	N(2)	C(8)	123.37(12)	C(12)	C(11)	C(10)	118.57(13)
C(10)	N(3)	C(14)	117.37(12)	C(11)	C(12)	C(13)	119.30(13)
C(15)	N(4)	C(16)	104.90(11)	C(12)	C(13)	C(14)	118.36(13)
C(15)	N(5)	C(22)	106.44(11)	N(3)	C(14)	C(13)	123.25(13)
C(15)	N(5)	C(23)	129.07(12)	N(3)	C(14)	C(15)	118.43(12)
C(22)	N(5)	C(23)	124.37(12)	C(13)	C(14)	C(15)	118.31(12)
N(1)	C(1)	C(7)	109.76(12)	N(4)	C(15)	N(5)	112.95(12)
N(1)	C(1)	C(2)	129.94(13)	N(4)	C(15)	C(14)	122.00(12)
C(7)	C(1)	C(2)	120.30(13)	N(5)	C(15)	C(14)	125.04(12)
C(3)	C(2)	C(1)	118.51(14)	N(4)	C(16)	C(17)	130.19(13)
C(2)	C(3)	C(5)	119.79(14)	N(4)	C(16)	C(22)	110.04(12)
C(2)	C(3)	C(4)	120.50(15)	C(17)	C(16)	C(22)	119.77(14)
C(5)	C(3)	C(4)	119.71(14)	C(18)	C(17)	C(16)	119.22(14)
C(6)	C(5)	C(3)	122.91(13)	C(17)	C(18)	C(20)	119.59(14)
C(5)	C(6)	C(7)	116.26(14)	C(17)	C(18)	C(19)	120.56(15)
N(2)	C(7)	C(1)	106.29(12)	C(20)	C(18)	C(19)	119.84(15)
N(2)	C(7)	C(6)	131.47(14)	C(21)	C(20)	C(18)	122.61(14)
C(1)	C(7)	C(6)	122.23(13)	C(20)	C(21)	C(22)	116.74(14)
N(1)	C(9)	N(2)	113.16(12)	N(5)	C(22)	C(21)	132.26(13)
N(1)	C(9)	C(10)	120.72(13)	N(5)	C(22)	C(16)	105.67(12)
N(2)	C(9)	C(10)	126.11(12)	C(21)	C(22)	C(16)	122.07(13)

Table S5 Selected least-squares planes data for ligand **L5**.

Least-squares planes

Least-squares planes description	Abbreviation	Max. deviation/Å	Atom
Benzimidazole 1 C(1) C(2) C(3) C(5) C(6) C(7) N(2) C(9) N(1)	Bz1	0.012	N(2)
Pyridine N(3) C(10) C(11) C(12) C(13) C(14)	Py	0.003	C(11)
Benzimidazole 2 C(16) C(17) C(18) C(20) C(21) C(22) N(5) C(15) N(4)	Bz2	0.006	C(16) C(22)

Interplanar angles (°)

	Bz1	Py	Bz2
Bz1		13.25(4)	34.72(4)
Py			25.54(4)
Bz2			

Table S6 Selected bond distances (Å) and bond angles (°) for ligand **L6**.

Bond distances (Å)

Atom 1	Atom 2	Distance	Atom 1	Atom 2	Distance
N(1)	C(4)	1.317(2)	C(3)#1	C(4)#1	1.476(2)
N(1)#1	C(4)#1	1.317(2)	C(5)	C(6)	1.394(2)
N(1)	C(5)	1.379(2)	C(5)#1	C(6)#1	1.394(2)
N(1)#1	C(5)#1	1.379(2)	C(5)	C(12)	1.397(2)
N(2)	C(4)	1.376(2)	C(5)#1	C(12)#1	1.397(2)
N(2)#1	C(4)#1	1.376(2)	C(6)	C(7)	1.379(2)
N(2)	C(12)	1.378(2)	C(6)#1	C(7)#1	1.379(2)
N(2)#1	C(12)#1	1.378(2)	C(7)	C(10)	1.408(3)
N(2)	C(13)	1.456(2)	C(7)#1	C(10)#1	1.408(3)
N(2)#1	C(13)#1	1.456(2)	C(8)	C(9B)	1.476(19)
N(3)	C(3)	1.3381(19)	C(8)#1	C(9B)#1	1.476(19)
N(3)	C(3)#1	1.3381(19)	C(8)	C(9A)	1.488(4)
C(1)	C(2)	1.370(2)	C(8)#1	C(9A)#1	1.488(4)
C(1)	C(2)#1	1.370(2)	C(10)	C(11)	1.381(3)
C(2)	C(3)	1.397(2)	C(10)#	C(11)#1	1.381(3)
C(2)#1	C(3)#1	1.397(2)	C(11)	C(12)	1.395(2)
C(3)	C(4)	1.476(2)	C(11)#1	C(12)#1	1.395(2)

Symmetry operation #1 $-x+1/2,y,-z+2$

Angles (°)

At. 1	At. 2	At. 3	Angle	At. 1	At. 2	At. 3	Angle
C(4)	N(1)	C(5)	105.48(14)	N(1)#1	C(5)#1	C(12)#1	109.71(15)
C(4)#1	N(1)#1	C(5)#1	105.48(14)	C(6)	C(5)	C(12)	119.83(15)
C(4)	N(2)	C(12)	106.14(13)	C(6)#1	C(5)#1	C(12)#1	119.83(15)
C(4)#1	N(2)#1	C(12)#1	106.14(13)	C(7)	C(6)	C(5)	119.55(17)
C(4)	N(2)	C(13)	129.96(14)	C(7)#1	C(6)#1	C(5)#1	119.55(17)
C(4)	N(2)	C(13)	129.96(14)	C(6)	C(7)	C(10)	119.59(17)
C(12)	N(2)	C(13)	123.85(14)	C(6)#1	C(7)#1	C(10)#1	119.59(17)
C(12)	N(2)	C(13)	123.85(14)	C(6)	C(7)	C(8)	120.27(17)
C(3)#1	N(3)	C(3)	117.78(19)	C(6)#1	C(7)#1	C(8)#1	120.27(17)
C(2)	C(1)	C(2)#1	119.5(2)	C(10)	C(7)	C(8)	120.13(17)
C(1)	C(2)	C(3)	118.66(18)	C(10)#1	C(7)#1	C(8)#1	120.13(17)
C(1)	C(2)#1	C(3)#1	118.66(18)	C(9B)	C(8)	C(9A)	49.0(8)
N(3)	C(3)	C(2)	122.67(16)	C(9B)#1	C(8)#1	C(9A)#1	49.0(8)
N(3)	C(3)#1	C(2)#1	122.67(16)	C(9B)	C(8)	C(7)	117.4(6)
N(3)	C(3)	C(4)	120.94(15)	C(9B)#1	C(8)#1	C(7)#1	117.4(6)
N(3)	C(3)#1	C(4)#1	120.94(15)	C(9A)	C(8)	C(7)	113.60(19)
C(2)	C(3)	C(4)	116.39(15)	C(9A)#1	C(8)#1	C(7)#1	113.60(19)
C(2)#1	C(3)#1	C(4)#1	116.39(15)	C(11)	C(10)	C(7)	122.13(17)
N(1)	C(4)	N(2)	112.67(14)	C(11)#1	C(10)#1	C(7)#1	122.13(17)
N(1)#1	C(4)#1	N(2)#1	112.67(14)	C(10)	C(11)	C(12)	117.20(17)
N(1)	C(4)	C(3)	120.64(15)	C(10)#1	C(11)#1	C(12)#1	117.20(17)
N(1)#1	C(4)#1	C(3)#1	120.64(15)	N(2)	C(12)	C(11)	132.30(16)
N(2)	C(4)	C(3)	126.69(14)	N(2)#1	C(12)#1	C(11)#1	132.30(16)
N(2)#1	C(4)#	C(3)#1	126.69(14)	N(2)	C(12)	C(5)	105.99(14)
N(1)	C(5)	C(6)	130.46(16)	N(2)#1	C(12)#1	C(5)#1	105.99(14)
N(1)#1	C(5)#1	C(6)#1	130.46(16)	C(11)	C(12)	C(5)	121.71(16)
N(1)	C(5)	C(12)	109.71(15)	C(11)#1	C(12)#1	C(5)#1	121.71(16)

Symmetry operation #1 $-x+1/2,y,-z+2$

Table S7 Selected least-squares planes data for ligand **L6**.

Least-Squares Planes

Least-squares planes description	Abbreviation	Max. deviation/Å	Atom
Benzimidazole 1 C(5) C(6) C(7) C(10) C(11) C(12) N(2) C(4) N(1)	Bz1	0.006	C(4)
Pyridine N(3) C(1) C(2) C(3) C(2)#1 C(3)#1	Py	0.003	C(2), C(3), C(2)#1, C(3)#1
Benzimidazole 2 C(5)#1 C(6)#1 C(7)#1 C(10)#1 C(11)#1 C(12)#1 N(2)#1 C(4)#1 N(1)#1	Bz2	0.006	C(7)#1

Interplanar angles (°)

	Bz1	Py	Bz2
Bz1		10.09(4)	18.48(6)
Py			10.09(4)
Bz2			

Table S8 Selected bond distances (Å) and bond angles (°) for ligand **L7**.[40]

Bond distances (Å)

Atom 1	Atom 2	Distance	Atom 1	Atom 2	Distance
C(1)	N(1)	1.317(7)	C(5)	N(1)	1.339(9)
C(1)	C(2)	1.349(8)	C(1)	C(6)	1.488(8)
C(2)	C(3)	1.388(9)	C(3)	C(4)	1.351(10)
C(4)	C(5)	1.391(10)	C(6)	N(2)	1.353(8)
C(10)	N(2)	1.349(7)	C(6)	C(7)	1.398(9)
C(7)	C(8)	1.376(9)	C(8)	C(9)	1.380(9)
C(9)	C(10)	1.396(8)	C(10)	C(11)	1.439(8)
C(11)	N(3)	1.350(8)	C(15)	N(3)	1.344(9)
C(11)	C(12)	1.391(9)	C(12)	C(13)	1.386(9)
C(13)	C(14)	1.366(10)	C(14)	C(15)	1.360(10)

Angles (°)

At. 1	At. 2	At. 3	Angle	At. 1	At. 2	At. 3	Angle
C(1)	N(1)	C(5)	118.4(5)	N(1)	C(1)	C(2)	123.3(5)
N(1)	C(1)	C(6)	116.1(5)	C(2)	C(1)	C(6)	120.5 (5)
C(1)	C(2)	C(3)	118.2(6)	C(2)	C(3)	C(4)	120.1(6)
C(3)	C(4)	C(5)	117.8(6)	N(1)	C(5)	C(4)	122.0(6)
C(6)	N(2)	C(10)	117.5(5)	C(1)	C(6)	N(2)	117.3(5)
C(1)	C(6)	C(7)	120.2(5)	N(2)	C(6)	C(7)	122.5(5)
C(6)	C(7)	C(8)	119.6(6)	C(7)	C(8)	C(9)	118.2(6)
C(8)	C(9)	C(10)	120.0(5)	N(2)	C(10)	C(9)	122.3(5)
N(2)	C(10)	C(11)	116.7(5)	C(9)	C(10)	C(11)	121.1(5)
C(11)	N(3)	C(15)	115.4(5)	C(10)	C(11)	N(3)	114.8(5)
C(10)	C(11)	C(12)	121.7(5)	N(3)	C(11)	C(12)	123.5(5)
C(11)	C(12)	C(13)	118.7(6)	C(12)	C(13)	C(14)	118.0(6)
C(13)	C(14)	C(15)	119.8(6)	N(3)	C(15)	C(14)	124.4(6)

Table S9 Selected least-squares planes data for ligand **L7**.

Least-squares planes

Least-squares planes description	Abbreviation	Max. deviation/Å	Atom
Pyridine 1 C(1) C(2) C(3) C(4) C(5) N(1)	Py1	0.023	C(4)
Pyridine 2 C(6) C(7) C(8) C(9) C(10) N(2)	Py2	0.012	C(6)
Pyridine 3 C(11) C(12) C(13) C(14) C(15) N(3)	Py3	0.027	C(14)

Interplanar angles (°)

	Py1	Py2	Py3
Py1		5.1(2)	7.2(8)
Py2			7.10(11)
Py3			

Table S10 Selected bond distances (Å) and bond angles (°) for ligand **L8**.

Bond distances (Å)

Atom 1	Atom 2	Distance	Atom 1	Atom 2	Distance
N(1)	C(1)	1.3357(19)	C(6)	C(7)	1.4857(18)
N(1)	C(6)	1.3423(16)	C(7)	C(8)	1.3944(19)
N(2)	C(11)	1.3403(16)	C(8)	C(9)	1.380(2)
N(2)	C(7)	1.3426(16)	C(9)	C(10)	1.3832(19)
N(3)	C(17)	1.3349(18)	C(10)	C(11)	1.3969(19)
N(3)	C(12)	1.3422(17)	C(11)	C(12)	1.4897(18)
C(1)	C(2)	1.385(2)	C(12)	C(13)	1.3949(19)
C(2)	C(4)	1.387(2)	C(13)	C(14)	1.3848(18)
C(2)	C(3)	1.503(2)	C(14)	C(15)	1.387(2)
C(4)	C(5)	1.3826(19)	C(15)	C(17)	1.394(2)
C(5)	C(6)	1.394(2)	C(15)	C(16)	1.5076(19)

Angles (°)

At. 1	At. 2	At. 3	angle	At. 1	At. 2	At. 3	angle
C(1)	N(1)	C(6)	117.44(13)	C(9)	C(8)	C(7)	119.04(12)
C(11)	N(2)	C(7)	118.14(11)	C(8)	C(9)	C(10)	119.04(13)
C(17)	N(3)	C(12)	117.81(12)	C(9)	C(10)	C(11)	118.63(13)
N(1)	C(1)	C(2)	125.04(13)	N(2)	C(11)	C(10)	122.71(12)
C(1)	C(2)	C(4)	116.56(13)	N(2)	C(11)	C(12)	116.82(11)
C(1)	C(2)	C(3)	121.72(14)	C(10)	C(11)	C(12)	120.47(12)
C(4)	C(2)	C(3)	121.72(15)	N(3)	C(12)	C(13)	121.97(12)
C(5)	C(4)	C(2)	119.96(14)	N(3)	C(12)	C(11)	116.84(12)
C(4)	C(5)	C(6)	118.98(12)	C(13)	C(12)	C(11)	121.19(12)
N(1)	C(6)	C(5)	122.01(12)	C(14)	C(13)	C(12)	118.99(12)
N(1)	C(6)	C(7)	116.72(12)	C(13)	C(14)	C(15)	119.96(13)
C(5)	C(6)	C(7)	121.26(11)	C(14)	C(15)	C(17)	116.61(12)
N(2)	C(7)	C(8)	122.43(12)	C(14)	C(15)	C(16)	122.34(14)
N(2)	C(7)	C(6)	117.14(11)	C(17)	C(15)	C(16)	121.05(13)
C(8)	C(7)	C(6)	120.42(12)	N(3)	C(17)	C(15)	124.66(13)

Table S11 Selected least-squares planes data for ligand **L8**.

Least-squares planes

Least-squares planes description	Abbreviation	Max. deviation/Å	Atom
Pyridine 1 C(1) C(2) C(4) C(5) C(6) N(1)	Py1	0.004	C(5), C(6)
Pyridine 2 C(7) C(8) C(9) C(10) C(11) N(2)	Py2	0.006	N(2)
Pyridine 3 C(12) C(13) C(14) C(15) C(17) N(3)	Py3	0.006	C(14), C(15)

Interplanar angles (°)

	Py1	Py2	Py3
Py1		9.79(5)	11.26(5)
Py2			8.49(5)
Py3			

Table S12 Selected bond distances (Å) and bond angles (°) for ligand **L9**.

Bond distances (Å)

Atom 1	Atom 2	Distance	Atom 1	Atom 2	Distance
N(1)	C(7)	1.3331(18)	C(6)	C(8)	1.4901(17)
N(1)	C(6)	1.3436(15)	C(8)	C(9)	1.3908(19)
N(2)	C(12)	1.3410(16)	C(9)	C(10)	1.3822(19)
N(2)	C(8)	1.3423(15)	C(10)	C(11)	1.3857(18)
N(3)	C(17)	1.3387(17)	C(11)	C(12)	1.3935(19)
N(3)	C(13)	1.3394(16)	C(12)	C(13)	1.4872(17)
C(1)	C(2)	1.495(2)	C(13)	C(14)	1.388(2)
C(2)	C(3)	1.5078(18)	C(14)	C(15)	1.3792(19)
C(3)	C(4)	1.3852(19)	C(15)	C(16)	1.3877(19)
C(3)	C(7)	1.389(2)	C(16)	C(17)	1.387(2)
C(4)	C(5)	1.3845(19)	C(16)	C(18)	1.5062(17)
C(5)	C(6)	1.3901(19)	C(18)	C(19)	1.498(2)

Angles (°)

At. 1	At. 2	At. 3	angle	At. 1	At. 2	At. 3	angle
C(7)	N(1)	C(6)	117.55(12)	C(10)	C(9)	C(8)	118.63(12)
C(12)	N(2)	C(8)	118.25(11)	C(9)	C(10)	C(11)	119.26(12)
C(17)	N(3)	C(13)	117.19(12)	C(10)	C(11)	C(12)	118.59(12)
C(1)	C(2)	C(3)	113.37(13)	N(2)	C(12)	C(11)	122.54(11)
C(4)	C(3)	C(7)	116.38(12)	N(2)	C(12)	C(13)	116.57(12)
C(4)	C(3)	C(2)	122.39(14)	C(11)	C(12)	C(13)	120.89(11)
C(7)	C(3)	C(2)	121.22(12)	N(3)	C(13)	C(12)	117.05(12)
C(5)	C(4)	C(3)	120.05(14)	C(14)	C(13)	C(12)	121.02(11)
C(4)	C(5)	C(6)	119.02(12)	C(15)	C(14)	C(13)	119.73(12)
N(1)	C(6)	C(5)	121.97(12)	C(14)	C(15)	C(16)	119.48(13)
N(1)	C(6)	C(8)	116.68(12)	C(17)	C(16)	C(15)	116.47(12)
C(5)	C(6)	C(8)	121.36(11)	C(17)	C(16)	C(18)	121.87(13)
N(1)	C(7)	C(3)	125.04(12)	C(15)	C(16)	C(18)	121.66(14)
N(2)	C(8)	C(9)	122.69(11)	N(3)	C(17)	C(16)	125.17(12)
N(2)	C(8)	C(6)	116.50(11)	C(19)	C(18)	C(16)	113.02(12)
C(9)	C(8)	C(6)	120.81(11)				

Table S13 Selected least-squares planes data for ligand **L9**.

Least-squares planes

Least-squares planes description	Abbreviation	Max. deviation/Å	Atom
Pyridine 1 C(3) C(4) C(5) C(6) C(7) N(1)	Py1	0.005	C(3)
Pyridine 2 C(8) C(9) C(10) C(11) C(12) N(2)	Py2	0.011	C(9), C(12)
Pyridine 3 C(13) C(14) C(15) C(16) C(17) N(3)	Py3	0.012	C(15)

Interplanar angles (°)

	Py1	Py2	Py3
Py1		4.03(4)	20.84(5)
Py2			20.25(5)
Py3			

Table S14 Summary of crystal data, intensity measurements and structure refinements for complexes $[Er(\mathbf{L4})_2(CF_3SO_3)_2](CF_3SO_3)\cdot 2CH_3CN$ (**1**), $[Er(\mathbf{L7})_2(CF_3SO_3)_2](CF_3SO_3)\cdot 1.5C_2H_5CN$ (**2**) and $[Er(\mathbf{L8})_2(CF_3SO_3)_3]$ (**3**).

	$[Er(\mathbf{L4})_2(O_3SCF_3)_2](CF_3SO_3)$	$[Er(\mathbf{L7})_2(O_3SCF_3)_2](CF_3SO_3)$	$Er(\mathbf{L8})_2(O_3SCF_3)_3$
Empirical formula	$C_{49}H_{40}ErF_9N_{12}O_9S_3$	$C_{37.5}H_{29.5}ErF_9N_{7.5}O_9S_3$	$C_{37}H_{30}ErF_9N_6O_9S_3$
Formula weight	1375.37	1163.63	1137.11
Temperature	180(2)K	180(2)K	180(2)K
Wavelength	1.54184 Å	1.54184 Å	1.54184 Å
Crystal System, Space group	Triclinic, *P* -1	Orthorhombic, *P nnm*	Triclinic, *P* -1
Unit cell dimensions	*a* = 11.6161(3) Å *b* = 15.2976(4) Å *c* = 16.1008(4) Å α = 87.341(2)° β = 75.733(3)° γ = 72.947(3)°	*a* = 11.5807(2) Å *b* = 14.2430(3) Å *c* = 27.0122(5) Å α = 90° β = 90° γ = 90°	*a* = 11.5993(7) Å *b* = 11.7864(6) Å *c* = 15.9722(9) Å α = 87.379(5)° β = 88.132(5)° γ = 76.233(5)°
Volume in Å^3	2649.90(13)	4455.52(14)	2118.2(2)
Z, Calculated density	2, 1.724 Mg/m^3	4, 1.735 Mg/m^3	2, 1.783 Mg/m^3
Absorption coefficient	4.931 mm^{-1}	5.702 mm^{-1}	5.969 mm^{-1}
F(000)	1374	2304	1126
Theta range for data collection	3.02 to 73.68 °	3.27 to 73.51°	3.86 to 73.69 °
Limiting indices	-14<=*h*<=9, -18<=*k*<=18, -20<=*l*<=19	-12<=*h*<=13, -11<=*k*<=17, -33<=*l*<=29	-12<=*h*<=14, -13<=*k*<=14, -18<=*l*<=19
Reflections collected / unique	17866 / 10348 [*R*(int) = 0.0245]	10914 / 4476 [*R*(int) = 0.0344]	14024 / 8244 [*R*(int) = 0.0213]
Completeness to theta	67.50°/ 99.9 %	67.50°/ 99.9 %	67.50°/ 99.8 %
Data / restraints / parameters	10348 / 0 / 754	4476 / 0 / 282	8244 / 0 / 590
Goodness-of-fit on F^2	1.037	1.037	1.050
Final *R* indices [$I>2\sigma(I)$]	R_1 = 0.0277, ωR_2 = 0.0703	R_1 = 0.0378, ωR_2 = 0.0981	R_1 = 0.0264, ωR_2 = 0.0690
R indices (all data)	R_1 = 0.0318, ωR_2 = 0.0739	R_1 = 0.0430, ωR_2 = 0.1027	R_1 = 0.0274, ωR_2 = 0.0698
Largest diff. peak and hole	0.739 and -0.710 e.Å^{-3}	0.625 and -1.499 e·Å^{-3}	0.609 and -1.093 e.Å^{-3}

Table S15 Selected bond distances (Å) and bond angles (°) for complex [Er(**L4**)$_2$(O$_3$SCF$_3$)$_2$](CF$_3$SO$_3$) (**1**).

Bond distances (Å)

Atom 1	Atom 2	Distance	Atom 1	Atom 2	Distance
Er(1)	O(1)	2.285(2)	Er(1)	N(4)	2.447(2)
Er(1)	O(4)	2.329(2)	Er(1)	N(3)	2.479(2)
Er(1)	N(1)	2.414(2)	Er(1)	N(8)	2.489(2)
Er(1)	N(9)	2.446(2)	Er(1)	N(6)	2.498(2)

Angles (°)

At. 1	At. 2	At. 3	angle	At. 1	At. 2	At. 3	angle
O(1)	Er(1)	O(4)	128.62(6)	N(4)	Er(1)	N(3)	65.62(6)
O(1)	Er(1)	N(1)	75.41(6)	O(1)	Er(1)	N(8)	76.23(6)
O(4)	Er(1)	N(1)	77.24(6)	O(4)	Er(1)	N(8)	128.69(6)
O(1)	Er(1)	N(9)	76.64(7)	N(1)	Er(1)	N(8)	150.30(6)
O(4)	Er(1)	N(9)	77.12(6)	N(9)	Er(1)	N(8)	65.64(6)
N(1)	Er(1)	N(9)	115.37(6)	N(4)	Er(1)	N(8)	75.53(6)
O(1)	Er(1)	N(4)	149.58(6)	N(3)	Er(1)	N(8)	127.96(6)
O(4)	Er(1)	N(4)	78.93(8)	O(1)	Er(1)	N(6)	80.41(6)
N(1)	Er(1)	N(4)	129.54(6)	O(4)	Er(1)	N(6)	147.93(6)
N(9)	Er(1)	N(4)	101.50(7)	N(1)	Er(1)	N(6)	101.63(6)
O(1)	Er(1)	N(3)	127.01(6)	N(9)	Er(1)	N(6)	128.97(6)
O(4)	Er(1)	N(3)	76.77(6)	N(4)	Er(1)	N(6)	77.59(6)
N(1)	Er(1)	N(3)	65.94(6)	N(3)	Er(1)	N(6)	73.78(6)
N(9)	Er(1)	N(3)	152.70(6)	N(8)	Er(1)	N(6)	64.89(6)

Table S16 Selected least-squares planes data for complex $[Er(\mathbf{L4})_2(O_3SCF_3)_2](CF_3SO_3)$ (**1**).

Least-squares planes

Least-squares planes description	Abbreviation	Max. deviation/Å	Atom
Pyridine 1 N(3) C(9) C(10) C(11) C(12) C(13)	Py1	0.027	C(9)
Benzimidazole 1 C(1) C(2) C(3) C(4) C(5) C(6) N(1) C(8) N(2)	Bz1	0.018	C(3), C(1)
Benzimidazole 2 C(16) C(17) C(18) C(19) C(20) C(21) N(4) C(14) N(5)	Bz2	0.030	C(14)
Pyridine 2 N(8) C(30) C(31) C(32) C(33) C(34)	Py2	0.015	C(34)
Benzimidazole 3 C(22) C(23) C(24) C(25) C(26) C(27) N(6) C(29) N(7)	Bz3	0.042	N(6)
Benzimidazole 4 C(37) C(38) C(39) C(40) C(41) C(42) N(9) C(35) N(10)	Bz4	0.020	N(10)

Interplanar angles (°)

	Py1	Bz1	Bz2	Py2	Bz3	Bz4
Py1		16.143(1)	16.86(1)	43.991(1)	28.487(1)	44.020(1)
Bz1			25.715(1)	35.595(1)	30.941(1)	29.623(1)
Bz2				35.744(1)	13.590(1)	43.873(1)
Py2					24.645(1)	19.579(1)
Bz3						37.907(1)
Bz4						

Table S17 Selected bond distances (Å), bond angles (°) for complex [Er(**L7**)$_2$(O$_3$SCF$_3$)$_2$](CF$_3$SO$_3$) (**2**).

Bond distances (Å)

Atom 1	Atom 2	Distance	Atom 1	Atom 2	Distance
Er(1)	O(1)	2.264(2)	Er(1)	N(3)#1	2.479(3)
Er(1)	O(1)#1	2.264(2)	Er(1)	N(3)	2.479(3)
Er(1)	N(2)#1	2.476(2)	Er(1)	N(1)	2.519(3)
Er(1)	N(2)	2.476(2)	Er(1)	N(1)#1	2.519(3)

Symmetry operation (#1) -x,-y+1,z

Angles (°)

At. 1	At. 2	At. 3	Angle	At. 1	At. 2	At. 3	Angle
O(1)	Er(1)	O(1)#1	105.76(12)	N(3)#1	Er(1)	N(3)	92.10(12)
O(1)	Er(1)	N(2)#1	135.03(9)	O(1)	Er(1)	N(1)	76.22(9)
O(1)#1	Er(1)	N(2)#1	83.97(8)	O(1)#1	Er(1)	N(1)	75.03(9)
O(1)	Er(1)	N(2)	83.97(8)	N(2)#1	Er(1)	N(1)	146.89(9)
O(1)#1	Er(1)	N(2)	135.04(8)	N(2)	Er(1)	N(1)	64.73(8)
N(2)#1	Er(1)	N(2)	120.12(11)	N(3)#1	Er(1)	N(1)	87.68(9)
O(1)	Er(1)	N(3)#1	157.06(8)	N(3)	Er(1)	N(1)	127.71(8)
O(1)#1	Er(1)	N(3)#1	85.22(9)	O(1)	Er(1)	N(1)#1	75.03(9)
N(2)#1	Er(1)	N(3)#1	65.00(8)	O(1)#1	Er(1)	N(1)#1	76.22(9)
N(2)	Er(1)	N(3)#1	74.33(8)	N(2)#1	Er(1)	N(1)#1	64.73(8)
O(1)	Er(1)	N(3)	85.22(9)	N(2)	Er(1)	N(1)#1	146.89(9)
O(1)#1	Er(1)	N(3)	157.06(8)	N(3)#1	Er(1)	N(1)#1	127.71(8)
N(2)#1	Er(1)	N(3)	74.33(8)	N(3)	Er(1)	N(1)#1	87.68(9)
N(2)	Er(1)	N(3)	65.00(8)	N(1)	Er(1)	N(1)#1	131.41(12)

Table S18 Selected least-squares planes data for complex [Er(**L7**)$_2$(O$_3$SCF$_3$)$_2$](CF$_3$SO$_3$) (**2**).

Least-squares planes

Least-squares planes description	Abbreviation	Max. deviation/Å	Atom
Pyridine 1	Py1		
N(1) C(1) C(2) C(3) C(4) C(5)		0.004	N(1), C(3)
Pyridine 2	Py2		
N(2) C(6) C(7) C(8) C(9) C(10)		0.032	N(2)
Pyridine 3	Py3		
N(3) C(11) C(12) C(13) C(14) C(15)		0.009	N(3)
Pyridine 1#1	Py1#1		
N(1)#1 C(1)#1 C(2)#1 C(3)#1 C(4)#1 C(5)#1		0.004	N(1), C(3)
Pyridine 2#1	Py2#1		
N(2)#1 C(6)#1 C(7)#1 C(8)#1 C(9)#1 C(10)#1		0.032	N(2)
Pyridine 3#1	Py3#1		
N(3)#1 C(11)#1 C(12)# C(13)#1 C(14)#1 C(15)#1		0.009	N(3)

Interplanar angles (°)

	Py1	Py2	Py3	Py1#1	Py2#1	Py3#1
Py1		21.29(11)	31.24(11)	44.52(15)	48.07(12)	65.87(11)
Py2			17.81(11)	48.07(12)	40.72(16)	57.16(11)
Py3				65.87(11)	57.16(11)	72.16(17)
Py1#1					21.29(11)	31.24(11)
Py2#1						17.81(11)
Py3#1						

Table S19 Selected bond distances (Å), bond angles (°) for complex Er(**L8**)$_2$(O_3SCF_3)$_3$ (**3**)

Bond distances (Å)

Atom 1	Atom 2	Distance	Atom 1	Atom 2	Distance
Er(1)	O(1)	2.3333(17)	Er(1)	N(5)	2.5272(19)
Er(1)	O(7)	2.3458(17)	Er(1)	N(2)	2.5395(19)
Er(1)	O(4)	2.4254(16)	Er(1)	N(4)	2.552(2)
Er(1)	N(6)	2.496(2)	Er(1)	N(3)	2.554(2)
Er(1)	N(1)	2.500(2)			

Angles (°)

At. 1	At. 2	At. 3	Angle	At. 1	At. 2	At. 3	Angle
O(1)	Er(1)	O(7)	144.50(6)	N(6)	Er(1)	N(2)	137.00(6)
O(1)	Er(1)	O(4)	73.73(6)	N(1)	Er(1)	N(2)	64.27(6)
O(7)	Er(1)	O(4)	70.93(6)	N(5)	Er(1)	N(2)	118.72(6)
O(1)	Er(1)	N(6)	93.01(7)	O(1)	Er(1)	N(4)	72.11(6)
O(7)	Er(1)	N(6)	79.27(6)	O(7)	Er(1)	N(4)	138.47(6)
O(4)	Er(1)	N(6)	71.73(6)	O(4)	Er(1)	N(4)	140.64(6)
O(1)	Er(1)	N(1)	77.79(6)	N(6)	Er(1)	N(4)	128.72(7)
O(7)	Er(1)	N(1)	88.72(6)	N(1)	Er(1)	N(4)	81.12(6)
O(4)	Er(1)	N(1)	73.04(6)	N(5)	Er(1)	N(4)	64.51(6)
N(6)	Er(1)	N(1)	144.76(6)	N(2)	Er(1)	N(4)	70.35(6)
O(1)	Er(1)	N(5)	70.98(6)	O(1)	Er(1)	N(3)	140.43(6)
O(7)	Er(1)	N(5)	131.87(6)	O(7)	Er(1)	N(3)	72.62(6)
O(4)	Er(1)	N(5)	120.58(6)	O(4)	Er(1)	N(3)	136.81(6)
N(6)	Er(1)	N(5)	64.24(6)	N(6)	Er(1)	N(3)	79.46(6)
N(1)	Er(1)	N(5)	138.94(6)	N(1)	Er(1)	N(3)	128.37(7)
O(1)	Er(1)	N(2)	129.57(6)	N(5)	Er(1)	N(3)	70.81(6)
O(7)	Er(1)	N(2)	68.98(6)	N(2)	Er(1)	N(3)	64.10(7)
O(4)	Er(1)	N(2)	120.66(6)	N(4)	Er(1)	N(3)	82.55(6)

Table S20 Selected least-squares planes data for complex Er(**L8**)$_2$(O_3SCF_3)$_3$ (**3**).

Least-squares planes

Least-squares planes description	Abbreviation	Max. deviation/Å	Atom
Pyridine 1	Py1		
N(1) C(1) C(2) C(3) C(4) C(5)		0.012	C(3)
Pyridine 2	Py2		
N(2) C(6) C(7) C(8) C(9) C(1AA)		0.007	C(6)
Pyridine 3	Py3		
N(3) C(10) C(11) C(12) C(13) C(14)		0.019	N(3), C(10)
Pyridine 4	Py4		
N(4) C(17) C(18) C(19) C(20) C(21)		0.036	N(4)
Pyridine 5	Py5		
N(5) C(22) C(23) C(24) C(25) C(26)		0.020	N(5)
Pyridine 6	Py6		
N(6) C(27) C(28) C(29) C(30) C(31)		0.012	N(6)

Interplanar angles (°)

	Py1	Py2	Py3	Py4	Py5	Py6
Py1		7.31(8)	18.20(9)	115.61(9)	100.01(8)	90.49(8)
Py2			10.89(9)	120.61(8)	103.39(8)	95.23(8)
Py3				127.31(9)	107.90(9)	102.03(9)
Py4					22.03(8)	25.42(9)
Py5						15.54(9)
Py6						

Table S21 Summary of crystal data, intensity measurements and structure refinements for complexes [Er(**L6**)$_3$](ClO$_4$)$_3$·2CH$_3$CN (**4**), [Er(**L7**)$_3$](ClO$_4$)$_3$ (**5**), [Er(**L8**)$_3$](ClO$_4$)$_3$ (**6**) and [Er(**L9**)$_3$](ClO$_4$)$_3$·1.5CH$_3$CN (**7**).

	[Er(**L6**)$_3$](ClO$_4$)$_3$	[Er(**L7**)$_3$](ClO$_4$)$_3$	[Er(**L8**)$_3$](ClO$_4$)$_3$	[Er(**L9**)$_3$](ClO$_4$)$_3$
Empirical formula	$C_{79}H_{81}Cl_3ErN_{17}O_{12}$	$C_{45}H_{33}Cl_3ErN_9O_{12}$	$C_{102}H_{90}C_{l6}Er_2N_{18}O_{24}$	$C_{60}H_{61.5}Cl_3ErN_{10.5}O_{12}$
Formula weight	1734.21	1165.41	2499.14	1395.31
Temperature	180(2)K	180(2)K	180(2) K	180(2)K
Wavelength	1.54184 Å	1.54184 Å	1.54184 Å	1.54184 Å
Crystal System, Space group	Orthorhombic, *P bcm*	Monoclinic, *C* 2/*c*	Monoclinic, *P* 2/*c*	Hexagonal, *P* 6$_3$
Unit cell dimensions	*a* = 15.00938(15) Å *b* = 18.4400(2) Å *c* = 29.3855(4) Å α = 90° β = 90° γ = 90°	*a* = 17.5447(4) Å *b* = 20.7433(5) Å *c* = 12.2263(3) Å α = 90° β = 94.638(2)° γ = 90°	*a* = 22.8203(3) Å *b* = 12.70104(15) Å *c* = 18.9988(3) Å α = 90° β = 110.6651(16)° γ = 90°	*a* = 12.77903(19) Å *b* = 12.77903 (19) Å *c* = 24.2818(4) Å α = 90° β = 90° γ = 120°
Volume in Å^3	8133.11(17)	4435.00(19)	5152.35(12)	3434.05(9)
Z, Calculated density	4, 1.416 Mg/m^3	4, 1.745 Mg/m^3	2, 1.611 Mg/m^3	2, 1.349 Mg/m^3
Absorption coefficient	3.402 mm^{-1}	5.835 mm^{-1}	5.065 mm^{-1}	3.862 mm^{-1}
F(000)	3556	2324	2516	1420
Theta range for data collection	3.80 to 73.30 °	3.31 to 73.57 °	4.05 to 73.35°	3.99 to 73.37 °
Limiting indices	-18<=*h*<=18, -22<=*k*<=22, -35<=*l*<=36	-21<=*h*<=17, -24<=*k*<=25, -13<=*l*<=14	-22<=*h*<=28, -14<=*k*<=15, -23<=*l*<=22	-11<=*h*<=15, -15<=*k*<=15, -24<=*l*<=29
Reflections collected / unique	20324 / 8154 [*R*(int) = 0.0317]	8622 / 4340 [*R*(int) = 0.0244]	20072 / 10096 [*R*(int) = 0.0309]	8289 / 3926 [*R*(int) = 0.0293]
Completeness to theta	67.50°/ 99.9 %	67.50°/ 99.9 %	67.50°/ 99.9 %	67.50°/ 100.0%
Data / restraints / parameters	8154 / 10 / 531	4340 / 0 / 318	10096 / 0 / 708	3926 / 8 / 287
Goodness-of-fit on F^2	1.076	1.042	1.010	1.224
Final *R* indices [$I>2\sigma(I)$]	R_1 = 0.0630, ωR_2 = 0.1651	R_1 = 0.0353, ωR_2 = 0.0934	R_1 = 0.0375, ωR_2 = 0.0969	R_1 = 0.0506, ωR_2 = 0.1495
R indices (all data)	R_1 = 0.0796, ωR_2 = 0.1778	R_1 = 0.0362, ωR_2 = 0.0944	R_1 = 0.0416, ωR_2 = 0.1009	R_1 = 0.0519, ωR_2 = 0.1513
Largest diff. peak and hole	0.925 and -0.925 e.Å^{-3}	1.184 and -1.900 e.Å^{-3}	1.049 and -1.855 e.Å^{-3}	0.700 and -0.742 e.Å^{-3}

Table S22 Selected bond distances (Å) and bond angles (°) for complex $[Er(\mathbf{L6})_3](ClO_4)_3$ (**4**).

Bond distances (Å)

Atom 1	Atom 2	Distance	Atom 1	Atom 2	Distance
Er(1)	N(4)	2.476(5)	Er(1)	N(5)	2.547(4)
Er(1)	N(2)#1	2.482(4)	Er(1)	N(5)#1	2.547(4)
Er(1)	N(2)	2.482(4)	Er(1)	N(7)#1	2.606(4)
Er(1)	N(1)	2.489(4)	Er(1)	N(7)	2.606(4)
Er(1)	N(1)#1	2.489(4)			

Symmetry operation (#1) x,-y+1/2,-z+1

Angles (°)

At. 1	At. 2	At. 3	angle	At. 1	At. 2	At. 3	angle
N(4)	Er(1)	N(2)#1	73.69(8)	N(1)	Er(1)	N(5)#1	74.62(13)
N(4)	Er(1)	N(2)	73.69(8)	N(1)#1	Er(1)	N(5)#1	142.95(13)
N(2)#1	Er(1)	N(2)	147.37(17)	N(5)	Er(1)	N(5)#1	129.07(18)
N(4)	Er(1)	N(1)	128.29(9)	N(4)	Er(1)	N(7)#1	132.24(9)
N(2)#1	Er(1)	N(1)	139.15(13)	N(2)#1	Er(1)	N(7)#1	76.66(12)
N(2)	Er(1)	N(1)	65.90(13)	N(2)	Er(1)	N(7)#1	127.47(13)
N(4)	Er(1)	N(1)#1	128.29(9)	N(1)	Er(1)	N(7)#1	63.34(13)
N(2)#1	Er(1)	N(1)#1	65.90(13)	N(1)#1	Er(1)	N(7)#1	67.40(13)
N(2)	Er(1)	N(1)#1	139.15(13)	N(5)	Er(1)	N(7)#1	139.29(12)
N(1)	Er(1)	N(1)#1	103.42(18)	N(5)#1	Er(1)	N(7)#1	79.63(12)
N(4)	Er(1)	N(5)	64.54(9)	N(4)	Er(1)	N(7)	132.23(9)
N(2)#1	Er(1)	N(5)	74.93(13)	N(2)#1	Er(1)	N(7)	127.48(13)
N(2)	Er(1)	N(5)	91.06(13)	N(2)	Er(1)	N(7)	76.66(12)
N(1)	Er(1)	N(5)	142.95(13)	N(1)	Er(1)	N(7)	67.40(13)
N(1)#1	Er(1)	N(5)	74.61(13)	N(1)#1	Er(1)	N(7)	63.34(13)
N(4)	Er(1)	N(5)#1	64.53(9)	N(5)	Er(1)	N(7)	79.63(12)
N(2)#1	Er(1)	N(5)#1	91.06(13)	N(5)#1	Er(1)	N(7)	139.29(12)
N(2)	Er(1)	N(5)#1	74.93(13)	N(7)#1	Er(1)	N(7)	95.53(19)

Table S23 Selected least-squares planes data for complex $[Er(\mathbf{L6})_3](ClO_4)_3$ (**4**).

Least-squares planes

Least-squares planes description	Abbreviation	Max. deviation/Å	Atom
Pyridine 1 N(1) C(2) C(3) C(26) C(27) C(28)	Py1	0.016	C(2)
Benzimidazole 1 C(5) C(6) C(7) C(8) C(9) C(10) N(2) C(1) N(3)	Bz1	0.027	N(2)
Benzimidazole 3#1 C(31)#1 C(32)#1 C(33)#1 C(34)#1 C(35)#1 C(36)#1 N(7)#1 C(36)#1 N(8)#1	Bz3#1	0.055	N(7)#1
Pyridine 2 N(4) C(13) C(14) C(15) C(14)#1 C(15)#1	Py2	0.005	C(14) C(15) C(14)#1 C(15)#1
Benzimidazole 2 C(18) C(19) C(20) C(21) C(22) C(23) N(5) C(16) N(6)	Bz2	0.043	C(16)
Benzimidazole 2#1 C(18)#1 C(19)#1 C(20)#1 C(21)#1 C(22)#1 C(23)#1 N(5)#1 C(16)#1 N(6)#1	Bz2#1	0.043	C(16)
Pyridine 1#1 N(1)#1 C(2)#1 C(3)#1 C(26)#1 C(27)#1 C(28)#1	Py1#1	0.016	C(2)#1
Benzimidazole 3 C(31) C(32) C(33) C(34) C(35) C(36) N(7) C(36) N(8)	Bz3	0.055	N(7)
Benzimidazole 1#1 C(5)#1 C(6)#1 C(7)#1 C(8)#1 C(9)# C(10)#1 N(2)#1 C(1)#1 N(3)#1	Bz1#1	0.027	N(2)
F1 N(2), N(5), N(7)	F1		
F2 N(1), N(1)#1, N(4)	F2		
F3 N(2)#1, N(5)#1, N(7)#1	F3		

Interplanar angles (°)

	Py1	Bz1	Bz3#1	Py2	Bz2	Bz2#1	Py1#1	Bz3	Bz1#1	F1	F2	F3
Py1		23.03(16)	22.94(16)	56.8(2)	65.63(18)	43.8(2)	39.4(3)	21.37(17)	55.13(16)			
Bz1			44.48(12)	43.51(15)	63.25(13)	22.02(18)	55.13(16)	43.22(12)	62.24(12)			
Bz3#1				64.7(2)	61.14(14)	62.02(14)	21.37(17)	1.7(2)	43.22(12)			
Py2					28.31(15)	28.31(15)	56.8(2)	64.7(2)	43.51(15)			
Bz2						54.9(3)	43.8(2)	62.02(14)	22.02(18)			
Bz2#1							65.63(18)	61.14(14)	63.25(13)			
Py1#1								22.87(17)	23.10(16)			
Bz3									44.48(12)			
Bz1#1												
F1											8.8(1)	17.4(2)
F2												8.8(1)
F3												

Table S24 Selected bond distances (Å) and bond angles (°) for complex $[Er(\mathbf{L7})_3](ClO_4)_3$ (**5**).

Bond distances (Å)

Atom 1	Atom 2	Distance	Atom 1	Atom 2	Distance
Er(1)	N(5)	2.460(3)	Er(1)	N(4)#1	2.521(2)
Er(1)	N(3)#1	2.516(2)	Er(1)	N(4)	2.521(2)
Er(1)	N(3)	2.516(2)	Er(1)	N(1)#1	2.555(2)
Er(1)	N(2)	2.516(2)	Er(1)	N(1)	2.555(2)
Er(1)	N(2)#1	2.516(2)			

Symmetry operation (#1) -x+1,y,-z+3/2.

Angles (°)

At. 1	At. 2	At. 3	Angle	At. 1	At. 2	At. 3	Angle
N(5)	Er(1)	N(3)#1	138.39(5)	N(2)	Er(1)	N(4)	136.94(8)
N(5)	Er(1)	N(3)	138.39(6)	N(2)#1	Er(1)	N(4)	72.00(8)
N(3)#1	Er(1)	N(3)	83.23(11)	N(4)#1	Er(1)	N(4)	130.32(12)
N(5)	Er(1)	N(2)	120.12(6)	N(5)	Er(1)	N(1)#1	71.01(5)
N(3)#1	Er(1)	N(2)	71.42(8)	N(3)#1	Er(1)	N(1)#1	127.86(8)
N(3)	Er(1)	N(2)	64.42(8)	N(3)	Er(1)	N(1)#1	82.69(8)
N(5)	Er(1)	N(2)#1	120.12(5)	N(2)	Er(1)	N(1)#1	140.62(8)
N(3)#1	Er(1)	N(2)#1	64.42(8)	N(2)#1	Er(1)	N(1)#1	63.49(8)
N(3)	Er(1)	N(2)#1	71.42(8)	N(4)#1	Er(1)	N(1)#1	81.85(8)
N(2)	Er(1)	N(2)#1	119.76(11)	N(4)	Er(1)	N(1)#1	82.44(8)
N(5)	Er(1)	N(4)#1	65.16(6)	N(5)	Er(1)	N(1)	71.01(5)
N(3)#1	Er(1)	N(4)#1	143.39(8)	N(3)#1	Er(1)	N(1)	82.69(8)
N(3)	Er(1)	N(4)#1	79.94(8)	N(3)	Er(1)	N(1)	127.86(8)
N(2)	Er(1)	N(4)#1	72.00(8)	N(2)	Er(1)	N(1)	63.49(8)
N(2)#1	Er(1)	N(4)#1	136.94(8)	N(2)#1	Er(1)	N(1)	140.62(8)
N(5)	Er(1)	N(4)	65.16(6)	N(4)#1	Er(1)	N(1)	82.43(8)
N(3)#1	Er(1)	N(4)	79.94(8)	N(4)	Er(1)	N(1)	81.85(8)
N(3)	Er(1)	N(4)	143.39(8)	N(1)#1	Er(1)	N(1)	142.02(11)

Table S25 Selected least-squares planes data for complex $[Er(\mathbf{L7})_3](ClO_4)_3$ (**5**).

	Least-squares planes		
Least-squares planes description	Abbreviation	Max. deviation/Å	Atom
Pyridine 1 N(1) C(1) C(2) C(3) C(4) C(5)	Py1	0.021	N(1)
Pyridine 2 N(2) C(6) C(7) C(8) C(9) C(10)	Py2	0.010	N(2)
Pyridine 3 N(3) C(11) C(12) C(13) C(14) C(15)	Py3	0.049	C(11)
Pyridine 4 N(4) C(16) C(17) C(18) C(19) C(20)	Py4	0.024	C(20)
Pyridine 5 N(5) C(21) C(22) C(23) C(22)#1 C(23)#1	Py5	0.009	C(21), C(22), C(21)#1, C(22)#1
Pyridine 4#1 N(4)#1 C(16)#1 C(17)#1 C(18)#1 C(19)#1 C(20)#1	Py4#1	0.024	C(20)#1
Pyridine 1#1 N(1)#1 C(1)#1 C(2)#1 C(3)#1 C(4)#1 C(5)#1	Py1#1	0.021	N(1)#1
Pyridine 2#1 N(2)#1 C(6)#1 C(7)#1 C(8)#1 C(9)#1 C(10)#1	Py2#1	0.010	N(2)#1
Pyridine 3#1 N(3)#1 C(11)#1 C(12)#1 C(13) #1 C(14)#1 C(15)#1	Py3#1	0.049	C(11)#1
F1 N(1)#1, N(3), N(4)	F1		
F2 N(2), (2)#1, N(5)	F2		
F3 N(1), N(3)#1, N(4)	F3		

Interplanar angles (°)

	Py1	Py2	Py3	Py4	Py5	Py4#1	Py1#1	Py2#1	Py3#1	F1	F2	F3
Py1		11.49(11)	38.30(11)	67.23(11)	51.70(10)	40.04(11)	74.85(15)	69.83(11)	60.57(11)			
Py2			26.82(10)	70.48(11)	57.29(11)	48.73(10)	69.83(11)	63.01(14)	50.19(10)			
Py3				79.98(11)	73.34(13)	71.07(11)	60.57(11)	50.19(10)	27.94(14)			
Py4					18.20(90)	36.29(17)	40.04(11)	48.73(10)	71.07(11)			
Py5						18.20(90)	51.70(10)	57.29(11)	73.34(13)			
Py4#1							67.23(11)	70.48(11)	79.98(11)			
Py1#1								11.49(11)	38.30(11)			
Py2#1									26.82(10)			
Py3#1												
F1											1.80(8)	0.4(1)
F2												1.80(8)
F3												

Table S26 Selected bond distances (Å) and bond angles (°) for complex $[Er(\mathbf{L8})_3](ClO_4)_3$ (**6**).

Bond distances (Å)

Atom 1	Atom 2	Distance	Atom 1	Atom 2	Distance
Er(1)	N(2)	2.505(2)	Er(2)	N(7)	2.453(2)
Er(1)	N(2)#1	2.505(2)	Er(2)	N(7)#2	2.453(2)
Er(1)	N(4)	2.523(3)	Er(2)	N(9)	2.491(3)
Er(1)	N(1)	2.525(2)	Er(2)	N(6)	2.525(2)
Er(1)	N(1)#1	2.525(2)	Er(2)	N(6)#2	2.525(2)
Er(1)	N(3)	2.532(2)	Er(2)	N(10)	2.532(2)
Er(1)	N(3)#1	2.532(2)	Er(2)	N(10)#2	2.532(2)
Er(1)	N(5)	2.554(2)	Er(2)	N(8)	2.544(2)
Er(1)	N(5)#1	2.554(2)	Er(2)	N(8)#2	2.544(2)

Symmetry operation (#1) -x+1,y,-z+3/2 (#2) -x,y,-z+1/2.

Angles (°)

At. 1	At. 2	At. 3	Angle	At. 1	At. 2	At. 3	Angle
N(2)	Er(1)	N(2)#1	119.48(10)	N(7)#2	Er(2)	N(7)	123.34(11)
N(2)	Er(1)	N(4)	120.26(5)	N(7)#2	Er(2)	N(9)	118.33(6)
N(2)#1	Er(1)	N(4)	120.26(5)	N(7)	Er(2)	N(9)	118.33(6)
N(2)	Er(1)	N(1)#1	138.42(7)	N(7)#2	Er(2)	N(6)	137.11(8)
N(2)#1	Er(1)	N(1)#1	64.30(7)	N(7)	Er(2)	N(6)	65.29(8)
N(4)	Er(1)	N(1)#1	71.83(5)	N(9)	Er(2)	N(6)	70.64(6)
N(2)	Er(1)	N(1)	64.30(7)	N(7)#2	Er(2)	N(6)#2	65.29(8)
N(2)#1	Er(1)	N(1)	138.42(7)	N(7)	Er(2)	N(6)#2	137.11(8)
N(4)	Er(1)	N(1)	71.83(5)	N(9)	Er(2)	N(6)#2	70.64(6)
N(1)#1	Er(1)	N(1)	143.66(10)	N(6)	Er(2)	N(6)#2	141.28(11)
N(2)	Er(1)	N(3)	64.50(7)	N(7)#2	Er(2)	N(10)	70.20(7)
N(2)#1	Er(1)	N(3)	71.26(7)	N(7)	Er(2)	N(10)	138.17(8)
N(4)	Er(1)	N(3)	138.24(5)	N(9)	Er(2)	N(10)	64.64(5)
N(1)#1	Er(1)	N(3)	80.71(7)	N(6)	Er(2)	N(10)	79.07(7)
N(1)	Er(1)	N(3)	128.80(7)	N(6)#2	Er(2)	N(10)	84.58(7)
N(2)	Er(1)	N(3)#1	71.26(7)	N(7)#2	Er(2)	N(10)#2	138.17(8)
N(2)#1	Er(1)	N(3)#1	64.50(7)	N(7)	Er(2)	N(10)#2	70.21(7)
N(4)	Er(1)	N(3)#1	138.24(5)	N(9)	Er(2)	N(10)#2	64.64(5)
N(1)#1	Er(1)	N(3)#1	128.80(7)	N(6)	Er(2)	N(10)#2	84.59(7)
N(1)	Er(1)	N(3)#1	80.71(7)	N(6)#2	Er(2)	N(10)#2	79.07(7)
N(3)	Er(1)	N(3)#1	83.53(10)	N(10)	Er(2)	N(10)#2	129.28(10)
N(2)	Er(1)	N(5)#1	70.83(7)	N(7)#2	Er(2)	N(8)#2	64.88(8)
N(2)#1	Er(1)	N(5)#1	141.60(7)	N(7)	Er(2)	N(8)#2	71.85(8)
N(4)	Er(1)	N(5)#1	63.14(5)	N(9)	Er(2)	N(8)#2	140.86(5)
N(1)#1	Er(1)	N(5)#1	83.81(7)	N(6)	Er(2)	N(8)#2	82.64(8)
N(1)	Er(1)	N(5)#1	79.98(7)	N(6)#2	Er(2)	N(8)#2	129.97(8)
N(3)	Er(1)	N(5)#1	83.50(7)	N(10)	Er(2)	N(8)#2	82.95(7)
N(3)#1	Er(1)	N(5)#1	141.93(7)	N(10)#2	Er(2)	N(8)#2	141.92(7)
N(2)	Er(1)	N(5)	141.60(7)	N(7)#2	Er(2)	N(8)	71.85(8)
N(2)#1	Er(1)	N(5)	70.83(7)	N(7)	Er(2)	N(8)	64.88(8)
N(4)	Er(1)	N(5)	63.14(5)	N(9)	Er(2)	N(8)	140.86(5)
N(1)#1	Er(1)	N(5)	79.98(7)	N(6)	Er(2)	N(8)	129.97(8)
N(1)	Er(1)	N(5)	83.81(7)	N(6)#2	Er(2)	N(8)	82.64(8)
N(3)	Er(1)	N(5)	141.93(7)	N(10)	Er(2)	N(8)	141.91(7)
N(3)#1	Er(1)	N(5)	83.50(7)	N(10)#2	Er(2)	N(8)	82.95(7)
N(5)#1	Er(1)	N(5)	126.28(10)	N(8)#2	Er(2)	N(8)	78.28(11)

Table S27 Selected least-squares planes data for complex $[Er(\mathbf{L8})_3](ClO_4)_3$ (**6**).[a]

Least-squares planes

Least-squares planes description	Abbreviation	Max. deviation/Å	Atom
Pyridine 1 N(1) C(1) C(2) C(4) C(5) C(6)	Py1	0.027	C(6)
Pyridine 2 N(2) C(7) C(8) C(9) C(10) C(11)	Py2	0.009	C(8)
Pyridine 3 N(3) C(12) C(13) C(14) C(15) C(17)	Py3	0.030	N(3)
Pyridine 4 N(5) C(18) C(19) C(21) C(22) C(23)	Py4	0.027	N(5)
Pyridine 5 N(4) C(24) C(25) C(26) C(25)#1 C(24)#1	Py5	0.024	C(24), C(25), C(24)#1, C(25)#1
Pyridine 4#1 N(5)#1 C(18)#1 C(19)#1 C(21)#1 C(22)#1 C(23)#1	Py4#1	0.027	N(5)#1
Pyridine 1#1 N(1)#1 C(1)#1 C(2)#1 C(4)#1 C(5)#1 C(6)#1	Py1#1	0.027	C(6)#1
Pyridine 2#1 N(2)#1 C(7)#1 C(8)#1 C(9)#1 C(10)#1 C(11)#1	Py2#1	0.009	C(8)#1
Pyridine 3#1 N(3)#1 C(12)#1 C(13)#1 C(14)#1 C(15)#1 C(17)#1	Py3#1	0.030	N(3)#1
F1(Er1) N(1)#1, N(3), N(5)#1	F1(Er1)		
F2(Er1) N(2), N(2)#1, N(4)	F2(Er1)		
F3(Er1) N(1), N(3)#1, N(5)	F3(Er1)		

Least-squares planes

Least-squares planes description	Abbreviation	Max. deviation/Å	Atom
Pyridine 6 N(6) C(27) C(28) C(30) C(31) C(32)	Py6	0.042	N(6)
Pyridine 7 N(7) C(33) C(34) C(35) C(36) C(37)	Py7	0.008	C(36)
Pyridine 8 N(8) C(38) C(39) C(40) C(41) C(43)	Py8	0.020	N(8)
Pyridine 9 N(10) C(44) C(45) C(47) C(48) C(49)	Py9	0.023	N(10)
Pyridine 10 N(9) C(50) C(51) C(52) C(51)#2 C(52)#2	Py10	0.006	C(50), C(51), C(50)#2, C(51)#2
Pyridine 9#2 N(10)#2 C(44)#2 C(45)#2 C(47)#2 C(48)#2 C(49)#2	Py9#2	0.023	N(10)#2
Pyridine 6#2 N(6)#2 C(27)#2 C(28)#2 C(30)#2 C(31)#2 C(32)#2	Py6#2	0.042	N(6)#2
Pyridine 7#2 N(7)#2 C(33)#2 C(34)#2 C(35)#2 C(36)#2 C(37)#2	Py7#2	0.007	C(36)#2
Pyridine 8#2 N(8)#2 C(38)#2 C(39)#2 C(40)#2 C(41)#2 C(43)#2	Py8#2	0.020	N(8)#2
F1(Er2) N(6), N(8)#2, N(10)	F1(Er2)		
F2(Er2) N(7), N(7)#2, N(9)	F2(Er2)		
F3(Er2) N(6)#2, N(8), N(10)#2	F3(Er2)		

[a] The asymmetric unit in the crystal structure of 6 contains two slightly different cations of $[Er(\mathbf{L8})_3]^{3+}$.

Interplanar angles (°)[a]

	Py1	Py2	Py3	Py4	Py5	Py4#1	Py1#1	Py2#1	Py3#1	F1(Er1)	F2(Er1)	F3(Er1)
Py1		13.7(1)	34.5(1)	69.0(1)	50.4(8)	29.8(1)	83.3(1)	75.5(1)	62.4(1)			
Py2			20.8(1)	67.7(1)	53.3(1)	37.2(1)	75.5(1)	65.8(1)	50.5(1)			
Py3				65.5(1)	59.5(1)	51.3(1)	62.7(1)	50.5(1)	32.0(2)			
Py4					22.9(7)	45.1(1)	29.8(1)	37.2(1)	51.3(1)			
Py5						22.9(7)	50.4(8)	50.3(1)	59.5(1)			
Py4#1							69.0(1)	67.7(1)	65.5(1)			
Py1#1								13.7(1)	34.5(1)			
Py2#1									20.8(1)			
Py3#1												
F1(Er1)											1.84(6)	2.49(9)
F2(Er1)												1.84(6)
F3(Er1)												

	Py6	Py7	Py8	Py9	Py10	Py9#2	Py6#2	Py7#2	Py8#2	F1(Er2)	F2(Er2)	F3(Er2)
Py6		27.4(1)	46.0(1)	48.7(1)	33.8(9)	19.5(1)	58.2(1)	65.2(1)	64.2(1)			
Py7			20.2(1)	65.1(1)	55.2(1)	45.5(1)	65.2(1)	57.5(2)	64.2(1)			
Py8				71.4(1)	66.7(1)	61.7(1)	64.2(1)	47.0(1)	31.0(2)			
Py9					16.9(7)	33.8(1)	19.5(1)	45.5(1)	61.7(1)			
Py10						16.9(7)	33.8(9)	55.2(1)	66.7(1)			
Py9#2							48.7(1)	65.1(1)	71.4(1)			
Py6#2								27.4(1)	46.0(1)			
Py7#2									20.2(1)			
Py8#2												
F1(Er2)											2.08(8)	3.7(1)
F2(Er2)												2.08(8)
F3(Er2)												

[a] The asymmetric unit in the crystal structure of 6 contains two slightly different cations of $[Er(\mathbf{L8})_3]^{3+}$.

Table S28 Selected bond distances (Å) and bond angles (°) for complex [Er(**L9**)$_3$](ClO$_4$)$_3$ (**7**).

Bond distances (Å)

Atom 1	Atom 2	Distance	Atom 1	Atom 2	Distance
Er(1)	N(2)#1	2.488(5)	Er(1)	N(1)	2.529(7)
Er(1)	N(2)#2	2.488(5)	Er(1)	N(3)#1	2.543(6)
Er(1)	N(2)	2.488(5)	Er(1)	N(3)#2	2.543(6)
Er(1)	N(1)#1	2.529(7)	Er(1)	N(3)	2.543(6)
Er(1)	N(1)#2	2.529(7)			

Symmetry operation (#1) -x,-y,-z+1 (#2) -y,x-y,z

Angles (°)

At. 1	At. 2	At. 3	Angle	At. 1	At. 2	At. 3	Angle
N(2)#1	Er(1)	N(2)#2	120.000(3)	N(1)#1	Er(1)	N(3)#1	128.56(14)
N(2)#1	Er(1)	N(2)	120.000(2)	N(1)#2	Er(1)	N(3)#1	142.94(14)
N(2)#2	Er(1)	N(2)	119.999(2)	N(1)	Er(1)	N(3)#1	82.52(13)
N(2)#1	Er(1)	N(1)#1	64.61(16)	N(2)#1	Er(1)	N(3)#2	71.57(15)
N(2)#2	Er(1)	N(1)#1	71.38(16)	N(2)#2	Er(1)	N(3)#2	63.96(15)
N(2)	Er(1)	N(1)#1	138.69(19)	N(2)	Er(1)	N(3)#2	138.79(18)
N(2)#1	Er(1)	N(1)#2	138.69(19)	N(1)#1	Er(1)	N(3)#2	82.52(13)
N(2)#2	Er(1)	N(1)#2	64.61(16)	N(1)#2	Er(1)	N(3)#2	128.56(14)
N(2)	Er(1)	N(1)#2	71.37(16)	N(1)	Er(1)	N(3)#2	142.94(14)
N(1)#1	Er(1)	N(1)#2	81.38(18)	N(3)#1	Er(1)	N(3)#2	81.87(16)
N(2)#1	Er(1)	N(1)	71.38(15)	N(2)#1	Er(1)	N(3)	138.79(18)
N(2)#2	Er(1)	N(1)	138.69(18)	N(2)#2	Er(1)	N(3)	71.57(15)
N(2)	Er(1)	N(1)	64.61(16)	N(2)	Er(1)	N(3)	63.96(15)
N(1)#1	Er(1)	N(1)	81.38(18)	N(1)#1	Er(1)	N(3)	142.94(14)
N(1)#2	Er(1)	N(1)	81.38(18)	N(1)#2	Er(1)	N(3)	82.52(13)
N(2)#1	Er(1)	N(3)#1	63.96(15)	N(1)	Er(1)	N(3)	128.56(14)
N(2)#2	Er(1)	N(3)#1	138.79(18)	N(3)#1	Er(1)	N(3)	81.87(16)
N(2)	Er(1)	N(3)#1	71.57(15)	N(3)#2	Er(1)	N(3)	81.87(16)

Table S29 Selected least-squares planes data for complex $[Er(\mathbf{L9})_3](ClO_4)_3$ (**7**).

Least-squares planes

Least-squares planes description	Abbreviation	Max. deviation/Å	Atom
Pyridine 1 N(1) C(1) C(2) C(3) C(4) C(5)	Py1	0.028	C(3)
Pyridine 2 N(2) C(6) C(7) C(8) C(9) C(10)	Py2	0.009	C(9)
Pyridine 3 N(3) C(11) C(12) C(13) C(14) C(15)	Py3	0.034	C(11)
Pyridine 1#1 N(1)#1 C(1)#1 C(2)#1 C(3)#1 C(4)#1 C(5)#1	Py1#1	0.028	C(3)#1
Pyridine 2#1 N(2)#1 C(6)#1 C(7)#1 C(8)#1 C(9)#1 C(10)#1	Py2#1	0.009	C(9)#1
Pyridine 3#1 N(3)#1 C(11)#1 C(12)#1 C(13)#1 C(14)#1 C(15)#1	Py3#1	0.034	C(11)#1
Pyridine 1#2 N(1)#2 C(1)#2 C(2)#2 C(3)#2 C(4)#2 C(5)#2	Py1#2	0.028	C(3)#2
Pyridine 2#2 N(2)#2 C(6)#2 C(7)#2 C(8)#2 C(9)#2 C(10)#2	Py2#2	0.009	C(9)#2
Pyridine 3#2 N(3)#2 C(11)#2 C(12)#2 C(13)#2 C(14)#2 C(15)#2	Py3#2	0.034	C(11)#2
F1 N(1), N(1)#1, N(1)#2	F1		
F2 N(2), N(2)#1, N(2)#2	F2		
F3 N(3), N(3)#1, N(3)#2	F3		

Interplanar angles (°)

	Py1	Py2	Py3	Py1#1	Py2#1	Py3#1	Py1#2	Py2#2	Py3#2	F1	F2	F3
Py1		19.1(3)	38.9(3)	63.7(3)	69.6(2)	76.2(2)	63.7(3)	48.1(2)	33.0(3)			
Py2			19.8(3)	48.1(2)	58.7(3)	70.8(3)	69.6(2)	58.7(3)	48.7(3)			
Py3				33.0(3)	48.7(3)	65.6(3)	76.2(2)	70.8(3)	65.6(3)			
Py1#1					19.1(3)	38.9(3)	63.7(3)	69.6(2)	76.2(2)			
Py2#1						19.8(3)	48.1(2)	58.7(3)	70.8(3)			
Py3#1							33.0(3)	48.1(2)	33.0(3)			
Py1#2								19.1(3)	38.9(3)			
Py2#2									19.8(3)			
Py3#2												
F1											0.0	0.0
F2												0.0
F3												

Table S30 Average bond distances $\delta_{Ln,N}$ and $\delta_{Ln,O}$ (Å), average of bond valences (v_{ij}) [a] and bond valence sums (V_i) [b] in the crystal structures of 1:2 and 1:3 complexes of ligands **L4-L9** with Ln(III) (Ln = Er, Eu and Lu).

Complexes	Ln	Ln/**L*k***	Avg. $\delta_{Ln,N}$ / Å	Avg. $\delta_{Ln,O}$ / Å	Avg. $v_{Ln,N}$	Avg. $v_{Ln,O}$	V_{Ln}
[Er(**L4**)$_2$(O$_3$SCF$_3$)$_2$](CF$_3$SO$_3$)	Er	1:2	2.46(3)	2.31(3)	0.36(3)	0.41(4)	2.99(4)
[Er(**L7**)$_2$(O$_3$SCF$_3$)$_2$](CF$_3$SO$_3$)	Er	1:2	2.49(2)	2.26	0.33(2)	0.46	2.92(4)
Er(**L8**)$_2$(O$_3$SCF$_3$)$_3$	Er	1:2	2.53(2)	2.37(5)	0.32(2)	0.35(5)	2.95(4)
[Er(**L6**)$_3$](ClO$_4$)$_3$	Er	1:3	2.52(5)	-	0.32(4)	-	2.88(4)
[Eu(**L7**)$_3$](ClO$_4$)$_3$ [c]	Eu	1:3	2.57(3)	-	0.30(1)	-	2.88(4)
[Er(**L7**)$_3$](ClO$_4$)$_3$	Er	1:3	2.52(3)	-	0.32(2)	-	2.91(4)
[Lu(**L7**)$_3$](ClO$_4$)$_3$ [c]	Lu	1:3	2.50(3)	-	0.31(1)	-	2.84(4)
[Er(**L8**)$_3$](ClO$_4$)$_3$ [d]	Er	1:3	2.53(2)	-	0.31(1)	-	2.84(4)
[Er(**L8**)$_3$](ClO$_4$)$_3$ [d]	Er	1:3	2.51(4)	-	0.33(3)	-	2.98(4)
[Er(**L9**)$_3$](ClO$_4$)$_3$	Er	1:3	2.52(2)	-	0.32(2)	-	2.90(4)

[a] $v_{ij} = e^{[(R_{ij}-d_{ij})/b]}$, whereby d_{ij} is the Ln-donor atom j distance.[60] The valence bond parameters R_{ij} was taken from references 60e and 60f and b = 0.37 Å. [c] $V_i = \sum_j v_{ij}$. [c] Crystal data were taken from reference 34b. [d] The crystal structure of **6** shows that the asymmetric unit contains two slightly different molecules.

Table S31 Summary of crystal data, intensity measurements and structure refinements for dimer complexes [(**L4**)$_2$Er(OH)$_2$Er(**L4**)$_2$](ClO$_4$)$_4$ ·2C$_6$H$_5$CN·4CH$_3$CN (**8**), [(**L5**)$_2$Er(OH)$_2$Er(**L5**)$_2$](ClO$_4$)$_4$·C$_6$H$_5$CN·7.5CH$_3$CN (**9**) and [(**L4**)$_2$Er((CH$_3$)NO$_2$)$_2$Er(**L4**)$_2$](ClO$_4$)$_6$·CH$_3$NO$_2$ (**10**).

	[(**L4**)$_2$Er(OH)$_2$Er(**L4**)$_2$](ClO$_4$)$_4$	[(**L5**)$_2$Er(OH)$_2$Er(**L5**)$_2$](ClO$_4$)$_4$	[(**L4**)$_2$Er((CH$_3$)NO$_2$)$_2$Er(**L4**)$_2$](ClO$_4$)$_6$
Empirical formula	$C_{106}H_{92}Cl_4Er_2N_{26}O_{18}$	$C_{115}H_{115}Cl_4Er_2N_{29}O_{18}$	$C_{87}H_{77}Cl_6Er_2N_{23}O_{30}$
Formula weight	2494.38	2662.67	2471.93
Temperature	180(2)K	180(2)K	180(2)K
Wavelength	1.54184 Å	1.54184 Å	1.54184 Å
Crystal System, Space group	Monoclinic, *C* 2/*c*	Monoclinic, *C* 2/*c*	Monoclinic, *P* 2$_1$/*c*
Unit cell dimensions	*a* = 27.5175(4) Å *b* = 14.45677(19) Å *c* = 27.0356(5) Å α = 90° β = 107.1147(17)° γ = 90°	*a* = 24.0649(19) Å *b* = 30.860(2) Å *c* = 16.5690(11) Å α = 90° β = 107.371(8)° γ = 90°	*a* = 27.2009(5) Å *b* = 23.2822(5) Å *c* = 15.2320(2) Å α = 90° β = 94.6614(16)° γ = 90°
Volume in Å^3	10278.9(3)	11743.7(15)	9614.5(3)
Z, Calculated density	4, 1.612 Mg/m^3	4, 1.506 Mg/m^3	4, 1.708 Mg/m^3
Absorption coefficient	4.589 mm^{-1}	4.062 mm^{-1}	5.484 mm^{-1}
F(000)	5032	5424	4952
Theta range for data collection	3.42 to 73.33 °	3.849 to 67.404 °	3.260 to 73.573 °
Limiting indices	-32<=*h*<=33, -11<=*k*<=17, -31<=*l*<=33	-28<=*h*<=24, -18<=*k*<=36, -19<=*l*<=19	-33<=*h*<=22, -28<=*k*<=19, -18<=*l*<=18
Reflections collected / unique	18745 / 10046 [*R*(int) = 0.0229]	20752 / 10556 [*R*(int) = 0.0410]	34420 / 18724 [*R*(int) = 0.0490]
Completeness to theta	67.50°/ 99.7 %	67.50°/ 99.8 %	67.50°/ 99.6 %
Data / restraints / parameters	10046 / 1 / 689	10556 / 1 / 712	18724 / 1 / 1246
Goodness-of-fit on F^2	1.039	1.112	1.018
Final *R* indices [$I>2\sigma(I)$]	R_1 = 0.0363, ωR_2 = 0.0944	R_1 = 0.0654, ωR_2 = 0.1819	R_1 = 0.0571, ωR_2 = 0.1403
R indices (all data)	R_1 = 0.0401, ωR_2 = 0.0982	R_1 = 0.0736, ωR_2 = 0.1896	R_1 = 0.0812, ωR_2 = 0.1563
Largest diff. peak and hole	0.872 and -1.347 e.Å^{-3}	2.099 and -2.708 e.Å^{-3}	1.450 and -0.966 e.Å^{-3}

Table S32 Selected bond distances (Å), bond angles (°) in $[(\mathbf{L4})_2Er(OH)_2Er(\mathbf{L4})_2](ClO_4)_4$ (**8**).

Bond distances (Å)

Atom 1	Atom 2	Distance	Atom 1	Atom 2	Distance
Er(1)	O(1)	2.2375(18)	Er(2)	O(1)	2.2414(18)
Er(1)	O(1)#1	2.2376(18)	Er(2)	O(1)#1	2.2414(18)
Er(1)	N(1)#1	2.492(2)	Er(2)	N(9)	2.486(2)
Er(1)	N(1)	2.492(2)	Er(2)	N(9)#1	2.486(2)
Er(1)	N(3)	2.548(2)	Er(2)	N(8)#1	2.528(2)
Er(1)	N(3)#1	2.548(2)	Er(2)	N(8)	2.528(2)
Er(1)	N(4)	2.552(2)	Er(2)	N(6)	2.533(3)
Er(1)	N(4)#1	2.552(2)	Er(2)	N(6)#1	2.533(3)

Symmetry operation (#1) -x+1,y,-z+1/2

Angles (°)

At. 1	At. 2	At. 3	Angle	At. 1	At. 2	At. 3	Angle
O(1)	Er(1)	O(1)#1	70.60(9)	O(1)	Er(2)	N(9)	87.77(7)
O(1)	Er(1)	N(1)#1	82.46(7)	O(1)#1	Er(2)	N(9)	82.31(8)
O(1)#1	Er(1)	N(1)#1	87.05(7)	O(1)	Er(2)	N(9)#1	82.31(7)
O(1)	Er(1)	N(1)	87.05(7)	O(1)#1	Er(2)	N(9)#1	87.77(7)
O(1)#1	Er(1)	N(1)	82.46(7)	N(9)	Er(2)	N(9)#1	167.87(11)
N(1)#1	Er(1)	N(1)	167.15(11)	O(1)	Er(2)	N(8)#1	134.83(7)
O(1)	Er(1)	N(3)	77.32(7)	O(1)#1	Er(2)	N(8)#1	78.80(7)
O(1)#1	Er(1)	N(3)	134.45(7)	N(9)	Er(2)	N(8)#1	120.46(8)
N(1)#1	Er(1)	N(3)	120.16(8)	N(9)#1	Er(2)	N(8)#1	63.84(8)
N(1)	Er(1)	N(3)	64.12(8)	O(1)	Er(2)	N(8)	78.80(7)
O(1)	Er(1)	N(3)#1	134.45(7)	O(1)#1	Er(2)	N(8)	134.83(7)
O(1)#1	Er(1)	N(3)#1	77.32(7)	N(9)	Er(2)	N(8)	63.84(8)
N(1)#1	Er(1)	N(3)#1	64.12(8)	N(9)#1	Er(2)	N(8)	120.46(8)
N(1)	Er(1)	N(3)#1	120.16(8)	N(8)#1	Er(2)	N(8)	143.57(11)
N(3)	Er(1)	N(3)#1	145.74(10)	O(1)	Er(2)	N(6)	108.16(8)
O(1)	Er(1)	N(4)	104.32(7)	O(1)#1	Er(2)	N(6)	157.90(8)
O(1)#1	Er(1)	N(4)	157.10(7)	N(9)	Er(2)	N(6)	119.79(8)
N(1)#1	Er(1)	N(4)	70.07(8)	N(9)#1	Er(2)	N(6)	70.33(8)
N(1)	Er(1)	N(4)	120.07(8)	N(8)#1	Er(2)	N(6)	88.53(8)
N(3)	Er(1)	N(4)	61.85(7)	N(8)	Er(2)	N(6)	63.38(8)
N(3)#1	Er(1)	N(4)	92.87(7)	O(1)	Er(2)	N(6)#1	157.90(8)
O(1)	Er(1)	N(4)#1	157.10(7)	O(1)#1	Er(2)	N(6)#1	108.15(8)
O(1)#1	Er(1)	N(4)#1	104.31(7)	N(9)	Er(2)	N(6)#1	70.33(8)
N(1)#1	Er(1)	N(4)#1	120.07(8)	N(9)#1	Er(2)	N(6)#1	119.79(8)
N(1)	Er(1)	N(4)#1	70.07(8)	N(8)#1	Er(2)	N(6)#1	63.38(8)
N(3)	Er(1)	N(4)#1	92.87(7)	N(8)	Er(2)	N(6)#1	88.53(8)
N(3)#1	Er(1)	N(4)#1	61.85(7)	N(6)	Er(2)	N(6)#1	81.45(12)
N(4)	Er(1)	N(4)#1	88.58(11)	Er(1)	O(1)	Er(2)	109.47(7)
O(1)	Er(2)	O(1)#1	70.46(9)	Er(1)	O(1)#1	Er(2)	109.47(7)

Table S33 Selected least-squares planes data for [(**L4**)$_2$Er(OH)$_2$Er(**L4**)$_2$](ClO$_4$)$_4$ (**8**).

Least-squares planes

Least-squares planes description	Abbreviation	Max. deviation/Å	Atom
Pyridine 1 N(3) C(9) C(10) C(11) C(12) C(13)	Py1	0.018	N(3)
Benzimidazole 1 C(1) C(2) C(3) C(4) C(5) C(6) N(1) C(8) N(2)	Bz1	0.035	C(6)
Benzimidazole 2 C(15) C(16) C(17) C(18) C(19) C(20) N(4) C(14) N(5)	Bz2	0.046	C(14)
Pyridine 2 N(8) C(30) C(31) C(32) C(33) C(34)	Py2	0.029	C(34)
Benzimidazole 3 C(22) C(23) C(24) C(25) C(26) C(27) N(6) C(29) N(7)	Bz3	0.036	C(29)
Benzimidazole 4 C(36) C(37) C(38) C(39) C(40) C(41) N(9) C(35) N(10)	Bz4	0.026	C(35)
Pyridine 1#1 N(3)#1 C(9)#1 C(10)#1 C(11)#1 C(12)#1 C(13)#1	Py1#1	0.018	N(3)#1
Benzimidazole 1#1 C(1)#1 C(2)#1 C(3)#1 C(4)#1 C(5)#1 C(6)#1 N(1)#1 C(8)#1 N(2)#1	Bz1#1	0.035	C(6)#1
Benzimidazole 2#1 C(15)#1 C(16)#1 C(17)#1 C(18)#1 C(19)#1 C(20)#1 N(4)#1 C(14)#1 N(5)#1	Bz2#1	0.046	C(14)#1
Pyridine 2#1 N(8)#1 C(30)#1 C(31)#1 C(32)#1 C(33)#1 C(34)#1	Py2#1	0.029	C(34)#1
Benzimidazole 3#1 C(22)#1 C(23)#1 C(24)#1 C(25)#1 C(26)#1 C(27)#1 N(6)#1 C(29)#1 N(7)#1	Bz3#1	0.036	C(29)#1
Benzimidazole 4#1 C(36)#1 C(37)#1 C(38)#1 C(39)#1 C(40)#1 C(41)#1 N(9)#1 C(35)#1 N(10)#1	Bz4#1	0.026	C(35)#1

Interplanar angles (°)

	Py1	Bz1	Bz2	Py2	Bz3	Bz4	Py1#1	Bz1#1	Bz2#1	Py2#1	Bz3#1	Bz4#1
Py1		26.92(10)	18.40(8)	31.63(11)	15.73(9)	26.39(9)	37.38(14)	26.92(10)	18.40(8)	34.63(11)	42.80(8)	15.96(9)
Bz1			43.78(8)	44.50(11)	40.09(9)	26.25(7)	22.54(8)	33.27(12)	21.77(8)	11.39(11)	18.06(7)	10.97(9)
Bz2				23.60(11)	4.14(7)	31.64(9)	46.92(9)	21.77(8)	61.06(10)	52.69(10)	56.97(7)	33.12(8)
Py2					21.37(10)	19.89(11)	34.63(11)	11.39(11)	52.69(10)	55.81(18)	49.37(11)	37.59(10)
Bz3						27.62(8)	42.80(8)	18.06(7)	56.97(7)	49.37(11)	52.9(1)	29.61(8)
Bz4							15.96(9)	10.97(9)	33.12(8)	37.59(10)	29.61(8)	22.76(9)
Py1#1								26.92(10)	18.40(8)	31.63(11)	15.73(9)	26.39(9)
Bz1#1									43.78(8)	44.50(11)	40.09(9)	26.25(7)
Bz2#1										23.60(11)	4.14(7)	31.64(9)
Py2#1											21.37(10)	19.89(11)
Bz3#1												27.62(8)
Bz4#1												

Table S34 Selected bond distances (Å), bond angles (°) in $[(\mathbf{L5})_2Er(OH)_2Er(\mathbf{L5})_2](ClO_4)_4$ (**9**).

Bond distances (Å)

Atom 1	Atom 2	Distance	Atom 1	Atom 2	Distance
Er(1)	O(1)	2.221(4)	Er(1)#1	O(1)	2.256(4)
Er(1)	O(1)#1	2.256(4)	Er(1)#1	O(1)#1	2.221(4)
Er(1)	N(6)	2.466(4)	Er(1)#1	N(6)#1	2.466(4)
Er(1)	N(4)	2.468(5)	Er(1)#1	N(4)#1	2.468(5)
Er(1)	N(9)	2.481(5)	Er(1)#1	N(9)#1	2.481(5)
Er(1)	N(8)	2.495(5)	Er(1)#1	N(8)#1	2.495(4)
Er(1)	N(3)	2.500(5)	Er(1)#1	N(3)#1	2.500(5)
Er(1)	N(1)	2.586(4)	Er(1)#1	N(1)#1	2.586(4)

Symmetry operation (#1) -x+1,y,-z+3/2.

Angles (°)

At. 1	At. 2	At. 3	Angle	At. 1	At. 2	At. 3	Angle
O(1)	Er(1)	O(1)#1	71.30(16)	O(1)	Er(1)#1	N(6)#1	95.67(14)
O(1)	Er(1)	N(6)	95.67(14)	O(1)#1	Er(1)#1	N(6)#1	154.98(14)
O(1)#1	Er(1)	N(6)	154.98(14)	O(1)	Er(1)#1	N(4)#1	84.37(14)
O(1)	Er(1)	N(4)	84.37(14)	O(1)#1	Er(1)#1	N(4)#1	82.10(14)
O(1)#1	Er(1)	N(4)	82.10(14)	N(6)#1	Er(1)#1	N(4)#1	75.27(15)
N(6)	Er(1)	N(4)	75.27(15)	O(1)	Er(1)#1	N(9)#1	94.37(15)
O(1)	Er(1)	N(9)	94.37(15)	O(1)#1	Er(1)#1	N(9)#1	79.03(14)
O(1)#1	Er(1)	N(9)	79.03(14)	N(6)#1	Er(1)#1	N(9)#1	124.21(16)
N(6)	Er(1)	N(9)	124.21(16)	N(4)#1	Er(1)#1	N(9)#1	160.44(17)
N(4)	Er(1)	N(9)	160.44(17)	O(1)	Er(1)#1	N(8)#1	77.07(14)
O(1)	Er(1)	N(8)	77.07(14)	O(1)#1	Er(1)#1	N(8)#1	129.49(14)
O(1)#1	Er(1)	N(8)	129.49(14)	N(6)#1	Er(1)#1	N(8)#1	64.20(15)
N(6)	Er(1)	N(8)	64.20(15)	N(4)#1	Er(1)#1	N(8)#1	132.89(16)
N(4)	Er(1)	N(8)	132.89(16)	N(9)#1	Er(1)#1	N(8)#1	65.07(17)
N(9)	Er(1)	N(8)	65.07(17)	O(1)	Er(1)#1	N(3)#1	140.85(13)
O(1)	Er(1)	N(3)	140.85(13)	O(1)#1	Er(1)#1	N(3)#1	80.56(14)
O(1)#1	Er(1)	N(3)	80.56(14)	N(6)#1	Er(1)#1	N(3)#1	98.97(15)
N(6)	Er(1)	N(3)	98.97(15)	N(4)#1	Er(1)#1	N(3)#1	64.88(16)
N(4)	Er(1)	N(3)	64.88(16)	N(9)#1	Er(1)#1	N(3)#1	106.62(17)
N(9)	Er(1)	N(3)	106.62(17)	N(8)#1	Er(1)#1	N(3)#1	141.72(14)
N(8)	Er(1)	N(3)	141.72(14)	O(1)	Er(1)#1	N(1)#1	156.80(14)
O(1)	Er(1)	N(1)	156.80(14)	O(1)#1	Er(1)#1	N(1)#1	119.90(14)
O(1)#1	Er(1)	N(1)	119.90(14)	N(6)#1	Er(1)#1	N(1)#1	80.39(14)
N(6)	Er(1)	N(1)	80.39(14)	N(4)#1	Er(1)#1	N(1)#1	116.14(14)
N(4)	Er(1)	N(1)	116.14(14)	N(9)#1	Er(1)#1	N(1)#1	70.03(14)
N(9)	Er(1)	N(1)	70.03(14)	N(8)#1	Er(1)#1	N(1)#1	80.70(15)
N(8)	Er(1)	N(1)	80.70(15)	N(3)#1	Er(1)#1	N(1)#1	62.08(15)
N(3)	Er(1)	N(1)	62.08(15)	Er(1)	O(1)	Er(1)#1	108.32(16)
O(1)	Er(1)#1	O(1)#1	71.30(16)	Er(1)	O(1)#1	Er(1)#1	108.32(16)

Table S35 Selected least-squares planes data for [(**L5**)$_2$Er(OH)$_2$Er(**L5**)$_2$](ClO$_4$)$_4$ (**9**).

Least-squares planes

Least-squares planes description	Abbreviation	Max. deviation/Å	Atom
Pyridine 1 N(3) C(10) C(11) C(12) C(13) C(14)	Py1	0.035	N(3)
Benzimidazole 1 C(1) C(2) C(3) C(5) C(6) C(7) N(1) C(9) N(2)	Bz1	0.049	N(1)
Benzimidazole 2 C(16) C(17) C(18) C(20) C(21) C(22) N(4) C(15) N(5)	Bz2	0.043	C(15)
Pyridine 2 N(8) C(33) C(34) C(35) C(36) C(37)	Py2	0.017	C(37)
Benzimidazole 3 C(24) C(25) C(26) C(28) C(29) C(30) N(6) C(32) N(7)	Bz3	0.023	C(32)
Benzimidazole 4 C(39) C(40) C(41) C(43) C(44) C(45) N(9) C(38) N(10)	Bz4	0.010	C(43)
Pyridine 1#1 N(3)#1 C(10)#1 C(11)#1 C(12)#1 C(13)#1 C(14)#1	Py1#1	0.035	N(3)#1
Benzimidazole 1#1 C(1)#1 C(2)#1 C(3)#1 C(5)#1 C(6)#1 C(7)#1 N(1)#1 C(9)#1 N(2)#1	Bz1#1	0.049	N(1)#1
Benzimidazole 2#1 C(16)#1 C(17)#1 C(18)#1 C(20)#1 C(21)#1 C(22)#1 N(4)#1 C(15)#1 N(5)#1	Bz2#1	0.043	C(15)#1
Pyridine 2#1 N(8)#1 C(33)#1 C(34)#1 C(35)#1 C(36)#1 C(37)#1	Py2#1	0.017	C(37)#1
Benzimidazole 3#1 C(24)#1 C(25)#1 C(26)#1 C(28)#1 C(29)#1 C(30)#1 N(6)#1 C(32)#1 N(7)#1	Bz3#1	0.023	C(32)#1
Benzimidazole 4#1 C(39)#1 C(40)#1 C(41)#1 C(43)#1 C(44)#1 C(45)#1 N(9)#1 C(38)#1 N(10)#1	Bz4#1	0.010	C(43)#1

Interplanar angles (°)

	Py1	Bz1	Bz2	Py2	Bz3	Bz4	Py1#1	Bz1#1	Bz2#1	Py2#1	Bz3#1	Bz4#1
Py1		13.94(16)	26.01(16)	44.3(2)	50.76(16)	26.43(16)	44.4(3)	45.91(15)	18.51(16)	26.29(19)	14.49(17)	34.13(17)
Bz1			30.01(12)	36.93(17)	41.73(11)	17.17(15)	45.91(15)	42.67(15)	23.97(10)	13.08(17)	5.05(10)	27.10(15)
Bz2				29.50(16)	27.88(13)	24.35(12)	18.51(16)	23.97(10)	7.53(19)	32.99(17)	34.35(14)	22.66(10)
Py2					16.22(16)	19.78(19)	26.29(19)	13.08(17)	32.92(17)	27.8(3)	41.68(16)	44.4(2)
Bz3						18.35(18)	14.49(17)	5.05(10)	34.35(14)	41.68(16)	52.75(14)	21.91(14)
Bz4							34.13(17)	27.10(15)	22.66(10)	10.24(19)	21.91(14)	10.3(3)
Py1#1								13.94(16)	26.01(16)	44.3(2)	50.76(16)	26.43(16)
Bz1#1									30.01(12)	36.93(17)	47.71(11)	17.17(15)
Bz2#1										29.50(16)	27.88(13)	24.35(12)
Py2#1											16.22(16)	19.78(19)
Bz3#1												31.99(14)
Bz4#1												

Table S36 Selected bond distances (Å), bond angles (°) in $[(\mathbf{L4})_2Er((CH_3)NO_2)_2Er(\mathbf{L4})_2](ClO_4)_6$ (**10**).

Bond distances (Å)

Atom 1	Atom 2	Distance	Atom 1	Atom 2	Distance
Er(1)	O(3)	2.207(4)	Er(2)	O(2)	2.228(4)
Er(1)	O(1)	2.240(4)	Er(2)	O(4)	2.239(4)
Er(1)	N(4)	2.446(4)	Er(2)	N(16)	2.463(5)
Er(1)	N(9)	2.470(4)	Er(2)	N(19)	2.467(5)
Er(1)	N(6)	2.477(4)	Er(2)	N(14)	2.473(5)
Er(1)	N(1)	2.481(5)	Er(2)	N(11)	2.482(4)
Er(1)	N(8)	2.518(5)	Er(2)	N(13)	2.535(5)
Er(1)	N(3)	2.525(5)	Er(2)	N(18)	2.540(5)

Angles (°)

At. 1	At. 2	At. 3	angle	At. 1	At. 2	At. 3	angle
O(1)	Er(1)	N(1)	96.68(15)	O(2)	Er(2)	N(13)	139.97(15)
O(1)	Er(1)	N(3)	69.73(15)	O(2)	Er(2)	N(14)	155.64(16)
O(1)	Er(1)	N(4)	82.21(15)	O(2)	Er(2)	N(16)	88.14(17)
O(1)	Er(1)	N(6)	74.97(15)	O(2)	Er(2)	N(18)	69.75(15)
O(1)	Er(1)	N(8)	136.97(14)	O(2)	Er(2)	N(19)	89.30(17)
O(1)	Er(1)	N(9)	156.84(15)	O(4)	Er(2)	N(11)	80.52(16)
O(3)	Er(1)	O(1)	90.24(15)	O(4)	Er(2)	N(13)	71.21(16)
O(3)	Er(1)	N(1)	153.42(16)	O(4)	Er(2)	N(14)	100.22(17)
O(3)	Er(1)	N(3)	141.10(16)	O(4)	Er(2)	N(16)	155.98(16)
O(3)	Er(1)	N(4)	80.42(16)	O(4)	Er(2)	N(18)	137.32(16)
O(3)	Er(1)	N(6)	83.14(15)	O(4)	Er(2)	N(19)	77.58(17)
O(3)	Er(1)	N(8)	71.97(16)	N(11)	Er(2)	N(13)	64.48(16)
O(3)	Er(1)	N(9)	94.55(15)	N(11)	Er(2)	N(18)	128.17(16)
N(1)	Er(1)	N(3)	64.65(16)	N(13)	Er(2)	N(18)	145.33(16)
N(1)	Er(1)	N(8)	85.78(16)	N(14)	Er(2)	N(11)	125.32(17)
N(4)	Er(1)	N(1)	125.88(17)	N(14)	Er(2)	N(13)	64.38(16)
N(4)	Er(1)	N(3)	64.47(16)	N(14)	Er(2)	N(18)	87.56(16)
N(4)	Er(1)	N(6)	151.71(16)	N(16)	Er(2)	N(11)	75.91(15)
N(4)	Er(1)	N(8)	130.04(15)	N(16)	Er(2)	N(13)	94.21(17)
N(4)	Er(1)	N(9)	76.30(16)	N(16)	Er(2)	N(14)	89.81(17)
N(6)	Er(1)	N(1)	74.04(15)	N(16)	Er(2)	N(18)	64.23(16)
N(6)	Er(1)	N(3)	120.51(15)	N(16)	Er(2)	N(19)	126.40(16)
N(6)	Er(1)	N(8)	64.44(15)	N(19)	Er(2)	N(11)	154.14(17)
N(8)	Er(1)	N(3)	144.29(15)	N(19)	Er(2)	N(13)	119.75(17)
N(9)	Er(1)	N(1)	89.10(15)	N(19)	Er(2)	N(14)	72.54(18)
N(9)	Er(1)	N(3)	92.97(15)	N(19)	Er(2)	N(18)	64.82(17)
N(9)	Er(1)	N(6)	128.08(16)	N(21)	O(1)	Er(1)	146.1(3)
N(9)	Er(1)	N(8)	65.65(15)	N(21)	O(2)	Er(2)	146.8(4)
O(2)	Er(2)	O(4)	91.25(16)	N(22)	O(3)	Er(1)	161.4(4)
O(2)	Er(2)	N(11)	77.55(16)	N(22)	O(4)	Er(2)	155.9(4)

Table S37 Selected least-squares planes data for [(**L4**)$_2$Er((CH$_3$)NO$_2$)$_2$Er(**L4**)$_2$](ClO$_4$)$_6$ (**10**).

Least-squares planes

Least-squares planes description	Abbreviation	Max. deviation/Å	Atom
Pyridine 1 N(3) C(9) C(10) C(11) C(12) C(13)	Py1	0.021	C(9)
Benzimidazole 1 C(1) C(2) C(3) C(4) C(5) C(6) N(1) C(8) N(2)	Bz1	0.030	C(2)
Benzimidazole 2 C(16) C(17) C(18) C(19) C(20) C(21) N(4) C(14) N(5)	Bz2	0.046	C(14)
Pyridine 2 N(8) C(30) C(31) C(32) C(33) C(34)	Py2	0.025	N(8)
Benzimidazole 3 C(22) C(23) C(24) C(25) C(26) C(27) N(6) C(29) N(7)	Bz3	0.046	C(27) C(29)
Benzimidazole 4 C(37) C(38) C(39) C(40) C(41) C(42) N(9) C(35) N(10)	Bz4	0.025	N(9)
Pyridine 3 N(13) C(72) C(73) C(74) C(75) C(76)	Py3	0.015	N(13)
Benzimidazole 5 C(71) C(72) C(73) C(74) C(75) C(76) N(11) C(71) N(12)	Bz5	0.030	C(64)
Benzimidazole 6 C(79) C(80) C(81) C(82) C(83) C(84) N(14) C(77) N(15)	Bz6	0.020	C(83)
Pyridine 4 N(18) C(51) C(52) C(53) C(54) C(55)	Py4	0.022	C(51)
Benzimidazole 7 C(43) C(44) C(45) C(46) C(47) C(48) N(16) C(50) N(17)	Bz7	0.019	C(50)
Benzimidazole 8 C(58) C(59) C(60) C(61) C(62) C(63) N(19) C(56) N(20)	Bz8	0.027	C(63)

Interplanar angles (°)

	Py1	Bz1	Bz2	Py2	Bz3	Bz4	Py3	Bz5	Bz6	Py4	Bz7	Bz8
Py1		15.95(17)	16.17(17)	61.7(2)	33.67(16)	97.83(16)	51.3(2)	29.28(17)	56.76(17)	13.9(2)	9.97(19)	25.9(2)
Bz1			21.60(13)	52.81(18)	20.94(15)	112.28(13)	43.94(19)	29.92(11)	54.15(14)	13.12(17)	13.99(12)	12.39(19)
Bz2				48.64(19)	27.84(12)	105.35(13)	37.74(19)	13.39(15)	40.90(14)	27.97(19)	25.04(16)	23.45(15)
Py2					32.6(2)	33.31(19)	11.0(2)	36.8(2)	20.40(19)	65.9(2)	65.91(18)	40.8(2)
Bz3						48.62(13)	25.4(2)	25.50(14)	39.22(18)	33.97(18)	34.81(13)	8.5(2)
Bz4							42.2(2)	66.06(16)	53.37(15)	79.16(16)	98.60(11)	56.30(19)
Py3								25.8(2)	16.2(2)	56.8(2)	56.32(19)	32.7(2)
Bz5									27.53(15)	39.54(18)	37.30(15)	25.56(14)
Bz6										65.77(18)	64.15(15)	44.89(18)
Py4											4.27(19)	25.4(2)
Bz7												26.29(18)
Bz8												

Table S38 Photophysical data for ligands **L4**-**L9** in the solid-state and in acetonitrile solution (0.3 mM) at various temperatures.

Compounds	State / solvent	T / K	E /cm^{-1} [a] Absorption ($^1\pi^* \leftarrow {}^1\pi$)	E /cm^{-1} [a] Emission ($^1\pi^* \rightarrow {}^1\pi$)	$\tau(^1\pi^*)$ / ns
L4	Solid	77		27317 sh 25966 24575 23109 sh 21597 sh	
		293		25448 21201	
	CH_3CN[a]	77		27333 sh 26481 25053 sh	
		293	48808 45044 sh 40807 sh 31056 29851 sh	26991	1.6 (100%)
L5	Solid	77		25664 24735 23257 sh 21437 19983 sh	
		293		25522 sh 24487 23223	
	CH_3CN	77		26918 sh 25608 24096 sh	
		293	48870 45045 sh 41152 sh 36232 sh 31056 29940 sh	26455	2.0 (100%)

L6	Solid	77		26270 sh 25511 sh 24802 sh 23865 22410	
		293	43809 37339 sh 29597 26222 sh 22638 sh	25331 sh 24013 21027[d]	
	CH_3CN	77	47847 44053 sh 40650 sh	26248 sh 24654 23353 sh	
		293	36232 sh 30581 29326 sh	26497	1.9 (100%)
L7	Solid	77		25895 24537 sh 23311 21757 19735	
		293	46508 sh 40869 35889 32148, 29561 sh 21491	27021 26056 sh 23273 21863 sh 20687 19197 sh	
	CH_3CN[a]	77		30573, 29605, 28801 sh 28801 sh 26993	< 0.3 (100%)
		293	42194 39841 sh 36232 33113, 31949 sh	24831 sh 30817 sh 29985 28531 sh	

L8	Solid	77		29168 27709 sh 26160 25195 sh 21481	
		293		28860 sh 27704 26385 sh	
	CH_3CN	77		30187 sh 29066 27626 26245	
		293	42918 sh 40984 39062 sh 34843 32680 sh 31348 sh	30817 sh 29586 28129 sh	< 0.3 (83%) 1.7 (17%)
L9	Solid	77		29090 sh 27675 sh 26424 25682,24293, 22988 sh 21375	
		293		20804 28656 sh 27436 24096 sh	
	CH_3CN	77		22820 sh 30110 sh 28977 27531	
		293	42918 sh 40816 39062 sh 34843 32680, 31348 sh	26493 sh 30769 sh 29499 28050 sh	< 0.3 (91%) 0.6 (9%)

[a] Maximum of the band envelope.

Table S39 Photophysical data recorded for the complexes **1**-**3** in acetonitrile solution (3.0 mM) at different temperatures.

Compounds	*T* / K	*E* /cm^{-1} [a] Absorption ($^1\pi^* \leftarrow {}^1\pi$)	*E* /cm^{-1} [a] Emission ($^1\pi^* \rightarrow {}^1\pi$)
[Er(**L4**)$_2$(O$_3$SCF$_3$)$_2$](CF$_3$SO$_3$) (**1**)	77		24331 sh
			23613
	293	49330 sh	23669
		44682 sh	
		40462 sh	
		32921	
		27701	
[Er(**L7**)$_2$(O$_3$SCF$_3$)$_2$](CF$_3$SO$_3$) (**2**)	77		27663 sh
			26882
			25211 sh
			24323 sh
	293	35714 sh	28011 sh
		34602	26991
		30211	
		29070 sh	
Er(**L8**)$_2$(O$_3$SCF$_3$)$_3$ (**3**)	77		27027 sh
			26042
			24752
	293	25088 sh	27397 sh
		33898	26385
		29499	
		28571 sh	

[a] Maximum of the band envelope.

Table S40 Experimental lifetimes, radiative lifetimes and intrinsic quantum yields of the complexes **1**-**7** in the solid state at room temperature.

Compound	$\tau_{\mathrm{Er,obs}}^{^4\mathrm{I}_{13/2}}$ /μs	$\tau_{\mathrm{Er,rad}}^{^4\mathrm{I}_{13/2}}$ /ms [a]	$Q_{\mathrm{Er}}^{\mathrm{Er}}\left(^4\mathrm{I}_{13/2}\right)$ /% [b]	$\tau_{\mathrm{Er,obs}}^{^4\mathrm{S}_{3/2}}$ /ns	$\tau_{\mathrm{Er,rad}}^{^4\mathrm{S}_{3/2}}$ /μs [a]	$Q_{\mathrm{Er}}^{\mathrm{Er}}\left(^4\mathrm{S}_{3/2}\right)$ /% [b]
[Er(**L4**)$_2$(O_3SCF_3)$_2$](CF_3SO_3) (**1**)	4.06(2)	6.3	0.064	10.9(5)	546	0.0020
[Er(**L7**)$_2$(O_3SCF_3)$_2$](CF_3SO_3) (**2**)	1.61(1)	6.1	0.026	8.9(4)	515	0.0017
Er(**L8**)$_2$(O_3SCF_3)$_3$ (**3**)	2.76(2)	5.6	0.049	9.0(3)	453	0.0020
[Er(**L6**)$_3$](ClO_4)$_3$ (**4**)	5.57(6)	6.3	0.088		716	
[Er(**L7**)$_3$](ClO_4)$_3$ (**5**)	1.88(2)	6.4	0.029		476	
[Er(**L8**)$_3$](ClO_4)$_3$ (**6**)	2.18(1)	6.1	0.036		493	
[Er(**L9**)$_3$](ClO_4)$_3$ (**7**)	1.94(2)	6.1	0.032		495	

[a]Taken from Table 2. [b] $Q_{\mathrm{Er}}^{\mathrm{Er}}\left(^{2S+1}L_J\right)=\tau_{\mathrm{Er,exp}}^{^{2S+1}\mathrm{L}_J}\Big/\tau_{\mathrm{Er,rad}}^{^{2S+1}\mathrm{L}_J}$.

Table S41 Photophysical data for the complexes **4**-**7** in acetonitrile solution (3.0 mM) and in the solid-state at various temperatures.

Compounds	State / solvent	T / K	E /cm^{-1} [a] Absorption ($^1\pi^* \leftarrow {}^1\pi$)	E /cm^{-1} [a] Emission ($^1\pi^* \rightarrow {}^1\pi$)
[Er(**L6**)$_3$](ClO$_4$)$_3$ (**4**)	Solid	293	29176 24402	
	CH_3CN	77		23950 22849 sh 21275 sh
		293	44586 sh 39776 sh 32354 26653	24063 sh 23154
[Er(**L7**)$_3$](ClO$_4$)$_3$ (**5**)	Solid	293	42085 35527 33457 sh	27866 sh 26139
	CH_3CN	77	27821	27610 sh 26681 25339 sh 23225 sh
		293	42918 sh 37453 35461 sh 34130 30120 29170 sh	27854 sh 26792
[Er(**L8**)$_3$](ClO$_4$)$_3$ (**6**)	Solid	293		27076 sh 25596
	CH_3CN	77		27401 sh 26050 24488 sh
		293	47847 40161 sh 37879 sh 35088 sh 33898 29499 28571 sh	27173 sh 26359 23189 sh
[Er(**L9**)$_3$](ClO$_4$)$_3$ (**7**)	CH_3CN	77		26678 sh 25958 24582 sh
		293	49504 40000 sh 33445 29412 28329 sh	27208 26119 sh 23158 sh

[a] Maximum of the band envelope.

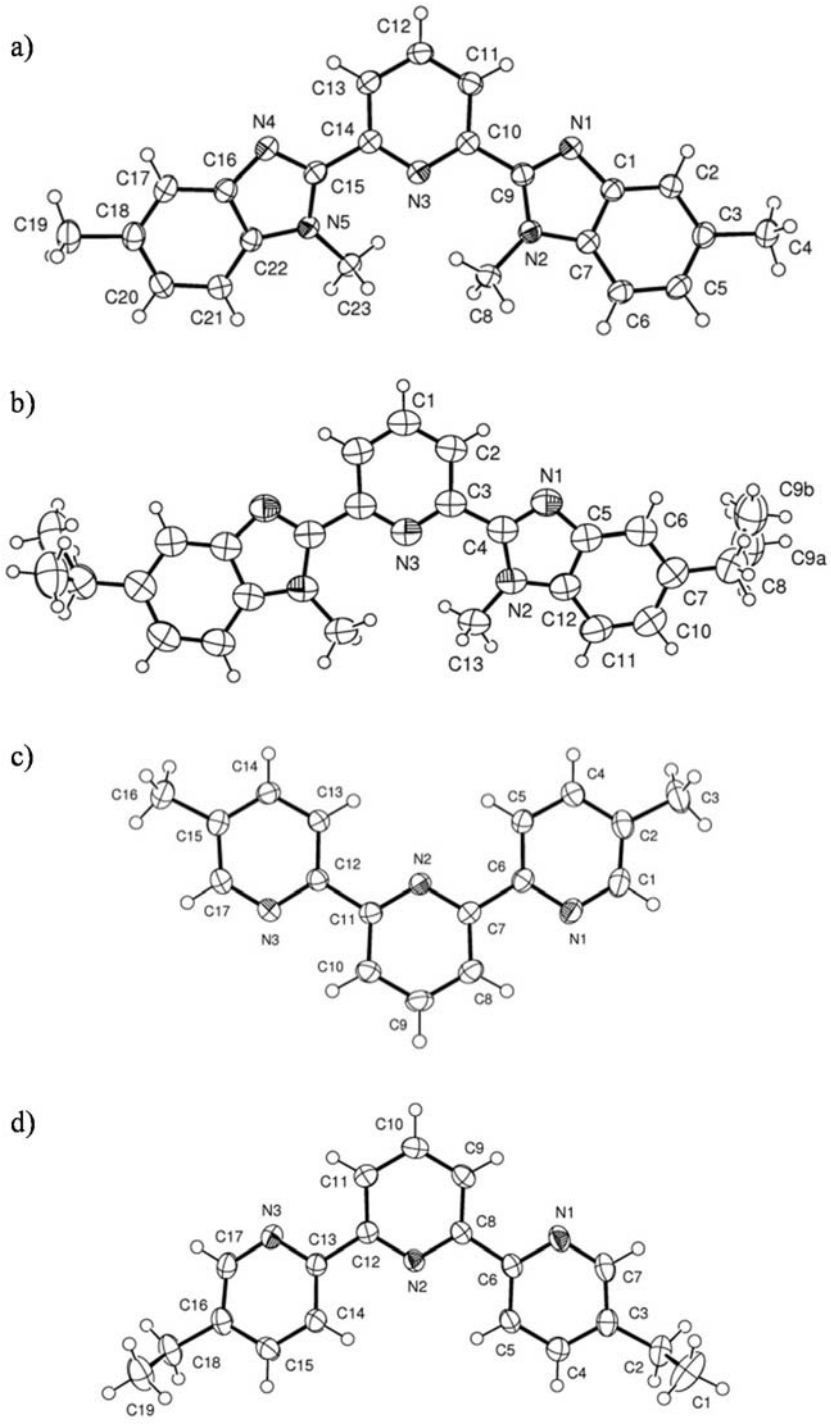

Figure S1 Molecular structures with numbering scheme of the asymmetric units of a) **L5**, b) **L6**, c) **L8** and d) **L9**. The thermal ellipsoids are represented at the 50% probability level.

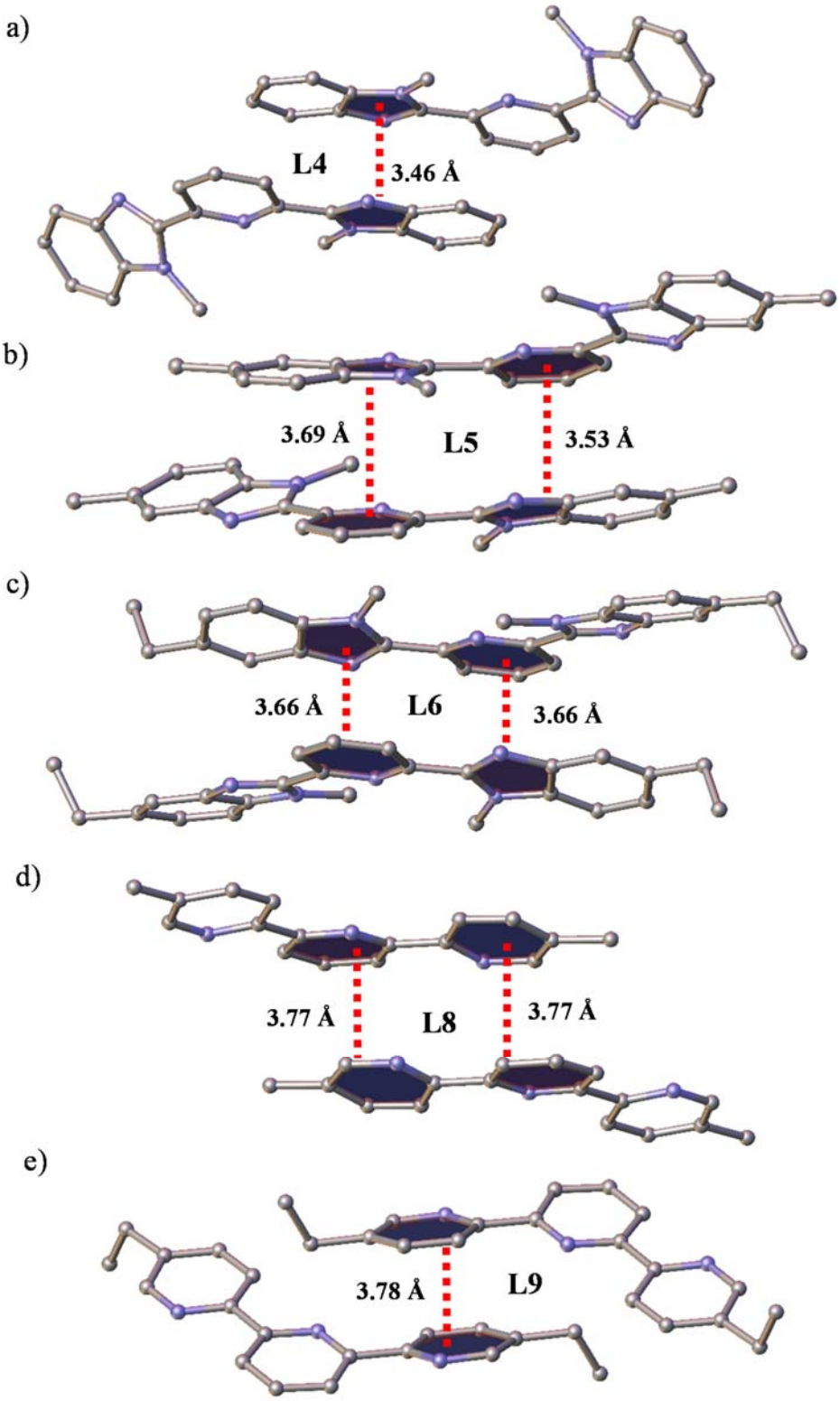

Figure S2 Perspective views of ligands a) **L4**, b) **L5**, c) **L6**, d) **L8** and e) **L9** showing the shortest intermolecular π-π interactions occurring between parallel aromatic units in the crystals.

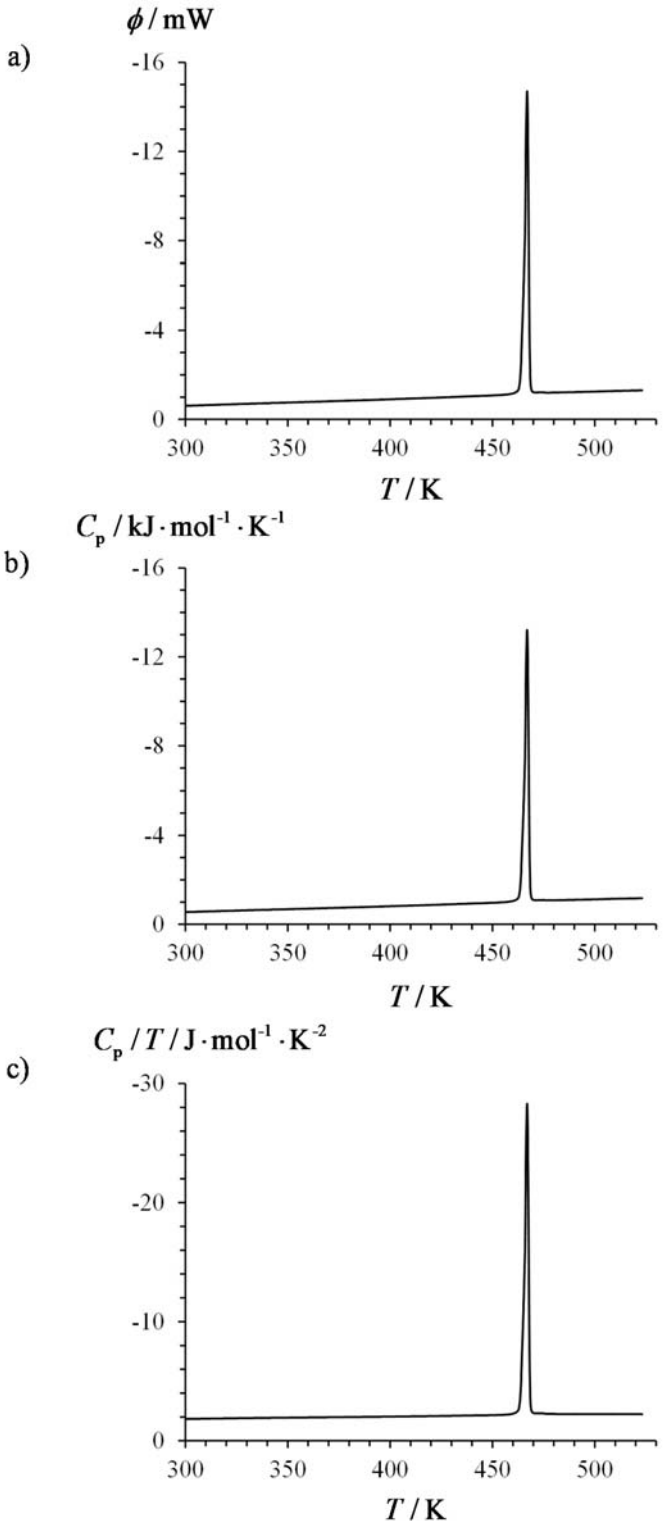

Figure S3 a) DSC traces recorded at 0.5 K/min for the ligand **L4** and its transformation into b) molar heat capacity ($\phi = \frac{\Delta W}{\Delta t} = \frac{nC_p\Delta T}{\Delta t} = nC_p\nu \Rightarrow C_p = \frac{\phi}{n\nu}$ with $\nu = \frac{\Delta T}{\Delta t}$ being the scanning rate and n the number of moles)[42a] and c) molar capacity per temperature unit.

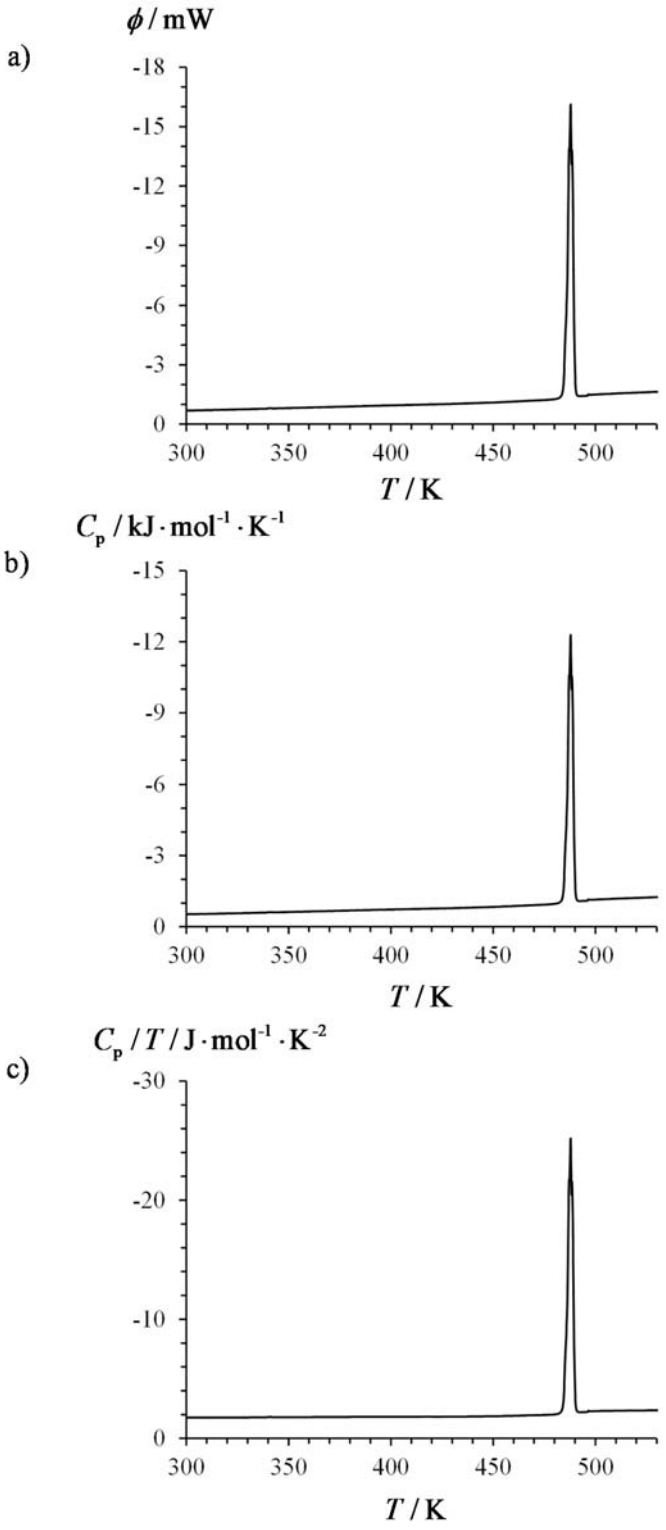

Figure S4 a) DSC traces recorded at 0.5 K/min for the ligand **L5** and its transformation into b) molar heat capacity ($\phi = \frac{\Delta W}{\Delta t} = \frac{nC_p\Delta T}{\Delta t} = nC_p\nu \Rightarrow C_p = \frac{\phi}{n\nu}$ with $\nu = \frac{\Delta T}{\Delta t}$ being the scanning rate and n the number of moles)[42a] and c) molar capacity per temperature unit.

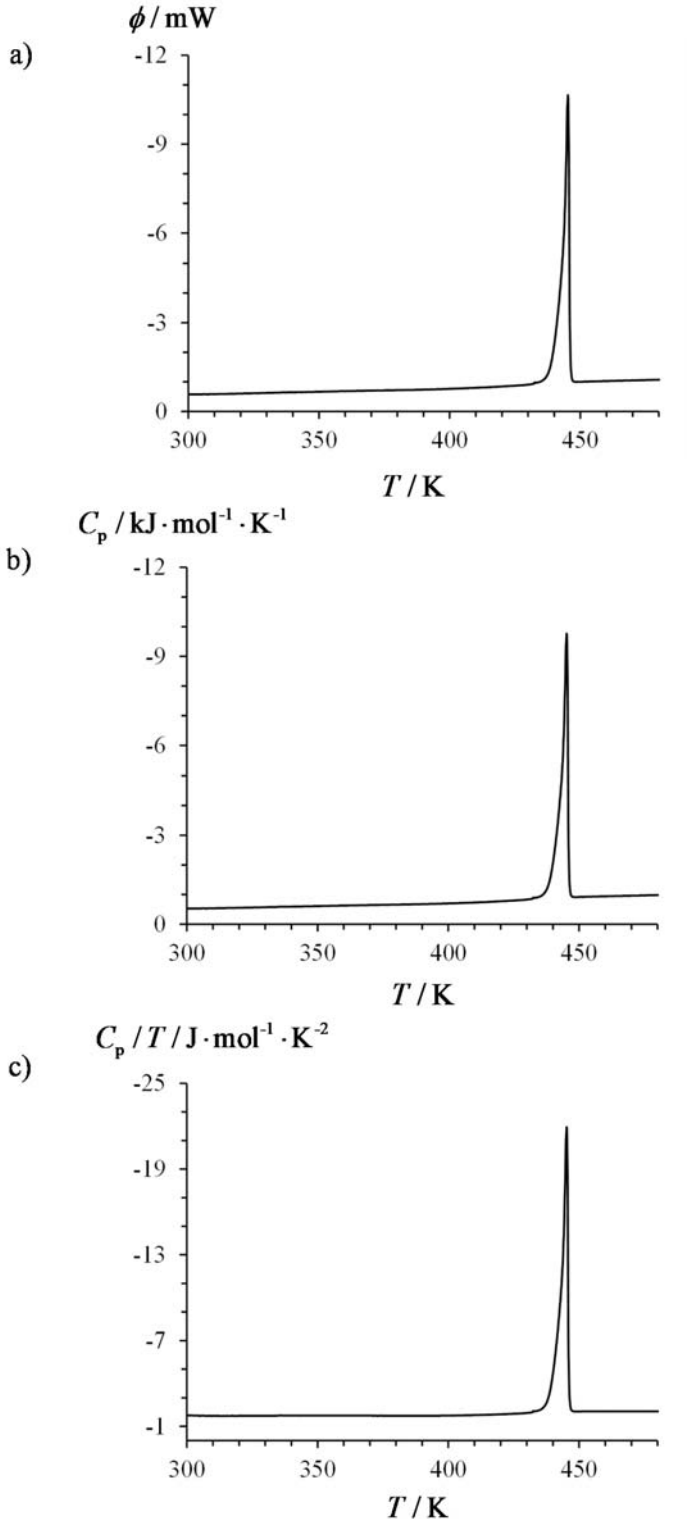

Figure S5 a) DSC traces recorded at 0.5 K/min for the ligand **L6** and its transformation into b) molar heat capacity ($\phi = \frac{\Delta W}{\Delta t} = \frac{nC_p\Delta T}{\Delta t} = nC_p\nu \Rightarrow C_p = \frac{\phi}{n\nu}$ with $\nu = \frac{\Delta T}{\Delta t}$ being the scanning rate and n the number of moles)[42a] and c) molar capacity per temperature unit.

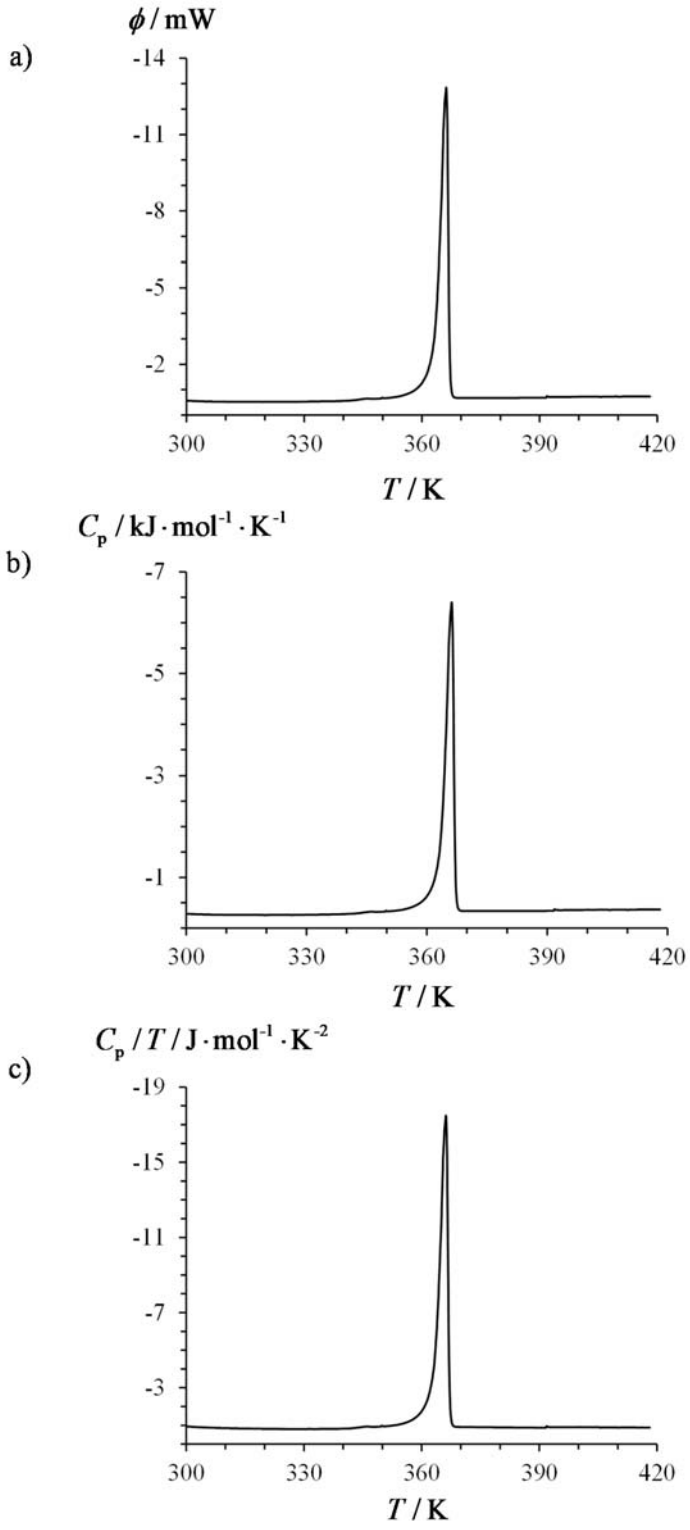

Figure S6 a) DSC traces recorded at 0.5 K/min for the ligand **L7** and its transformation into b) molar heat capacity ($\phi = \frac{\Delta W}{\Delta t} = \frac{nC_p\Delta T}{\Delta t} = nC_p\nu \Rightarrow C_p = \frac{\phi}{n\nu}$ with $\nu = \frac{\Delta T}{\Delta t}$ being the scanning rate and n the number of moles)[42a] and c) molar capacity per temperature unit.

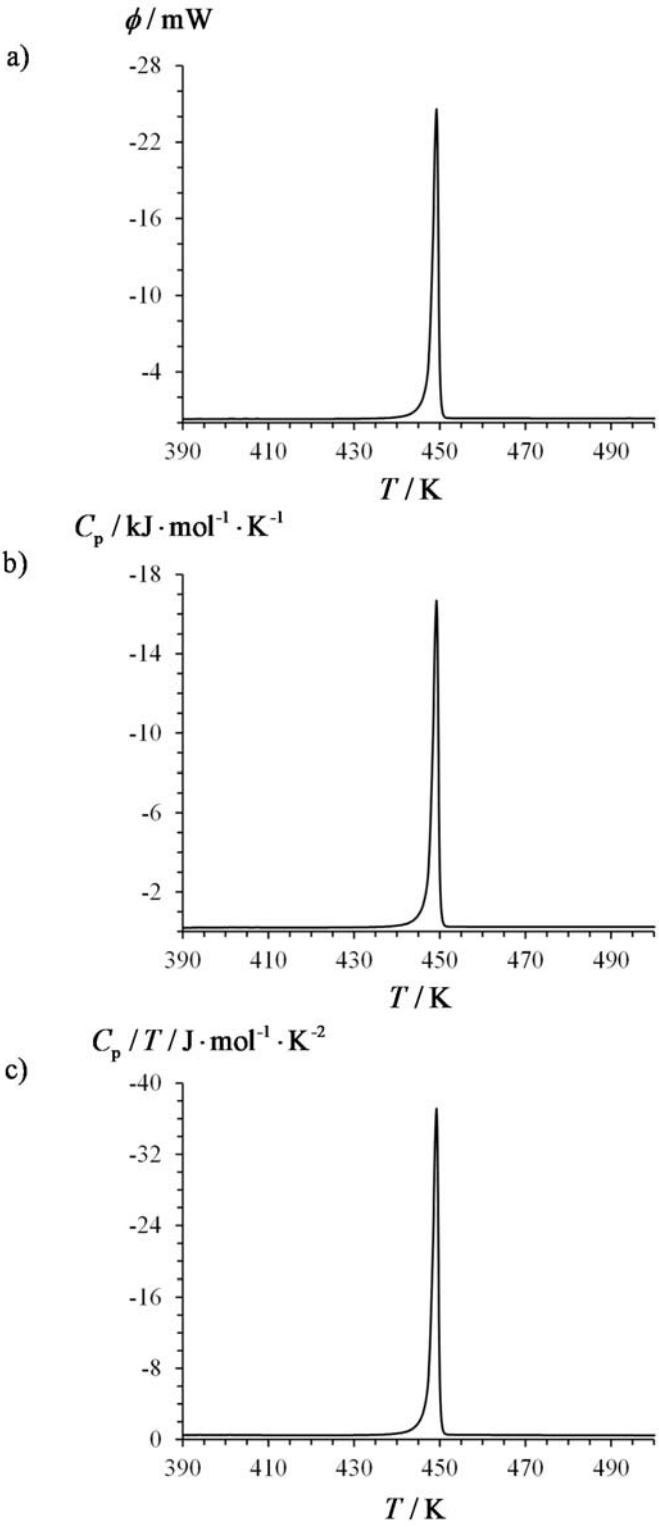

Figure S7 a) DSC traces recorded at 0.5 K/min for the ligand **L8** and its transformation into b) molar heat capacity ($\phi = \frac{\Delta W}{\Delta t} = \frac{nC_p\Delta T}{\Delta t} = nC_p\nu \Rightarrow C_p = \frac{\phi}{n\nu}$ with $\nu = \frac{\Delta T}{\Delta t}$ being the scanning rate and n the number of moles)[42a] and c) molar capacity per temperature unit.

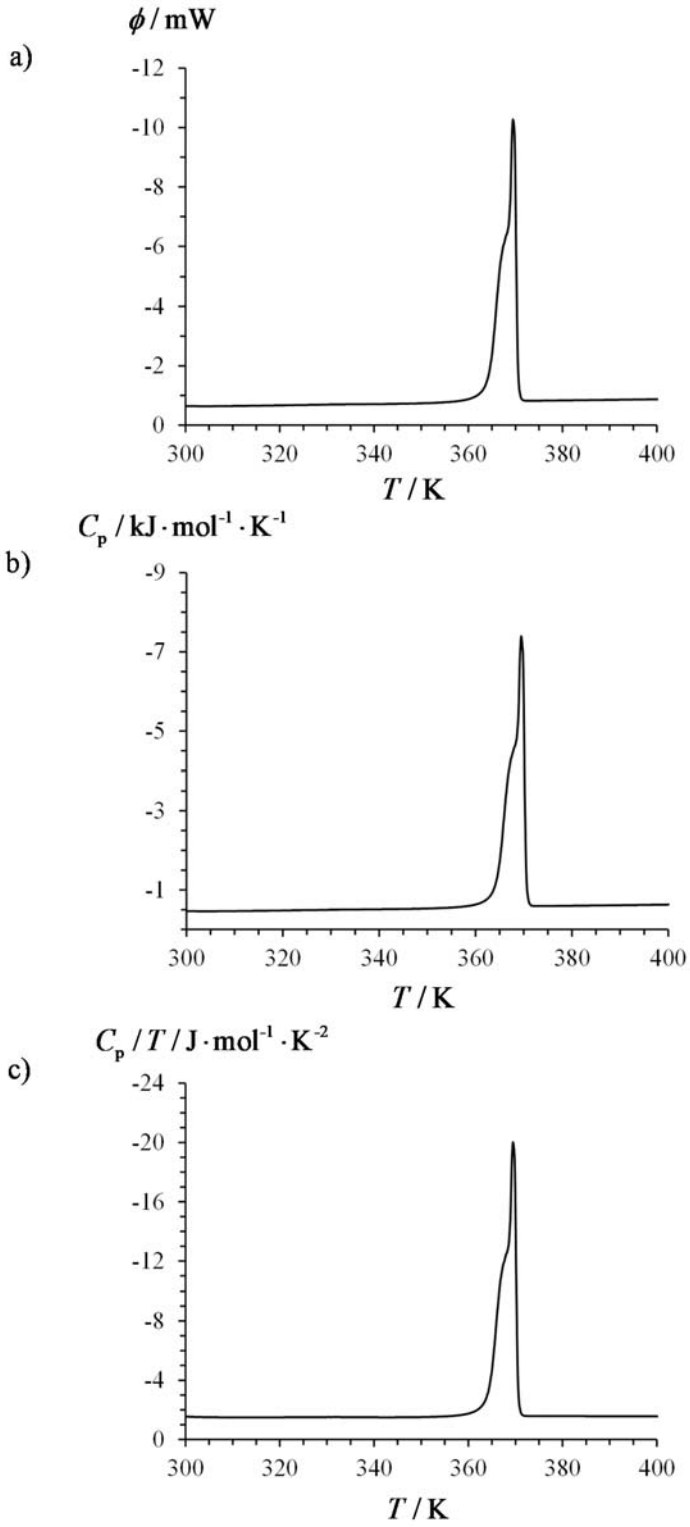

Figure S8 a) DSC traces recorded at 0.5 K/min for the ligand **L9** and its transformation into b) molar heat capacity ($\phi = \frac{\Delta W}{\Delta t} = \frac{nC_p\Delta T}{\Delta t} = nC_p\nu \Rightarrow C_p = \frac{\phi}{n\nu}$ with $\nu = \frac{\Delta T}{\Delta t}$ being the scanning rate and n the number of moles)[42a] and c) molar capacity per temperature unit.

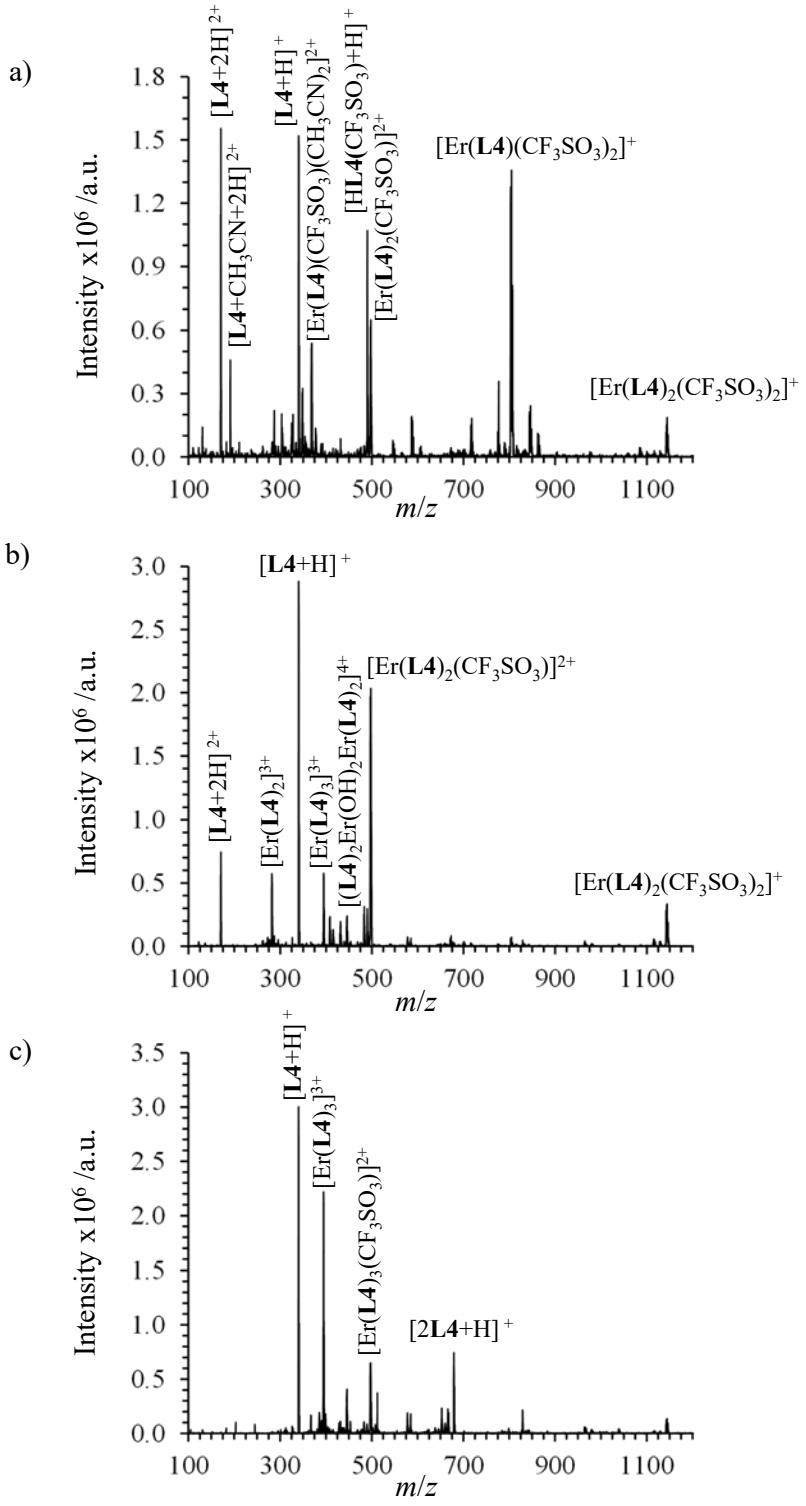

Figure S9 ESI-MS spectra recorded upon titration of **L4** with $Er(CF_3SO_3)_3$ (total ligand concentration: 2.0×10^{-3} M in acetonitrile, 298 K) for stoichiometric ratios a) $[Er]_{tot}/[\mathbf{L4}]_{tot} = 1.00$, b) $[Er]_{tot}/[\mathbf{L4}]_{tot} = 0.50$ and c) $[Er]_{tot}/[\mathbf{L4}]_{tot} = 0.33$.

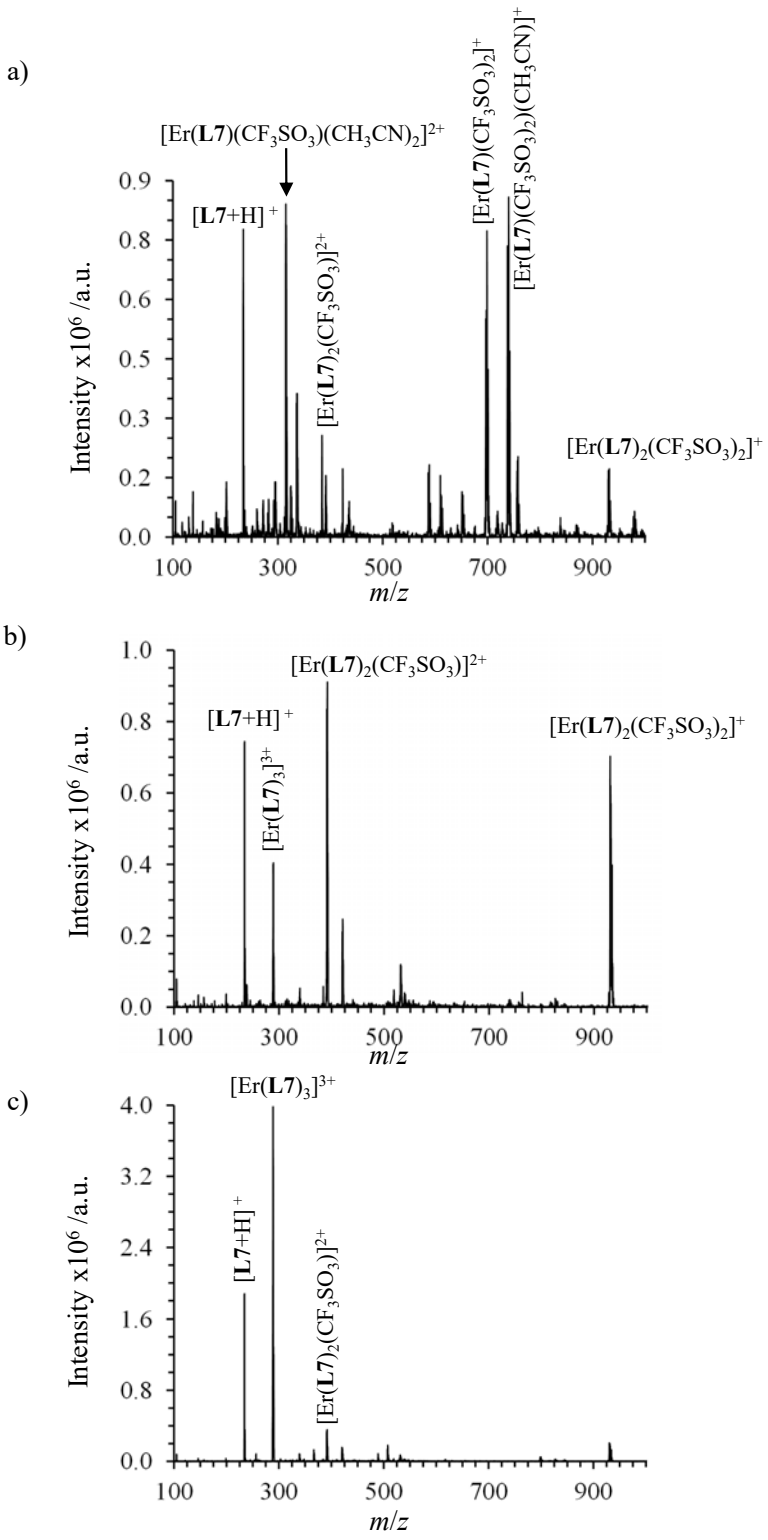

Figure S10 ESI-MS spectra upon titration of **L7** with $Er(CF_3SO_3)_3$ (total ligand concentration: 2.0×10^{-3} M in acetonitrile, 298 K) at stoichiometric ratios a) $[Er]_{tot}/\ [\mathbf{L7}]_{tot} = 1.00$, b) $[Er]_{tot}/\ [\mathbf{L7}]_{tot} = 0.50$ and c) $[Er]_{tot}/\ [\mathbf{L7}]_{tot} = 0.33$.

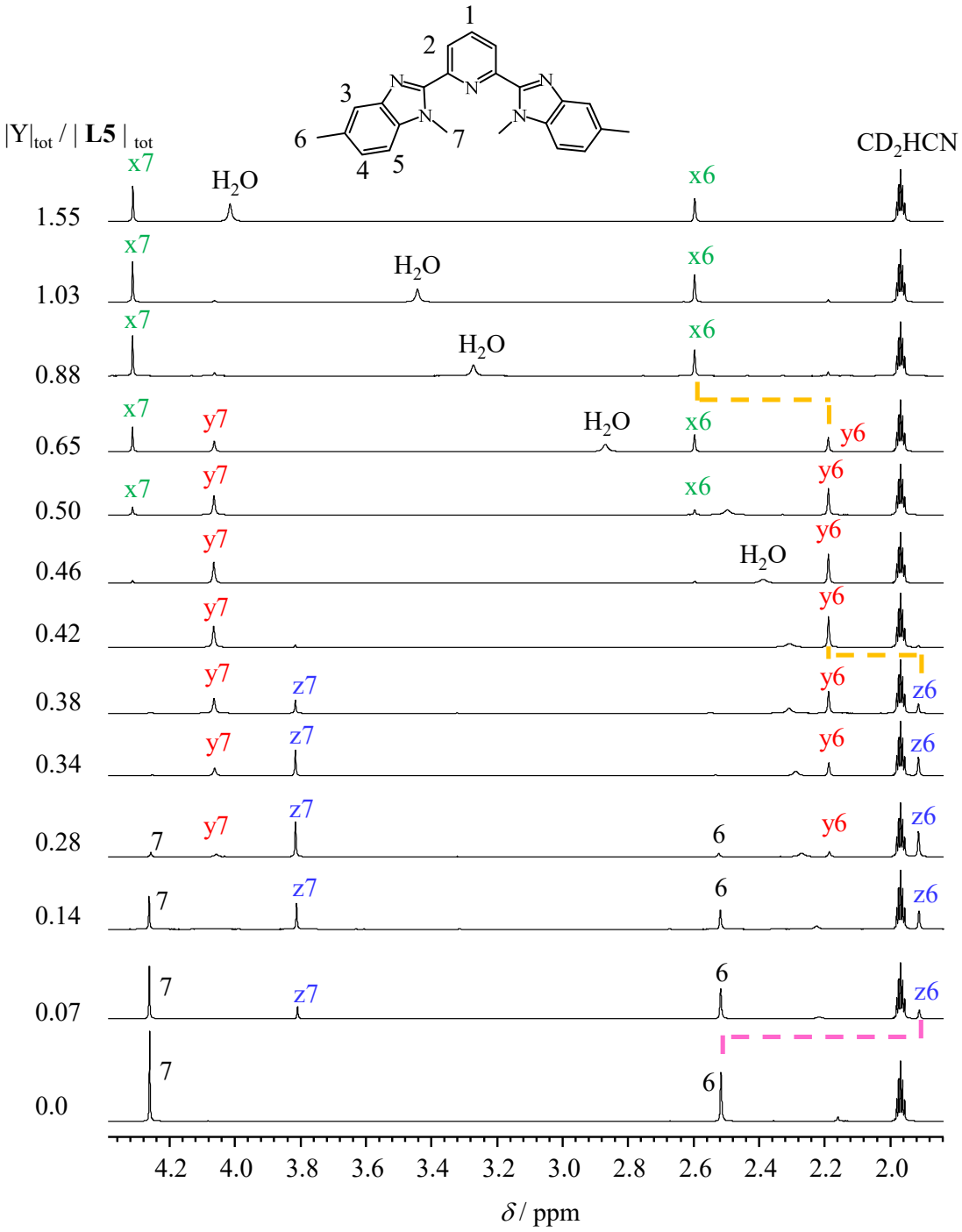

Figure S11 Aliphatic parts of the ^{1}H NMR spectra with numbering scheme recorded upon titration of **L5** with $Y(CF_3SO_3)_3$ in CD_3CN at 298 K with numbering scheme. ($5\times10^{-3} \leq |\mathbf{L5}|_{tot} \leq 9\times10^{-3}$ M and $6\times10^{-4} \leq |Y|_{tot} \leq 8\times10^{-3}$ M). The letters x, y and z denote signals arising from the 1:1 (green), 1:2 (red) and 1:3 (blue) species, respectively.

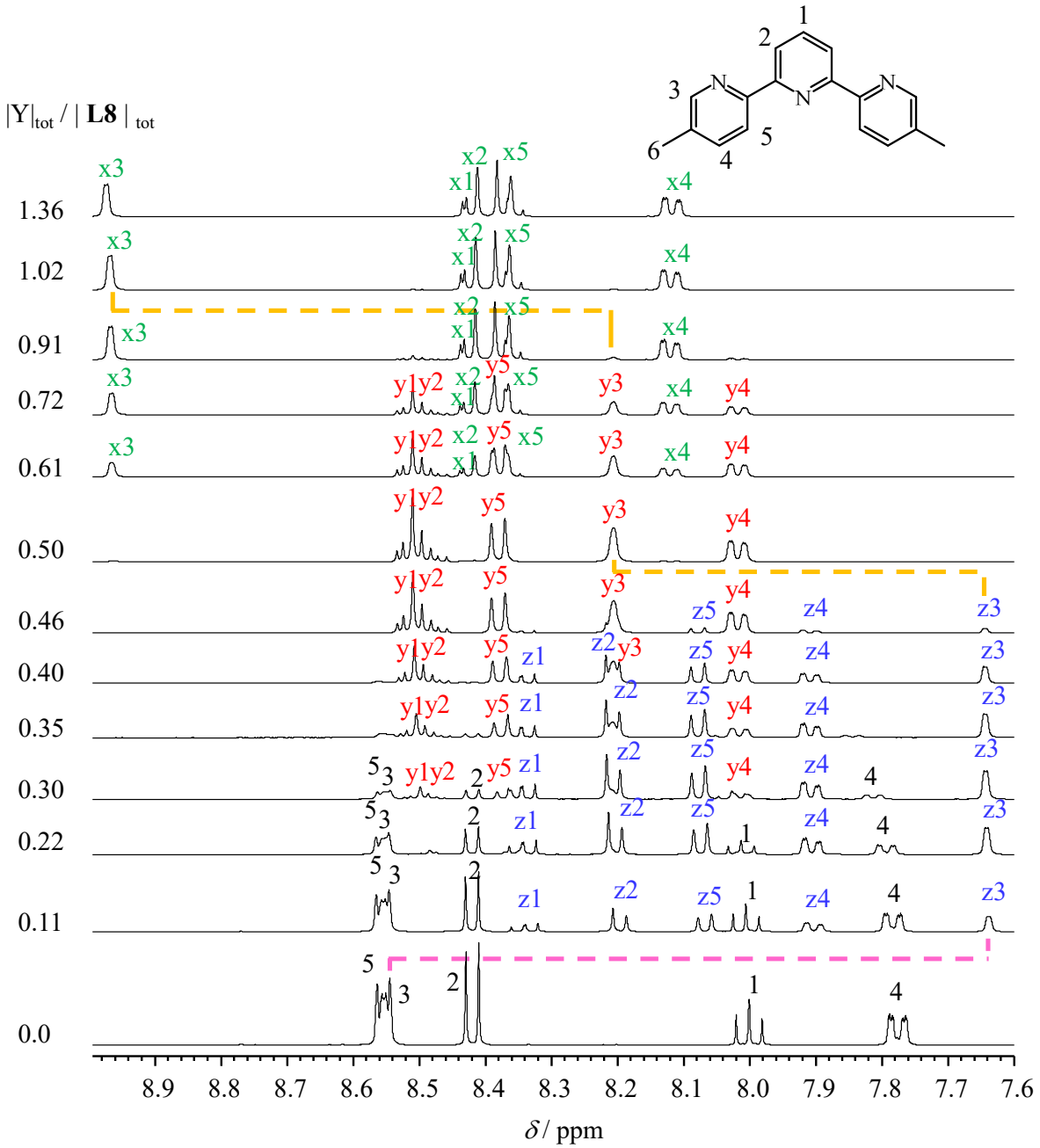

Figure S12 Aromatic parts of the ^{1}H NMR spectra with numbering scheme recorded upon titration of **L8** with $Y(CF_3SO_3)_3$ in CD_3CN at 298 K with numbering scheme. ($5\times10^{-3} \leq |\mathbf{L8}|_{tot} \leq 9\times10^{-3}$ M and $6\times10^{-4} \leq |Y|_{tot} \leq 8\times10^{-3}$ M). The letters x, y and z denote signals arising from the 1:1 (green), 1:2 (red) and 1:3 (blue) species, respectively.

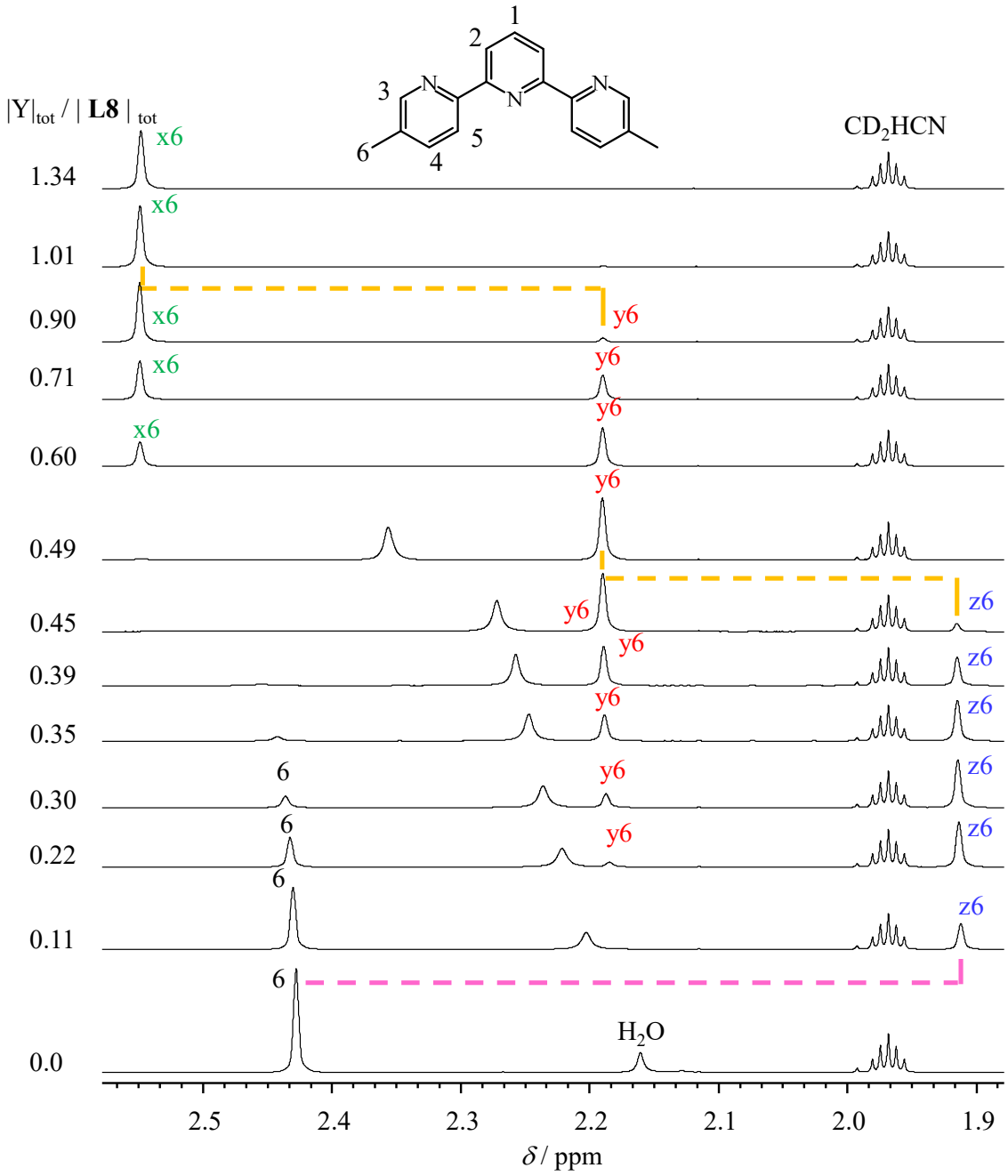

Figure S13 Aliphatic parts of the ^{1}H NMR spectra with numbering scheme recorded upon titration of **L8** with $Y(CF_3SO_3)_3$ in CD_3CN at 298 K with numbering scheme. ($5\times10^{-3} \leq |\mathbf{L8}|_{tot} \leq 9\times10^{-3}$ M and $6\times10^{-4} \leq |Y|_{tot} \leq 8\times10^{-3}$ M). The letters x, y and z denote signals arising from the 1:1 (green), 1:2 (red) and 1:3 (blue) species, respectively.

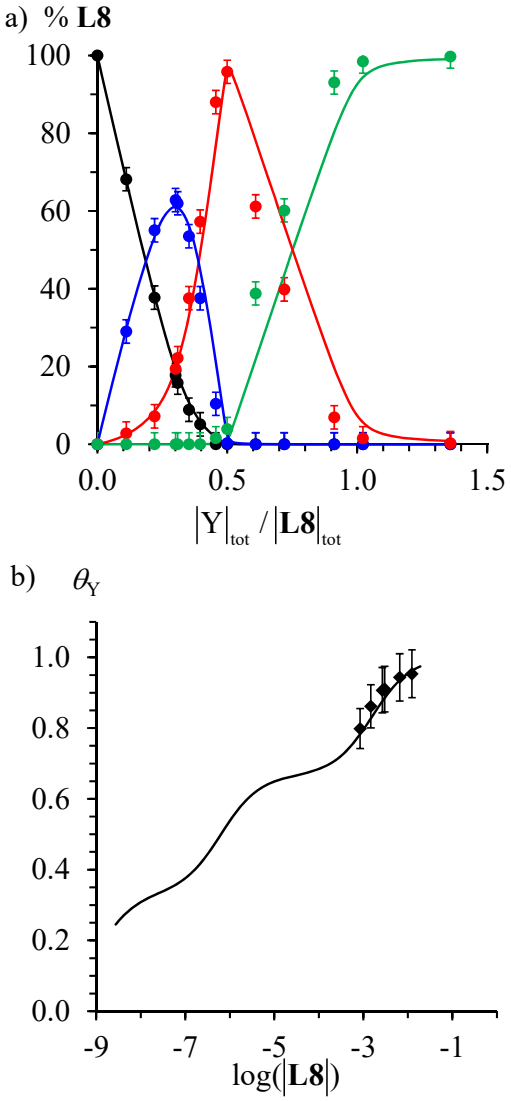

Figure S14 a) Macroscopic ligand speciations obtained by integration of ^{1}H NMR signals during the titration of **L8** (1.8×10^{-2} M) with $Y(CF_3SO_3)_3$ in CD_3CN at 298 K (discs, color code: black = **L8**, blue = $[Y(\mathbf{L8})_3]^{3+}$, red = $[Y(\mathbf{L8})_2]^{3+}$ and green = $[Y(\mathbf{L8})]^{3+}$) and b) associated binding isotherm (diamonds, Eq. (7)). The full traces correspond to the re-constructed a) distribution and b) binding isotherm computed for equilibria (4)-(6) with $\beta_{1,1}^{Y,\mathbf{L8}} = 9.0$, $\beta_{1,2}^{Y,\mathbf{L8}} = 15.2$ and $\beta_{1,3}^{Y,\mathbf{L8}} = 18.0$.

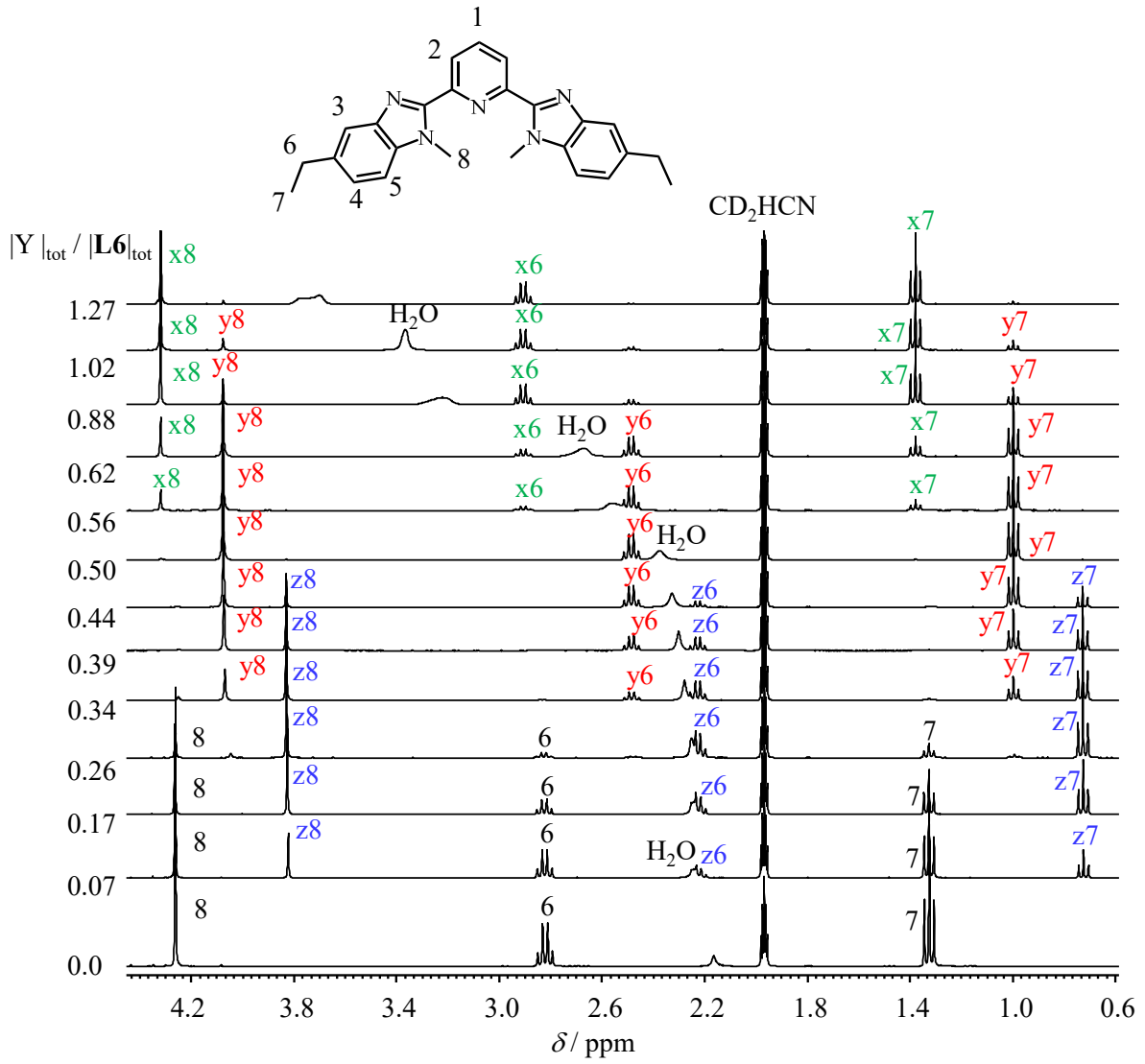

Figure S15 Aliphatic parts of the ^{1}H NMR spectra with numbering scheme recorded upon titration of **L6** with $Y(CF_3SO_3)_3$ in CD_3CN at 298 K with numbering scheme. ($5\times10^{-3} \leq |\mathbf{L6}|_{tot} \leq 9\times10^{-3}$ M and $6\times10^{-4} \leq |Y|_{tot} \leq 8\times10^{-3}$ M). The letters x, y and z denote signals arising from the 1:1 (green), 1:2 (red) and 1:3 (blue) species, respectively.

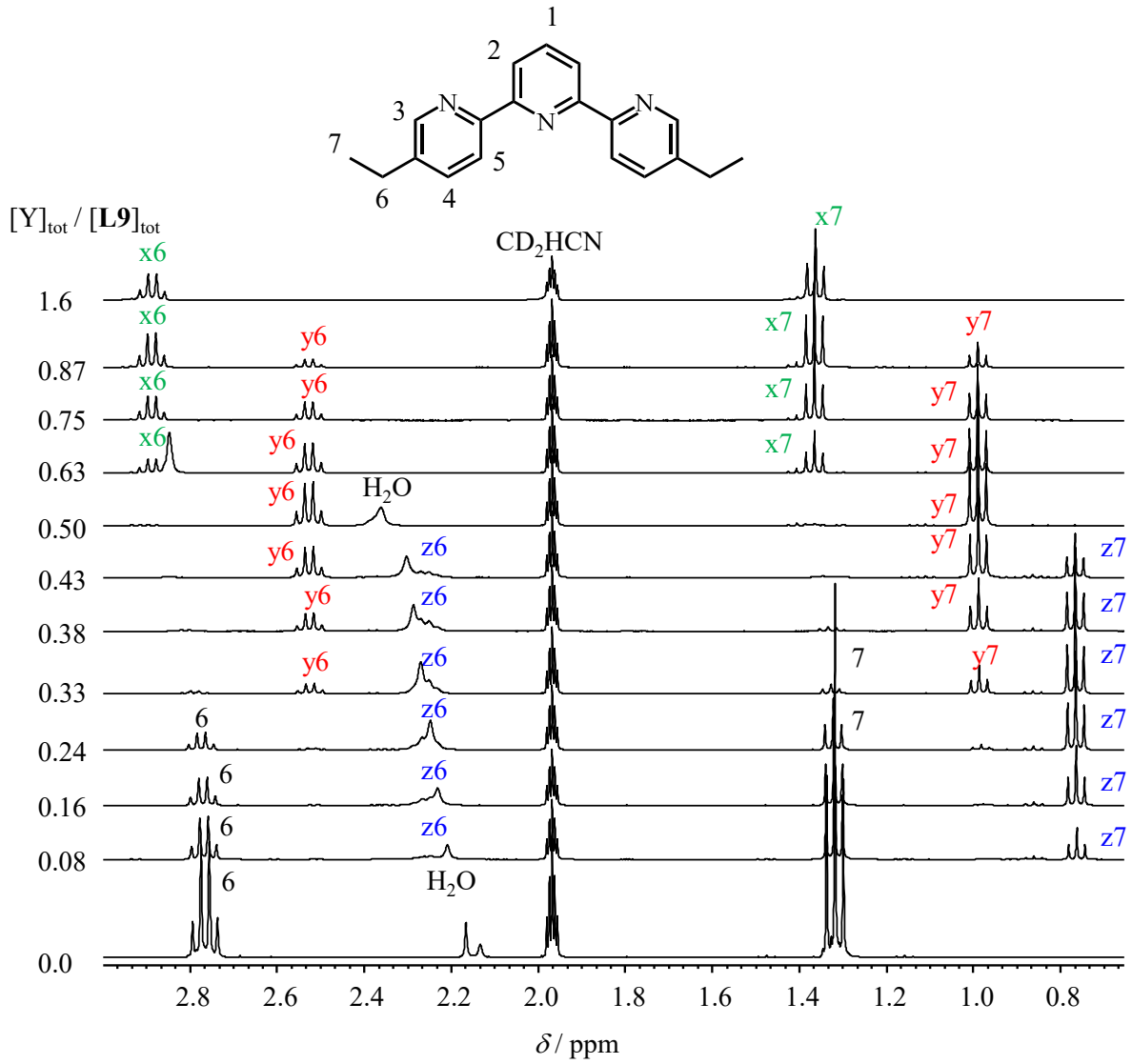

Figure S16 Aliphatic parts of the ^{1}H NMR spectra with numbering scheme recorded upon titration of **L9** with $Y(CF_3SO_3)_3$ in CD_3CN at 298 K with numbering scheme. ($5\times10^{-3} \leq |\mathbf{L9}|_{tot} \leq 9\times10^{-3}$ M and $6\times10^{-4} \leq |Y|_{tot} \leq 8\times10^{-3}$ M). The letters x, y and z denote signals arising from the 1:1 (green), 1:2 (red) and 1:3 (blue) species, respectively.

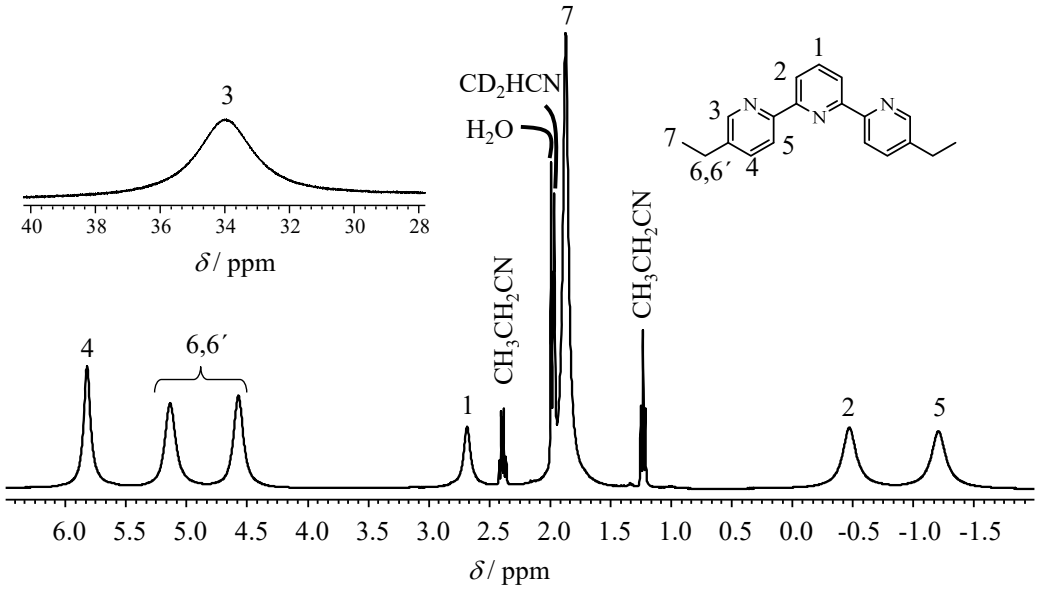

Figure S17 ^{1}H NMR spectrum with numbering scheme of [Er(**L9**)$_3$](ClO$_4$)$_3$·0.05CH$_3$CH$_2$CN ·0.7H$_2$O in CD$_3$CN ($4.5\cdot10^{-2}$ M) at 298 K.

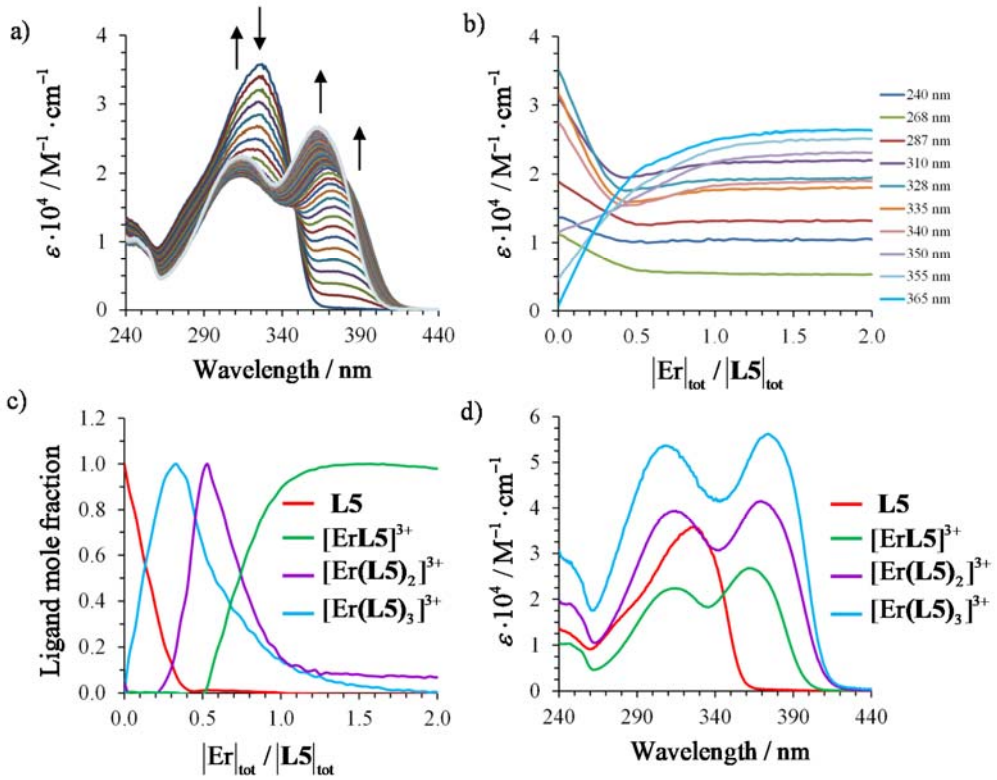

Figure S18. a) Variation of absorption spectra and b) corresponding variation of molar extinction at different wavelengths observed for the spectrophotometric titration of **L5** with Er(CF$_3$SO$_3$)$_3$ (total ligand concentration: $2.5\cdot10^{-4}$ mol·dm^{-3} in acetonitrile, 298 K). c) Evolving factor analysis[46] using four absorbing eigenvectors and d) reconstructed individual electronic absorption spectra.

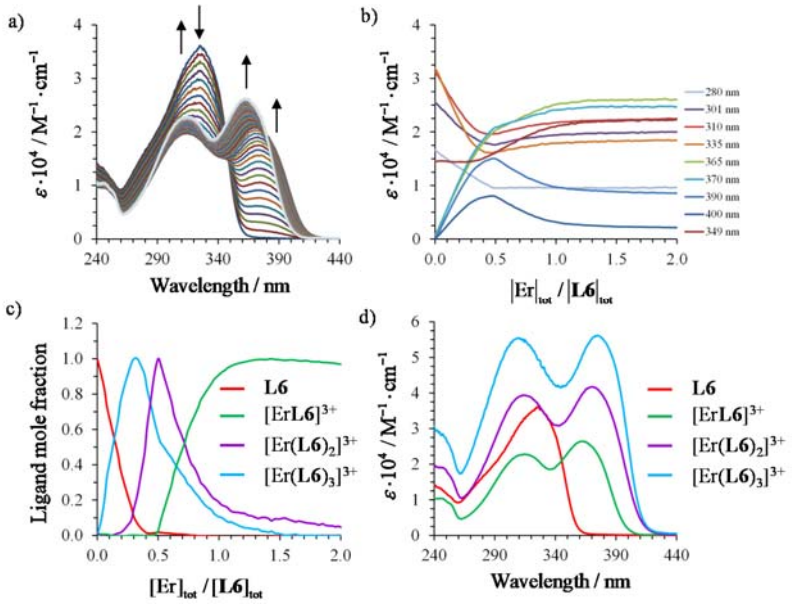

Figure S19. a) Variation of absorption spectra and b) corresponding variation of molar extinction at different wavelengths observed for the spectrophotometric titration of **L6** with $Er(CF_3SO_3)_3$ (total ligand concentration: $3.0 \cdot 10^{-4}$ mol·dm^{-3} in acetonitrile, 298 K). c) Evolving factor analysis[46] using four absorbing eigenvectors and d) reconstructed individual electronic absorption spectra.

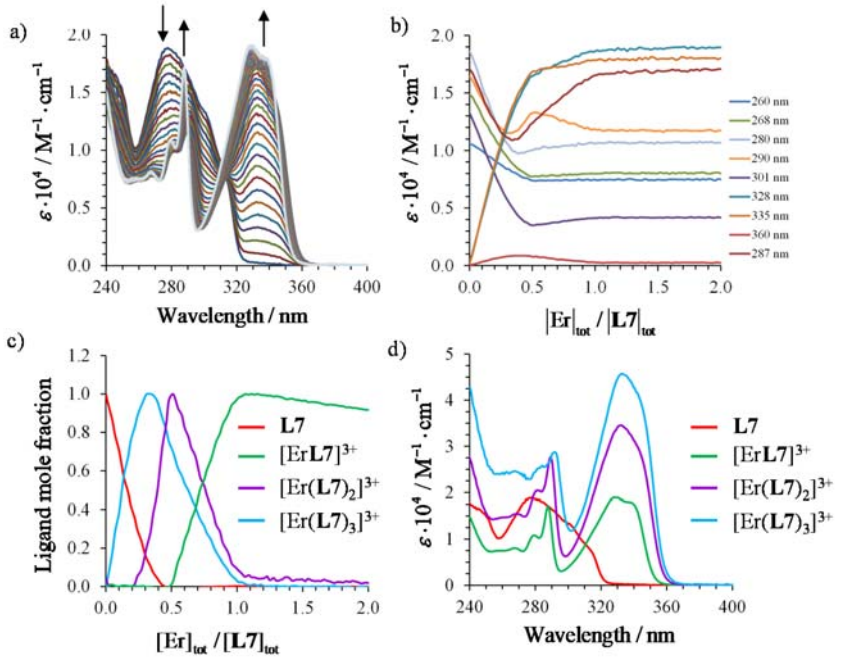

Figure S20. a) Variation of absorption spectra and b) corresponding variation of molar extinction at different wavelengths observed for the spectrophotometric titration of **L7** with $Er(CF_3SO_3)_3$ (total ligand concentration: $3.5 \cdot 10^{-4}$ mol·dm^{-3} in acetonitrile, 298 K). c) Evolving factor analysis[46] using four absorbing eigenvectors and d) reconstructed individual electronic absorption spectra.

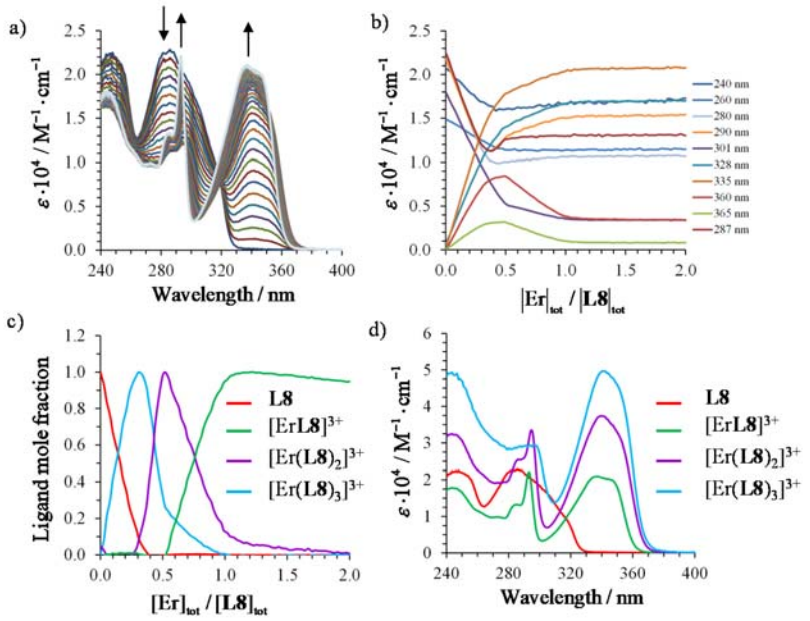

Figure S21. a) Variation of absorption spectra and b) corresponding variation of molar extinction at different wavelengths observed for the spectrophotometric titration of **L8** with $Er(CF_3SO_3)_3$ (total ligand concentration: $3.2 \cdot 10^{-4}$ mol·dm^{-3} in acetonitrile, 298 K). c) Evolving factor analysis[46] using four absorbing eigenvectors and d) reconstructed individual electronic absorption spectra.

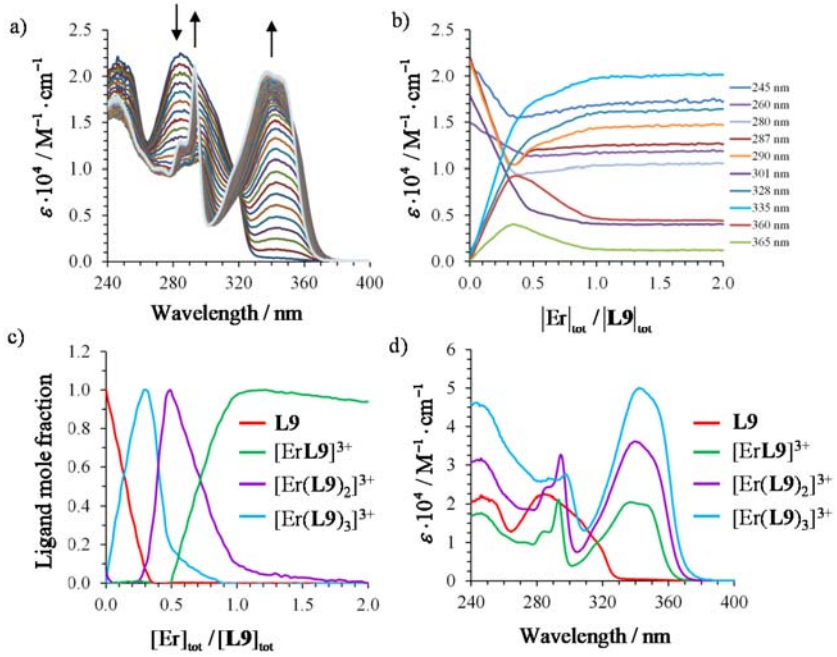

Figure S22. a) Variation of absorption spectra and b) corresponding variation of molar extinction at different wavelengths observed for the spectrophotometric titration of **L9** with $Er(CF_3SO_3)_3$ (total ligand concentration: $3.5 \cdot 10^{-4}$ mol·dm^{-3} in acetonitrile, 298 K). c) Evolving factor analysis[46] using four absorbing eigenvectors and d) reconstructed individual electronic absorption spectra.

a)

$$[Er(CH_3CN)_9]^{3+} + \textbf{L4} \xrightleftharpoons{\beta_{1,1}^{Er,\textbf{L4}}} [Er(\textbf{L4})(CH_3CN)_6]^{3+} + 3\ CH_3CN$$

Point group	D_{3h}	C_{2v}	C_{2v}	C_{3v}
σ_{ext}	6	2	2	3
σ_{int}	3^9	3^2	$3^2 \times 3^6$	1
σ_{mix}	1	1	1	1

$$\omega_{1,1}^{chiral} = \frac{1\times 1}{1\times (1)^3} = 1,\ \omega_{1,1}^{Er,\textbf{L4}} = \frac{6\times 3^9 \times 2\times 3^2}{2\times 3^2 \times 3^6 \times (3)^3} = 6 \Rightarrow K_{1,1}^{stat} = \omega_{1,1}^{chiral} \cdot \omega_{1,1}^{Er,\textbf{L4}} = 6$$

b)

$$[Er(CH_3CN)_9]^{3+} + 2\ \textbf{L4} \xrightleftharpoons{\beta_{1,2}^{Er,\textbf{L4}}} [Er(\textbf{L4})_2(CH_3CN)_3]^{3+} + 6\ CH_3CN$$

Point group	D_{3h}	C_{2v}	C_{2v}	C_{3v}
σ_{ext}	6	2	2	3
σ_{int}	3^9	3^2	$3^4 \times 3^3$	1
σ_{mix}	1	1	1	1

$$\omega_{1,2}^{chiral} = \frac{1\times 1^2}{1\times (1)^6} = 1,\ \omega_{1,2}^{Er,\textbf{L4}} = \frac{6\times 3^9 \times (2)^2 \times (3^2)^2}{2\times 3^4 \times 3^3 \times (3)^6} = 12 \Rightarrow K_{1,2}^{stat} = \omega_{1,2}^{chiral} \cdot \omega_{1,2}^{Er,\textbf{L4}} = 12$$

c)

$$[Er(CH_3CN)_9]^{3+} + 3\ \textbf{L4} \xrightleftharpoons{\beta_{1,3}^{Er,\textbf{L4}}} [Er(\textbf{L4})_3]^{3+} + 9\ CH_3CN$$

Point group	D_{3h}	C_{2v}	D_3	C_{3v}
σ_{ext}	6	2	6	3
σ_{int}	3^9	3^2	3^6	1
σ_{mix}	1	1	$\frac{1}{2}$	1

$$\omega_{1,3}^{chiral} = \frac{1\times 1^3}{\frac{1}{2}\times (1)^9} = 2,\ \omega_{1,3}^{Er,\textbf{L4}} = \frac{6\times 3^9 \times (2)^3 \times (3^2)^3}{6\times 3^6 \times (3)^9} = 8 \Rightarrow K_{1,3}^{stat} = \omega_{1,3}^{chiral} \cdot \omega_{1,3}^{Er,\textbf{L4}} = 16$$

Figure S23 Symmetry numbers obtained by *Benson*'s method and associated statistical factors computed for the formation of a) $[Er(\textbf{L4})]^{+3}$, b) $[Er(\textbf{L4})_2]^{+3}$ and c) $[Er(\textbf{L4})_3]^{+3}$.

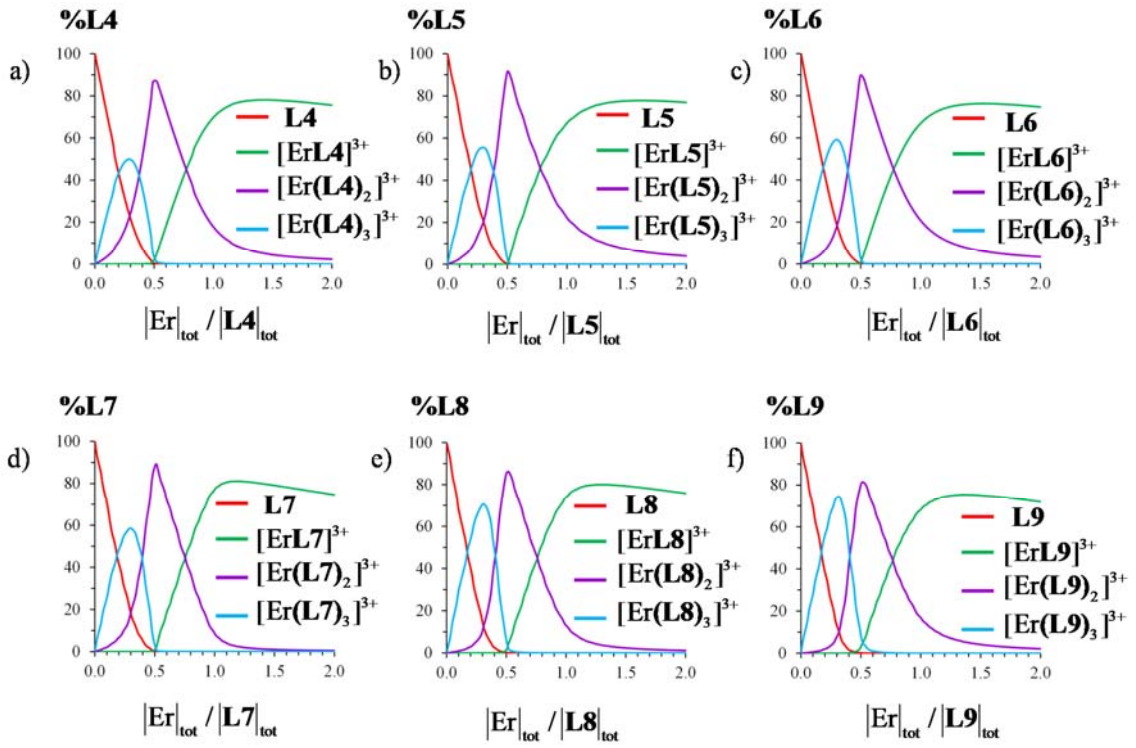

Figure S24 Macroscopic speciation curves computed for the spectrophotometric titrations of ligands **L4-L9** with $Er(CF_3SO_3)_3$ ($|\mathbf{Lk}|_{tot} \approx 3\times10^{-4}$ M in acetonitrile, 298 K).

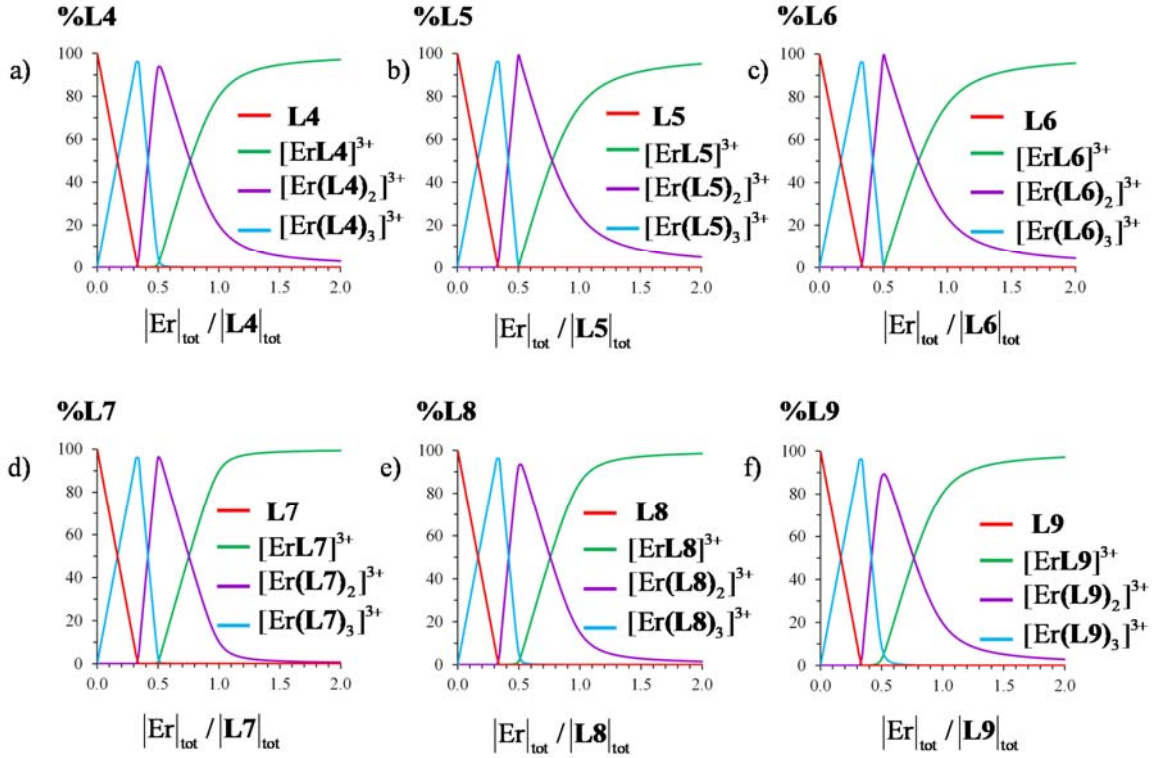

Figure S25 Macroscopic speciation curves computed for the spectrophotometric titrations of ligands **L4-L9** with $Er(CF_3SO_3)_3$ ($|\mathbf{Lk}|_{tot} \approx 1$M in acetonitrile, 298 K).

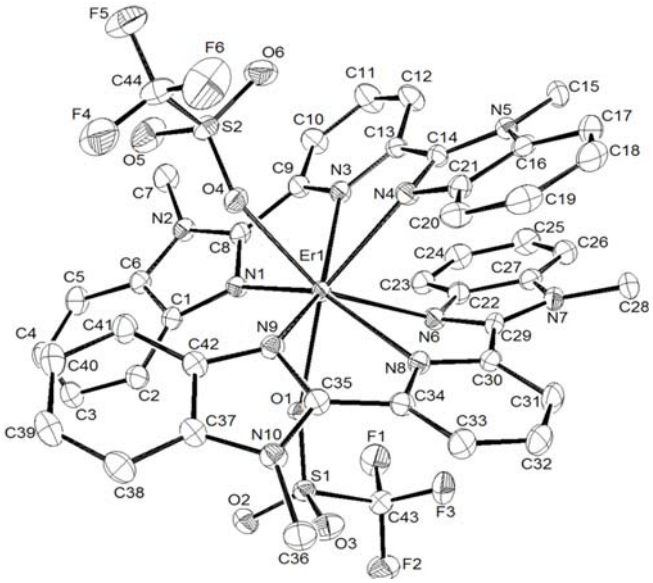

Figure S26 ORTEP molecular view with numbering scheme of the asymmetric unit for $[Er(\mathbf{L4})_2(O_3SCF_3)_2]^+$ in the crystal structure of **1**. Thermal ellipsoids are represented at the 40% probability level and hydrogen atoms are omitted for clarity.

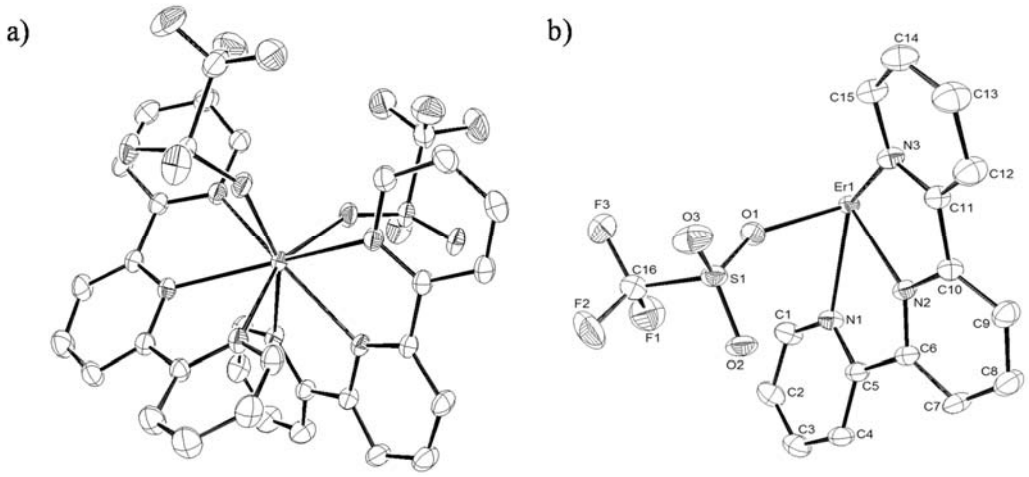

Figure S27 ORTEP molecular view of a) $[Er(\mathbf{L7})_2(O_3SCF_3)_2]^+$ in the crystal structure of **2** and b) numbering scheme of the asymmetric unit. Thermal ellipsoids are represented at the 40% probability level and hydrogen atoms are omitted for clarity.

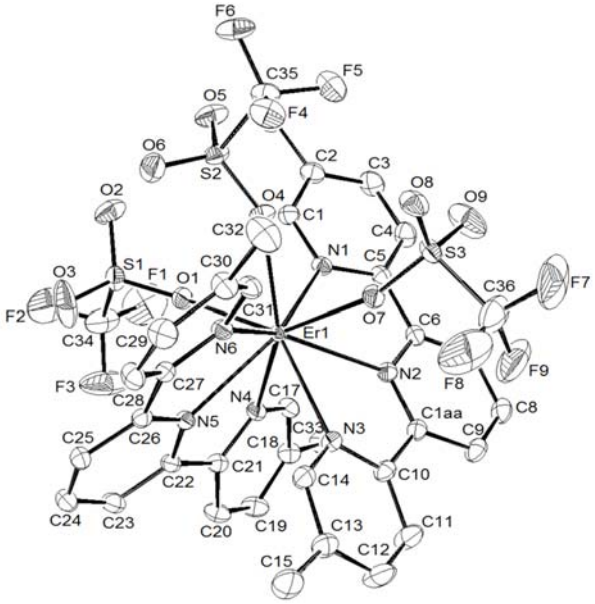

Figure S28 ORTEP molecular view with numbering scheme of the asymmetric unit for Er(**L8**)$_2$(O$_3$SCF$_3$)$_3$ in the crystal structure of **3**. Thermal ellipsoids are represented at the 40% probability level and hydrogen atoms are omitted for clarity.

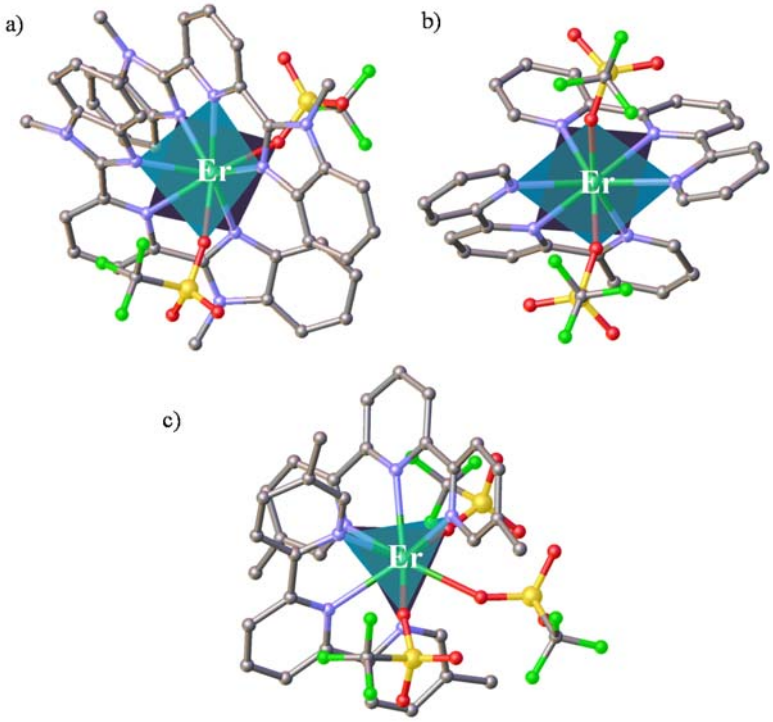

Figure S29 Perspective views of complexes a) [Er(**L4**)$_2$(O$_3$SCF$_3$)$_2$]$^+$ (**1**), b) [Er(**L7**)$_2$(O$_3$SCF$_3$)$_2$]$^+$ (**2**) and c) Er(**L8**)$_2$(O$_3$SCF$_3$)$_3$ (**3**) showing the pseudo-square antiprismatic (for complexes **1** and **2**) and distorted tricapped trigonal-prismatic (for complex **3**) arrangements around trivalent erbium.

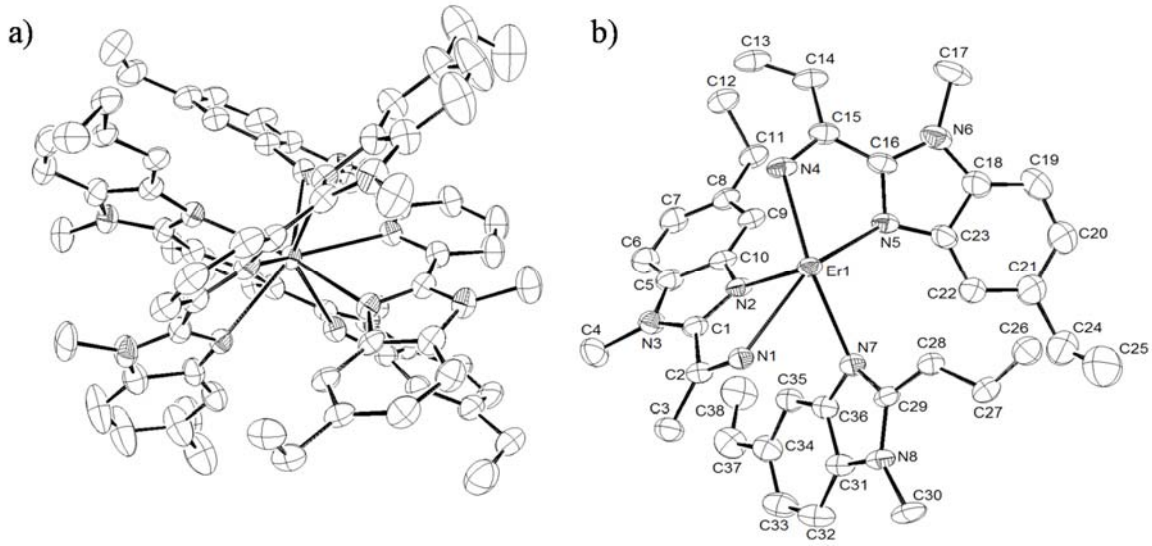

Figure S30 ORTEP molecular view of a) $[Er(\mathbf{L6})_3]^{3+}$ in the crystal structure of **4** and b) numbering scheme of the asymmetric unit. Thermal ellipsoids are represented at the 40% probability level and hydrogen atoms are omitted for clarity.

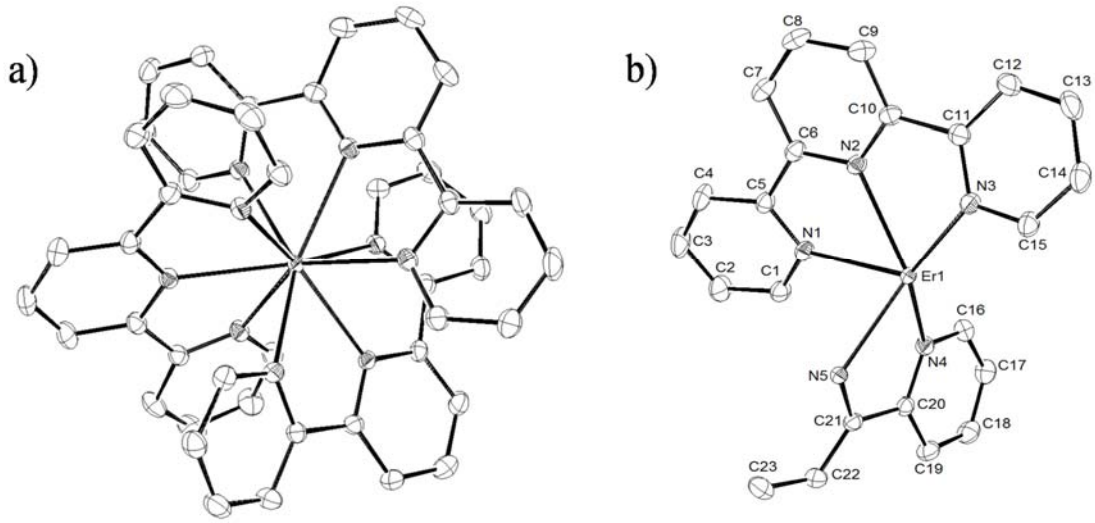

Figure S31 ORTEP molecular view of a) $[Er(\mathbf{L7})_3]^{3+}$ in the crystal structure of **5** and b) numbering scheme of the asymmetric unit. Thermal ellipsoids are represented at the 40% probability level and hydrogen atoms are omitted for clarity.

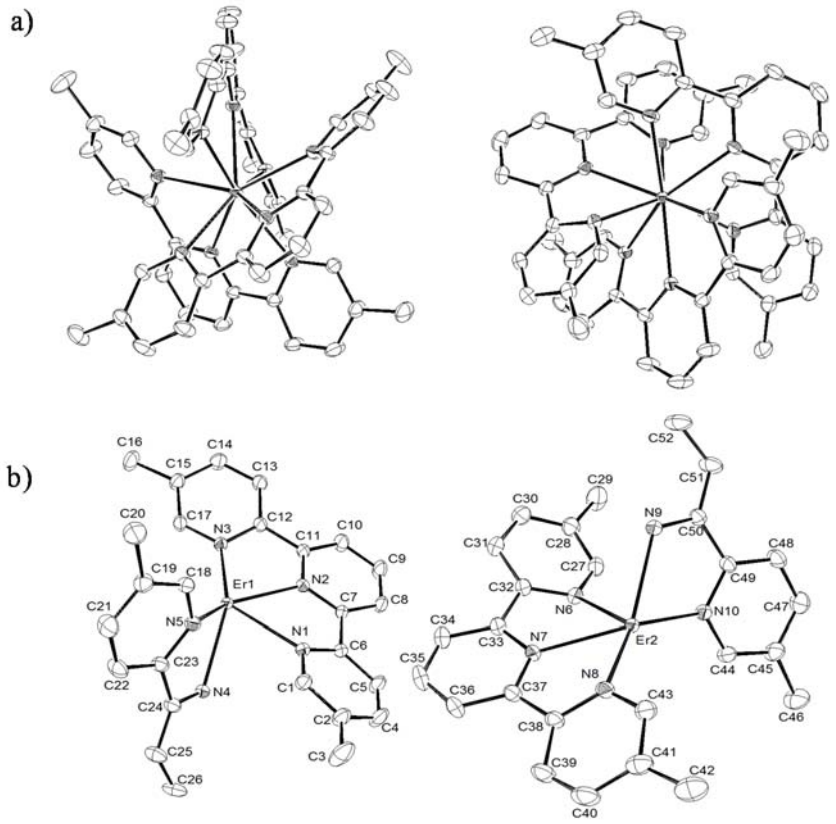

Figure S32 ORTEP molecular view of a) $[Er(\mathbf{L8})_3]^{3+}$ in the crystal structure of **6** and b) numbering scheme of the asymmetric unit (the asymmetric unit in the crystal structure of **6** contains two slightly different $[Er(\mathbf{L8})_3]^{3+}$ cations). Thermal ellipsoids are represented at the 40% probability level and hydrogen atoms are omitted for clarity.

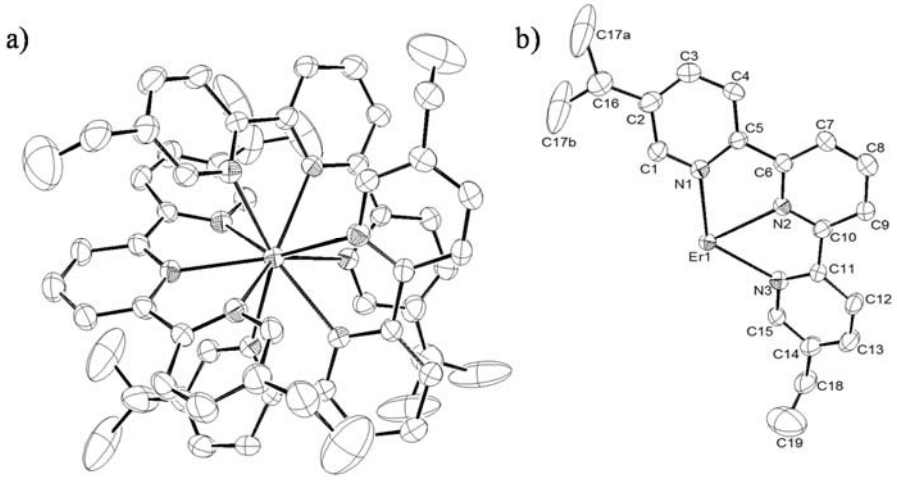

Figure S33 ORTEP molecular view of a) $[Er(\mathbf{L9})_3]^{3+}$ in the crystal structure of **7** and b) numbering scheme of the asymmetric unit. Thermal ellipsoids are represented at the 40% probability level and hydrogen atoms are omitted for clarity.

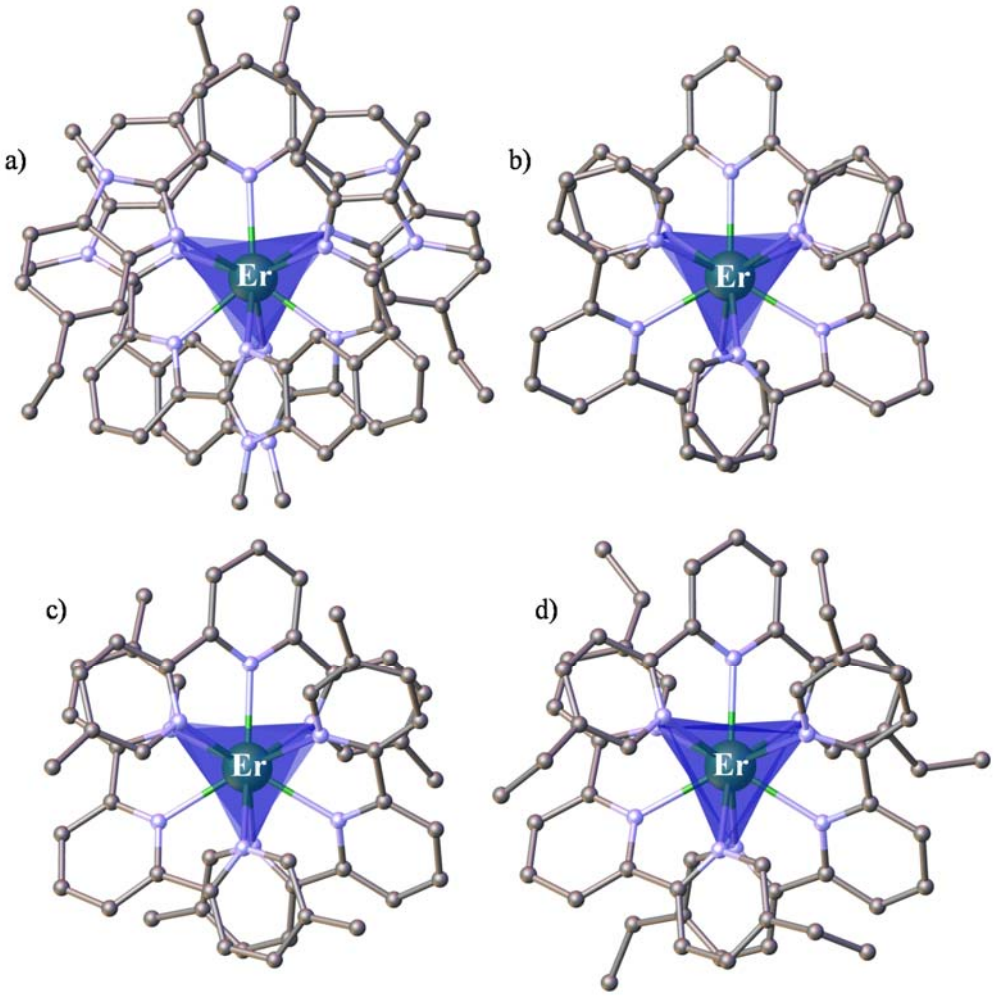

Figure S34 Perspective views of complexes a) $[Er(\mathbf{L6})_3]^{3+}$, b) $[Er(\mathbf{L7})_3]^{3+}$, c) $Er(\mathbf{L8})_3]^{3+}$ and d) $[Er(\mathbf{L9})_3]^{3+}$ along the pseudo-C_3 axis which highlight the distorted tricapped trigonal-prismatic arrangements around trivalent erbium.

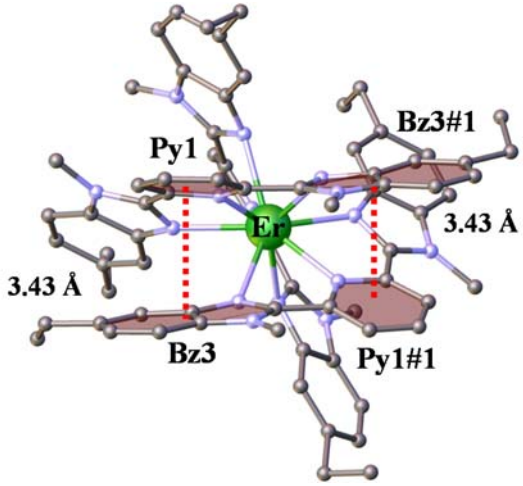

Figure S35 Perspective view of complex $[Er(\mathbf{L6})_3]^{3+}$ perpendicular to the pseudo-C_3 axis showing the intramolecular π-π interactions.

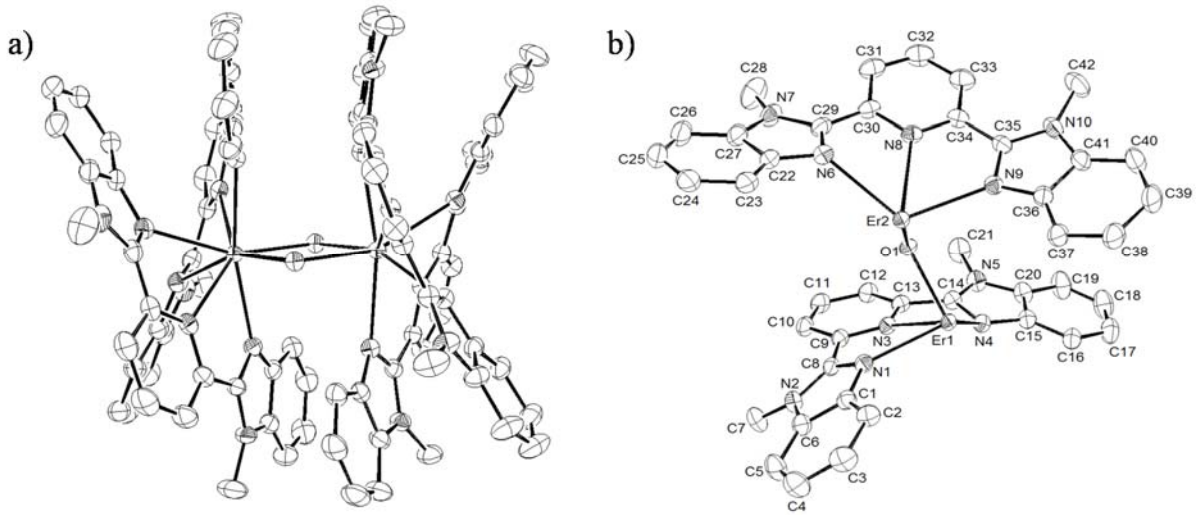

Figure S36 ORTEP molecular view of a) $[(\mathbf{L4})_2Er(OH)_2Er(\mathbf{L4})_2]^{4+}$ in the crystal structure of **8** and b) numbering scheme of the asymmetric unit. Thermal ellipsoids are represented at the 40% probability level and hydrogen atoms are omitted for clarity.

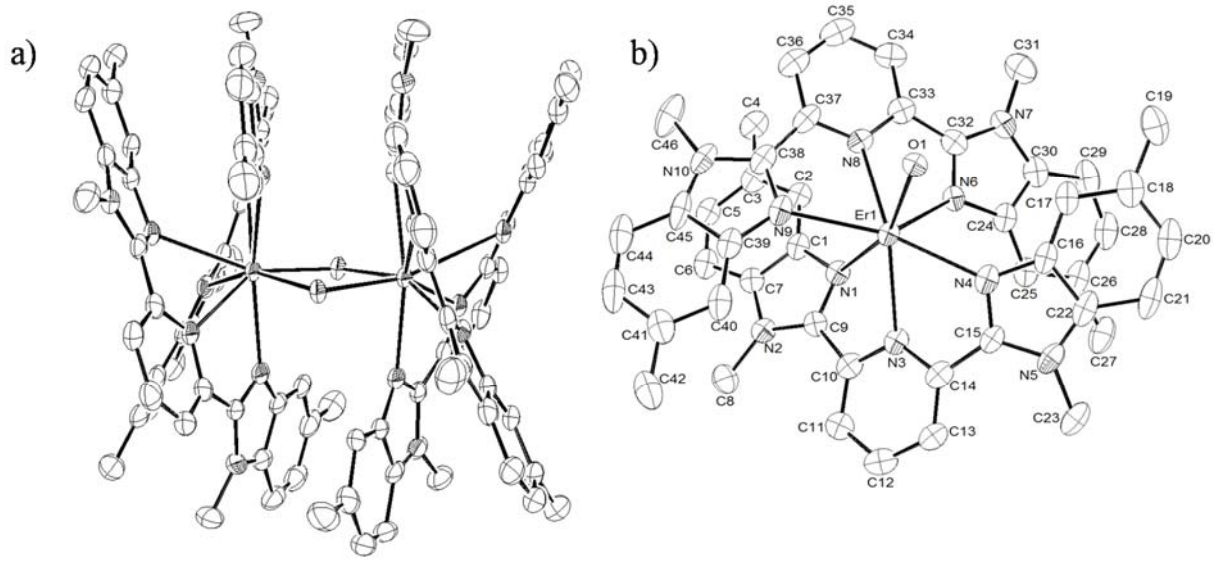

Figure S37 ORTEP molecular view of a) $[(\mathbf{L5})_2Er(OH)_2Er(\mathbf{L5})_2]^{4+}$ in the crystal structure of **9** and b) numbering scheme of the asymmetric unit. Thermal ellipsoids are represented at the 40% probability level and hydrogen atoms are omitted for clarity.

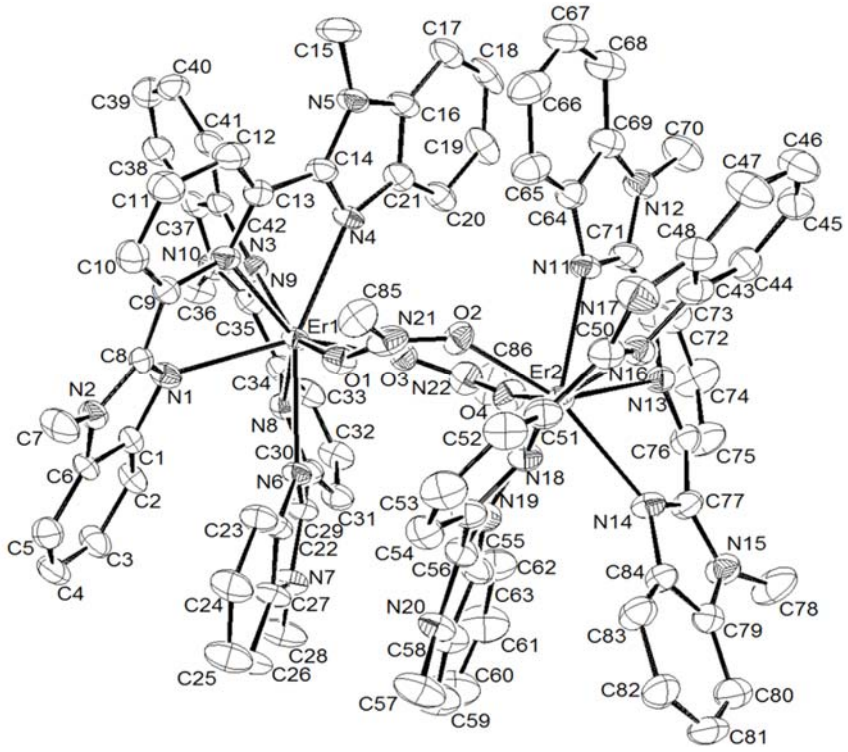

Figure S38 ORTEP molecular view with numbering scheme of the asymmetric unit for $[(\mathbf{L4})_2Er((CH_3)NO_2)_2Er(\mathbf{L4})_2]^{6+}$ in the crystal structure of **10**. Thermal ellipsoids are represented at the 40% probability level and hydrogen atoms are omitted for clarity.

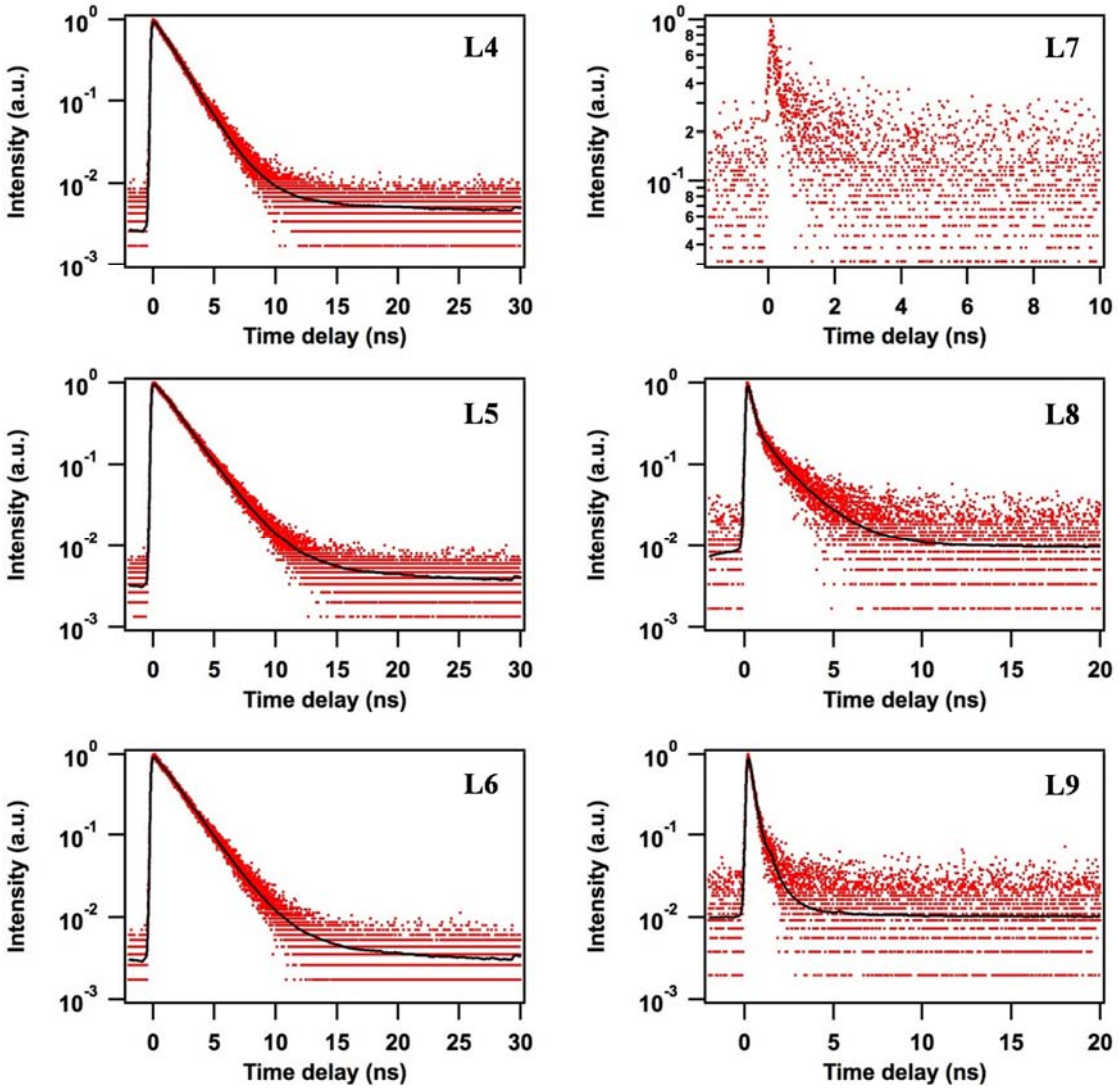

Figure S39 Fluorescence time profiles of **L4-L9** in acetonitrile upon excitation at 320 nm. The black solid traces represent best fits to the data points. The quality of the experimental data obtained with **L7** (extremely low signal) prevented from an exponential fit to the data to properly converge; therefore only the raw data is shown.

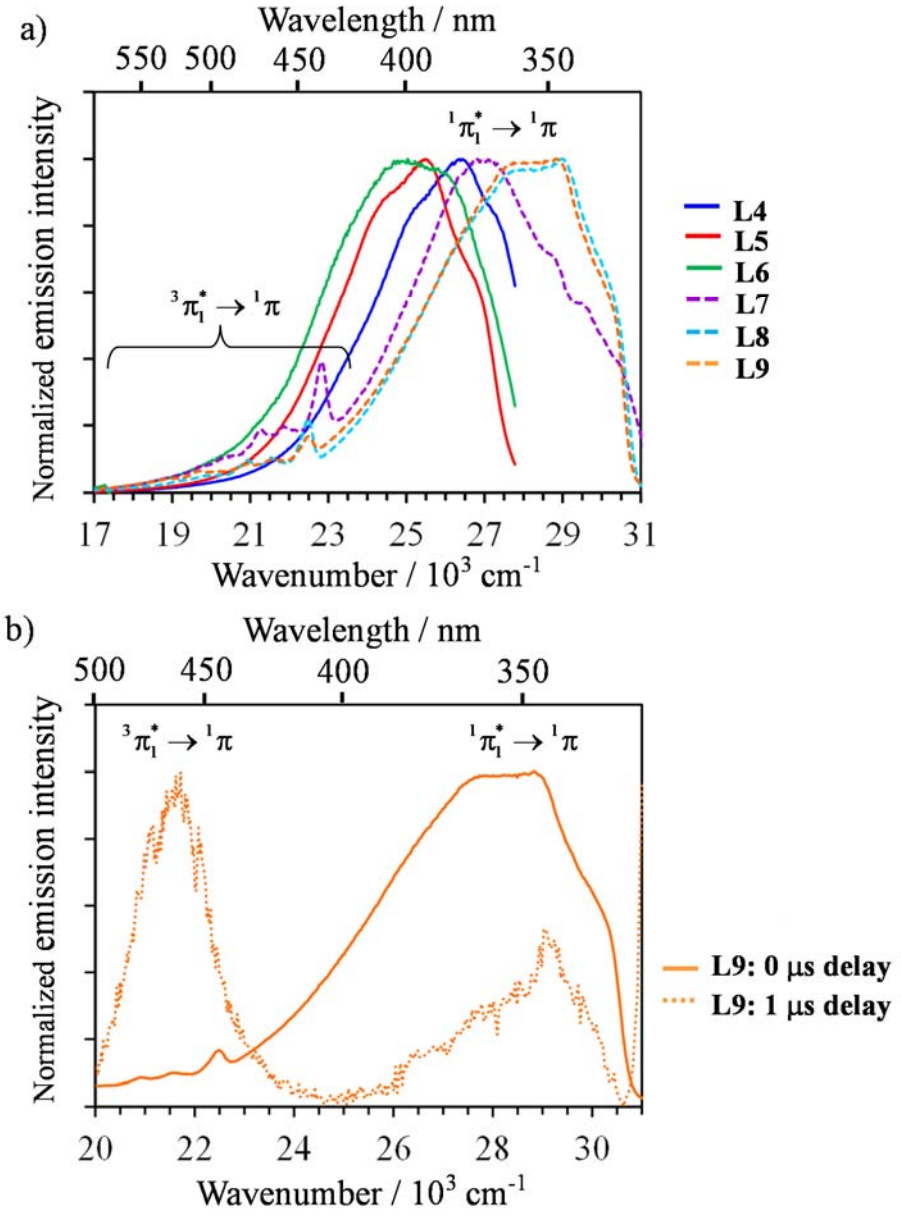

Figure S40 a) Normalized emission spectra recorded for ligands **L4-L6** (λ_{exc} = 330 nm, full traces) and **L7-L9** (λ_{exc} = 280 nm) in frozen acetonitrile (0.3 mM) at 77 K. b) Normalized emission (full trace) and time-gated (1.0 µs delay, dotted trace) recorded for **L9** (λ_{exc} = 280 nm) in frozen acetonitrile (0.3 mM) at 77 K highlighting the weak spin-forbidden $^3\pi_1 \rightarrow {}^1\pi$ transition.

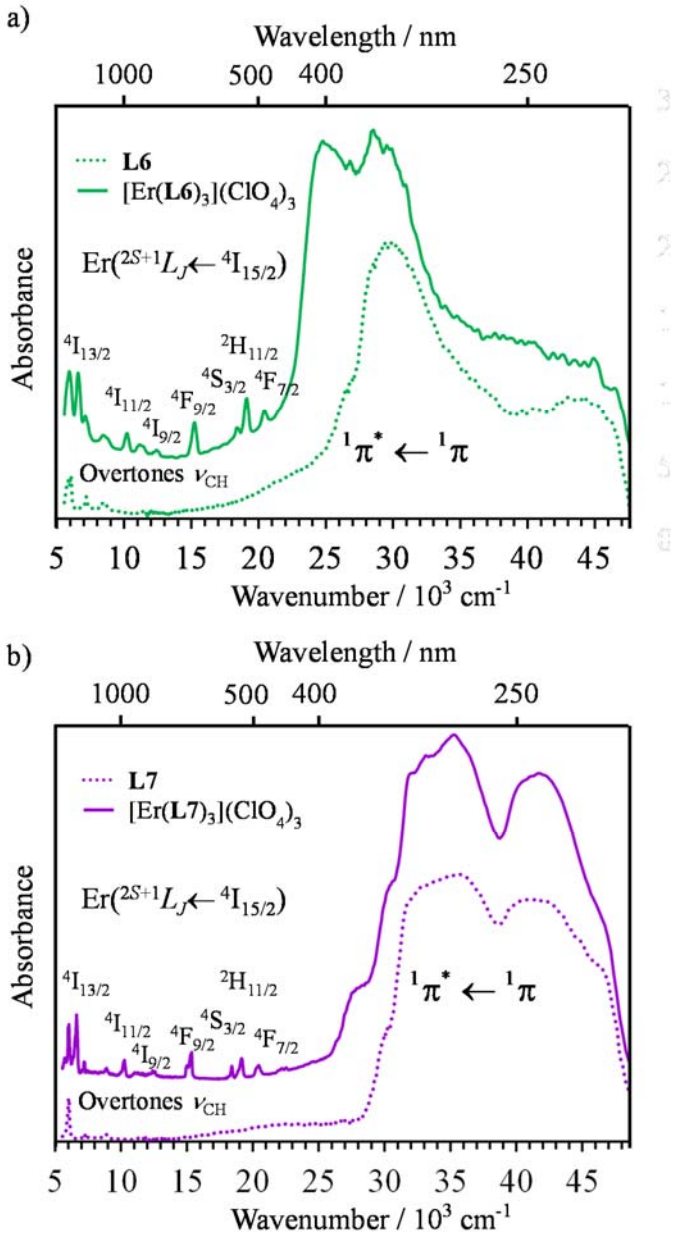

Figure S41 Comparison of the absorption spectra recorded a) ligand **L6** and its triple helical complex $[Er(\mathbf{L6})_3](ClO_4)_3$ (**4**) and b) ligand **L7** and its triple helical complex $[Er(\mathbf{L7})_3](ClO_4)_3$ (**5**) recorded in the solid-state at room temperature. The samples were diluted in MgO (85 wt %).

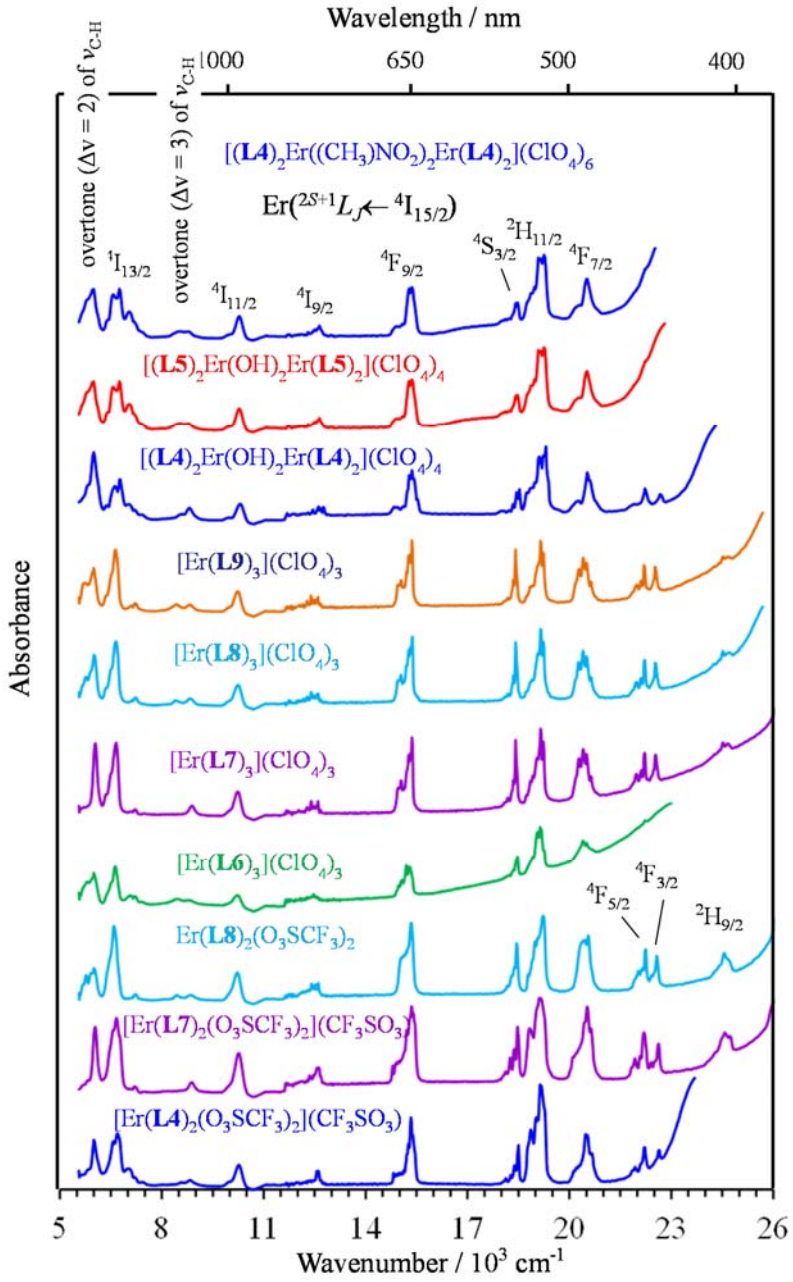

Figure S42 Vis to NIR absorption spectra of the complexes [Er(**L4**)$_2$(CF$_3$SO$_3$)$_2$](CF$_3$SO$_3$)·2CH$_3$CN (**1**), [Er(**L7**)$_2$(CF$_3$SO$_3$)$_2$](CF$_3$SO$_3$)·1.5C$_2$H$_5$CN (**2**),[21a] [Er(**L8**)$_2$(CF$_3$SO$_3$)$_3$] (**3**), [Er(**L6**)$_3$](ClO$_4$)$_3$·1.5CH$_3$CN (**4**), [Er(**L7**)$_3$](ClO$_4$)$_3$ (**5**), [Er(**L8**)$_3$](ClO$_4$)$_3$ (**6**) and [Er(**L9**)$_3$](ClO$_4$)$_3$·1.5CH$_3$CN (**7**) [(**L4**)$_2$Er(OH)$_2$Er(**L4**)$_2$](ClO$_4$)$_4$·2C$_6$H$_5$CN·4CH$_3$CN (**8**), [(**L5**)$_2$Er(OH)$_2$Er(**L5**)$_2$](ClO$_4$)$_4$·C$_6$H$_5$CN·8CH$_3$CN (**9**) and [(**L4**)$_2$Er(CH$_3$NO$_2$)$_2$Er(**L4**)$_2$](ClO$_4$)$_6$·CH$_3$NO$_2$ (**10**) recorded in the solid-state at room temperature and assigned as Er($^{2S+1}L_J \leftarrow {}^4I_{15/2}$) transitions.

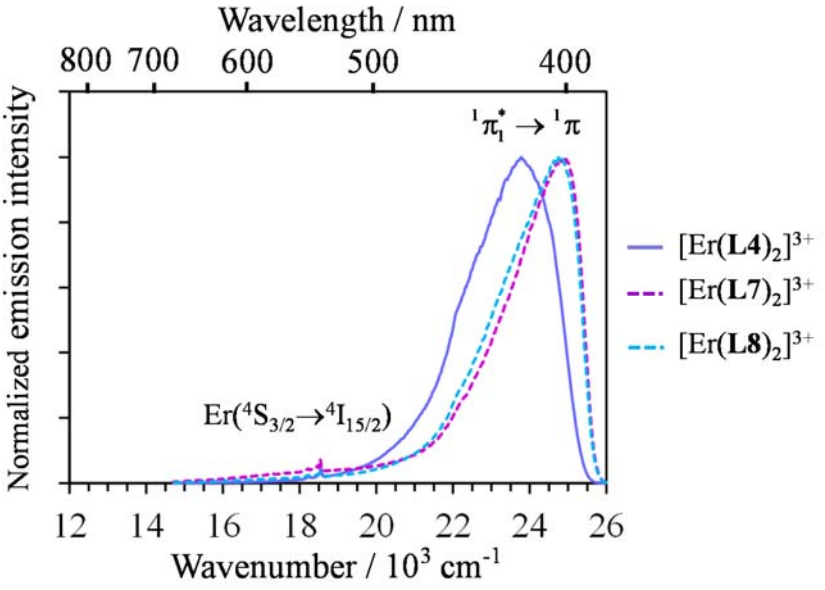

Figure S43 Visible emission spectra recorded for the complexes [Er(**L4**)$_2$]$^{3+}$ (λ_{exc} = 370 nm), [Er(**L7**)$_2$]$^{3+}$ and [Er(**L8**)$_2$]$^{3+}$ (λ_{exc} = 350 nm) in frozen acetonitrile solution (3.0 mM) at 77 K.

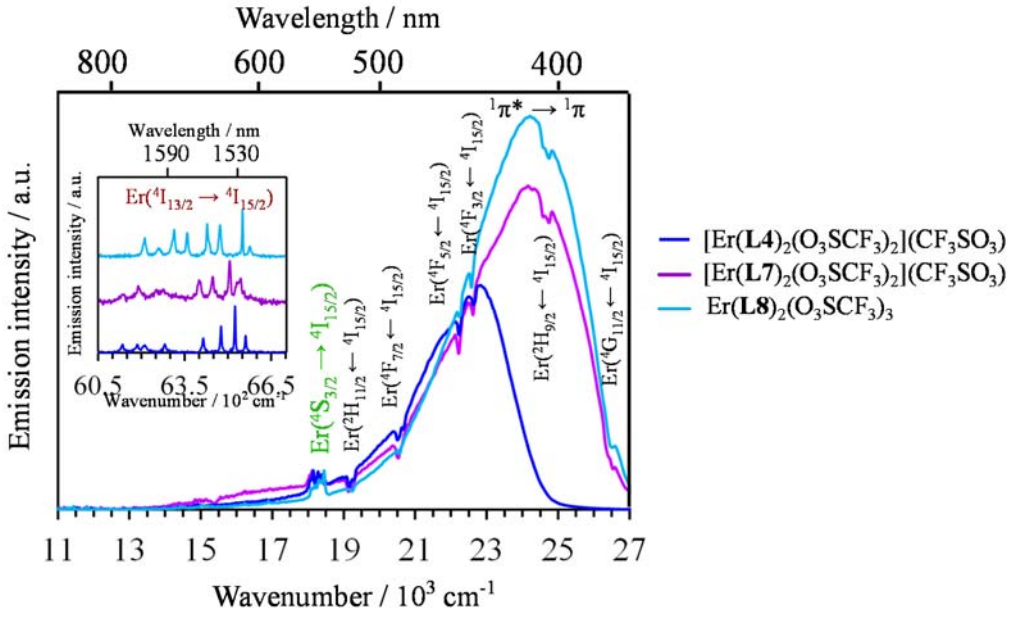

Figure S44 Visible emission spectra recorded for solid-state complexes [Er(**L4**)$_2$(CF$_3$SO$_3$)$_2$](CF$_3$SO$_3$) (**1**), [Er(**L7**)$_2$(CF$_3$SO$_3$)$_2$](CF$_3$SO$_3$) (**2**), [Er(**L8**)$_2$(CF$_3$SO$_3$)$_3$] (**3**) (λ_{exc} = 350 nm) at 7 K. The inset shows the associated near-infrared emission spectra (λ_{exc} = 447 nm, 11 K). The dual emission is assigned with color fonts, while the dips (assigned using black fonts) correspond to Er-centered re-absorption of the residual ligand-centered $^1\pi^*\rightarrow\pi$ emission.

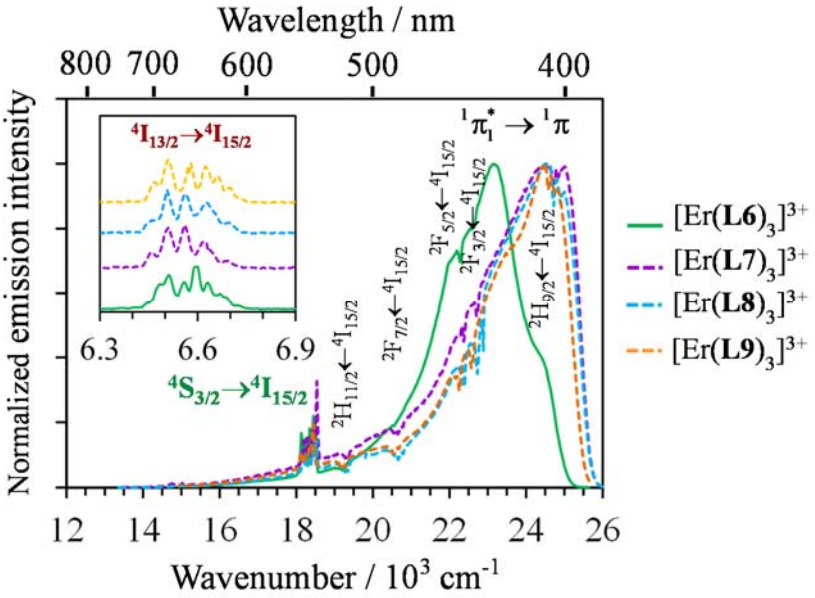

Figure S45 Dual visible (main plot) and near-infrared (inset) emission spectra recorded for the complexes **4** (λ_{exc} = 370 nm) and **5-7** (λ_{exc} = 340 nm) in the solid-state at 77K. The dual emission is assigned using color fonts, while the dips (assigned using black fonts) correspond to Er-centered re-absorption of the residual ligand-centered $^1\pi^*\rightarrow\pi$ emission.

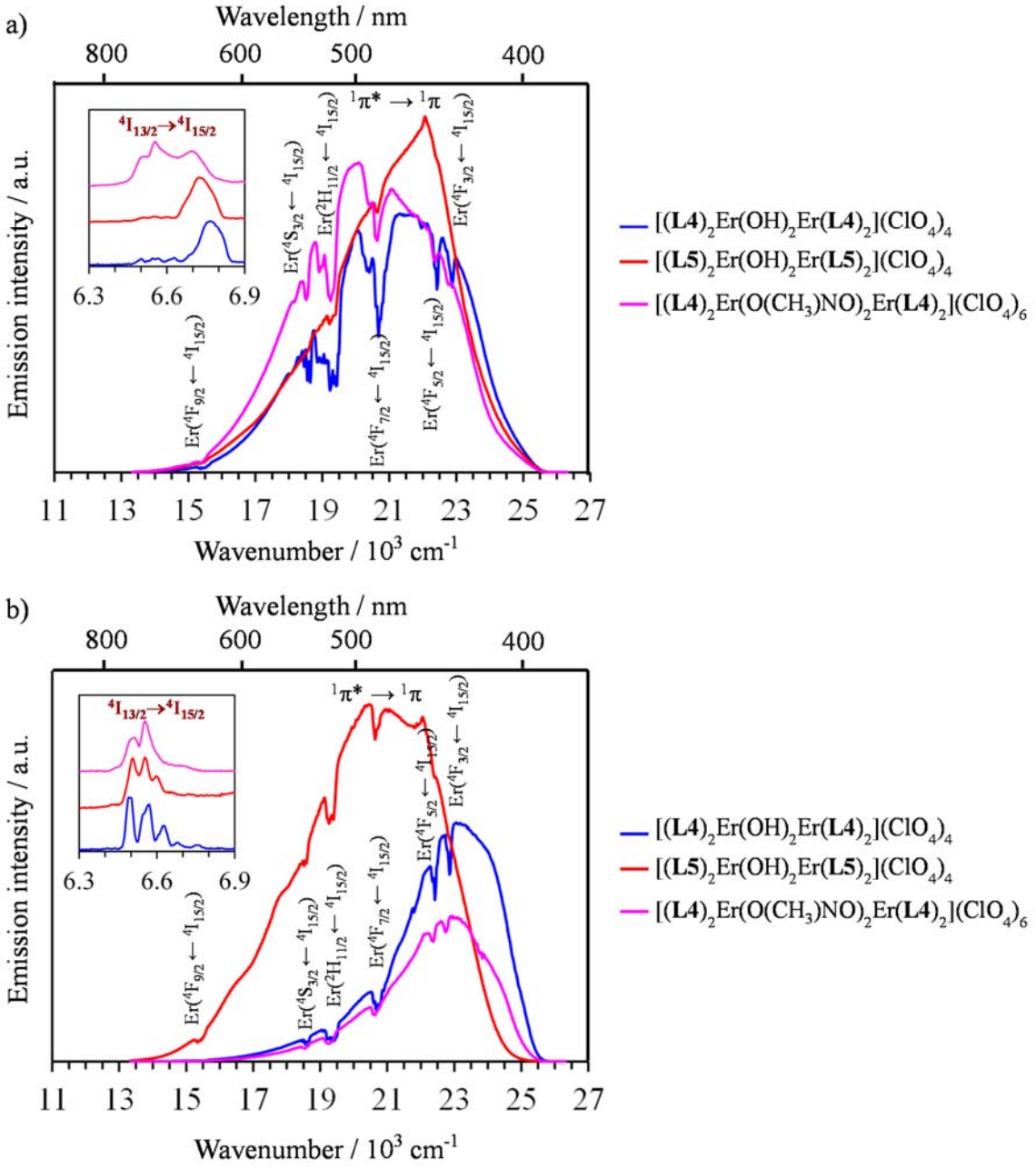

Figure S46 Emission spectra recorded for the dimeric complexes $[(\mathbf{L4})_2Er(OH)_2Er(\mathbf{L4})_2](ClO_4)_4$ (**8**), $[(\mathbf{L5})_2Er(OH)_2Er(\mathbf{L5})_2](ClO_4)_4$ (**9**) and $[(\mathbf{L4})_2Er(CH_3NO_2)_2Er(\mathbf{L4})_2](ClO_4)_6$ (**10**) (λ_{exc} = 370 nm) in the solid-state at a) 298 K and b) 77K. The dips (assigned using black fonts) correspond to Er-centered re-absorption of the residual ligand-centered $^1\pi^* \rightarrow \pi$ emission.